ABSTRACT

Title of Dissertation: SUBPLATE NEURONS AND THEIR ROLE IN THE FUNCTIONAL MATURATION OF THE BRAIN

Aminah Sheikh, Doctor of Philosophy, 2016

Dissertation directed by: Professor, Dr. Patrick O. Kanold, Department of Biology

Normal brain development is crucial for the proper maturation of neural circuits and cognitive functioning. White matter brain injury during development results in disruption of normal brain maturation and consequently increases risk of developing disorders such as epilepsy and cerebral palsy. Crucial for the proper development of thalamocortical circuits are a transient population of neurons in the developing subcortical white matter of the brain referred to as subplate neurons (SPNs). SPNs are among the first cortical neurons to be born and are necessary for normal functional development of the cerebral cortex. This dissertation begins by studying the effect of SPN removal in the neonatal rat somatosensory cortex (S1). After subplate ablation in the S1 barrel region, we find that removal of SPNs prevents the development of the barrel field in L4, and in vitro recordings reveal that thalamocortical inputs to layer 4 neurons are weak. This dissertation then progresses to investigating the effects of a more clinically relevant and common brain injury

among humans, neonatal hypoxia-ischemia (HI), which causes brain damage specific to different brain structures over development. In the preterm human, HI results in damage to subcortical developing white matter, referred to as periventricular leukomalacia (PVL). From other studies we know that HI can damage SPNs however, it is unclear how HI and its differing severities alters SPN circuits. This dissertation uses a rat model of HI in which either mild or moderate HI was induced at postnatal day (P)1. To investigate the functional synaptic connectivity changes of SPNs and layer 4 neurons in both injury categories, this dissertation also uses laser-scanning photostimulation (LSPS) combined with whole-cell patch clamp recordings in acute thalamocortical slices of rat A1 over development. Our results suggest that SPNs are uniquely susceptible to HI and that HI causes a rearrangement of SPN circuits. This leads to abnormal cortical function observed after HI. Results from these studies help fill in crucial gaps in the understanding of not only how important SPNs are in the proper development of multiple sensory regions, but also how vulnerable they are to hypoxic-ischemic brain injury.

SUBPLATE NEURONS AND THEIR ROLE IN THE FUNCTIONAL MATURATION OF THE BRAIN

by

Aminah Sheikh

Dissertation submitted to the Faculty of the Graduate School of the
University of Maryland, College Park, in partial fulfillment
of the requirements for the degree of
Doctor of Philosophy
2016

Advisory Committee:
Professor, Dr. Patrick O. Kanold, Chair
Distinguished Professor, Dr. Catherine E. Carr
Associate Professor, Dr. Jens Herberholz
Assistant Professor, Dr. Masaaki Torii
Associate Professor, Dr. Matthew R. Roesch

Dedication

I dedicate this dissertation to my mother, Patricia L. Sheikh, for being incredibly supportive, always believing in me, and for her unconditional love.

Acknowledgements

I want to acknowledge my mother, and my brothers for their love & support: Patricia L. Sheikh, Abdul Aleem Sheikh, and Abdul Azeem Sheikh.

To my PI, Dr. Patrick O. Kanold, Ph.D., for giving me a chance when I came to you as an undergraduate with no lab experience & for believing in me; from undergraduate to Ph.D.

I want to thank my dissertation committee for helping guide me through this journey: Dr. Catherine Carr, Ph.D.; Dr. Jens Herberholz, Ph.D.; Dr. Matthew Roesch, Ph.D.; and Dr. Masaaki Torii, Ph.D.

I want to thank the following members of the Kanold Lab, present and past, for their continual support, advice, and friendship: Dr. Daniel E. Winkowski, Ph.D., Dr. Xiangying Meng, Ph.D.; Dr. Daniel Nagode Ph.D.; Dr. Sarada Viswanathan, PhD; Dr. Amal Isaiah MD, PhD (UMD SOM); Dr. Sharba Bandyopadhyay, Ph.D.; Dr. Barak Shechter, Ph.D.; Dr. Nik Francis, Ph.D.; Dr. Paul V. Watkins, Ph.D.; Dr. Cuiping Zhao, M.D, Ph.D.; Dr. Berje Shammassian, M.D., Kevin Donaldson, Krystyna L. Solarana, Rongkang Deng, Ji Liu, Zac Bowen, Kevin Armengol, and Shahzeib Syed. I also want to thank all the past undergraduates for helping me with a mountain of histological processing over the years.

I want to thank Dr. Joseph PY Kao, Ph.D. (UMD SOM) for his continual supply of caged glutamate solution for which none of this would have been possible without.

I want to thank Dr. Loren Looger, PhD (HHMI Janelia Farms), for his continual motivation, support, and advice over the years.

Dr. Richard Payne, Ph.D., for his belief in me and for introducing me to my first research lab, the Kanold Lab.

Ms. Pam Komarek, Assistant Director of the NACS graduate program, for guiding me through program deadlines & her support.

I want to thank Dr. Heiko Luhmann, Ph.D.; Dr. Jerome Mordel, Ph.D.; and the rest of the Luhmann Lab of Mainz, Germany for giving me the chance to work overseas in my first international lab, for teaching me, and friendship.

I want to thank Dr. Hey-Kyoung Lee, Ph.D.; Dr. Kaiwen He, Ph.D.; Dr. Emily Petrus, Ph.D.; and Dr. Hui Wang, Ph.D. for inspiring me to go into the world of electrophysiology, and for their friendship and support.

I want to thank other professors and staff for their support over the years: Dr. Daniel A. Butts, Ph.D.; Dr. Rashidul Alam, Ph.D., and especially Dr. William J. Higgins, Ph.D. and Mr. Gene Ferrick for their unconditional support & friendship.

To my neighbor, Dr. Daron Freedberg, Ph.D. for keeping tabs on my graduate school progress, his friendship, and wonderful advice.

I want to thank my middle and high school teachers for introducing me into the world of science and for growing my leadership skills. *Music (especially an article from band class in middle school) is what led to me being initially interested in neuroscience, especially the auditory cortex*: Mr. Stephen Majkrzak (biology), Mr. Robert Hartswick (biology), Mr. Robert Dahlin (music), Mr. William J Hollin (music), and Mr. Tory Shaw (music).

Table of Contents

List of Figures

Chapter 1: Introduction

1.1) *Subplate development and the thalamus*

Subplate neurons are a transient population of neurons in the developing cortical white matter that help secure the connection and relay feedforward excitatory transmission from the thalamus to the cortex (Kanold et al., 2003; Kanold, 2009; Tolner et al., 2012). In the embryonic brain, the earliest cells come from the ventricular zone to then make up the preplate, which becomes divided into the marginal zone (MZ) and the deep subplate (SP) (Aboitiz, 2009; Hoerder-Suabedissen and Molnar, 2012). The cells between these layers make up the cortical plate (CP) (Aboitiz, 2009; Hoerder-Suabedissen and Molnar, 2012).

Subplate neurons (SPNs) are necessary for the proper development of the cerebral cortex (Ghosh and Shatz, 1993; Kanold et al., 2003; Kanold and Shatz, 2006; Kanold, 2009). Also, subplate neurons play a universal role in thalamocortical

development of mammals. They are amongst the earliest appearing neurons born at around E10.5-11.5 and disappear in the adult brain as thalamocortical connections become secure (Molyneaux et al., 2007). The cell bodies of subplate neurons are located in the developing white matter of all cortical regions (Luskin and Shatz, 1985; Valverde and Facal-Valverde, 1987; Kostovic and Rakic, 1990; Allendoerfer and Shatz, 1994; Kostovic et al., 2002; Kanold, 2009).

Over development, the subplate axons serve as a guide for growing thalamocortical axons, and eventually these subplate neurons die off as the species mature to the adult stage (Allendoerfer and Shatz, 1994; Kanold and Luhmann, 2010). During development, there is a period referred to as the critical period, which is when the circuitry of the brain is plastic and able to be re-wired easily as a result of experiences (Hensch and Fagiolini, 2004). This is referred to as experience-dependent plasticity, where experience drives the formation of circuitry in the brain and if there is a lack of activity in either a sensory region or injury to the brain, there is improper formation of circuitry or lack of established circuitry to the proper target areas of the brain. During embryonic ages, the subplate does not solely contain subplate neurons, but is also contains glial cells, extracellular matrix, axons, and migrating neurons (Vasung et al., 2010); (Jantzie et al., 2014).

Subplate neurons are present across cortical regions, and the removal of subplate neurons in for example, the primary somatosensory cortex, disrupts the anatomical organization of the barrel field in layer 4 of the cortex, and weakens thalamocortical transmission (Tolner et al., 2012). Therefore, subplate neurons are needed for the correct wiring of the cerebral cortex over development (Kanold et al.,

2003; Kanold, 2009). Nevertheless there is still much investigation needed on understanding the synaptic inputs received by subplate neurons (SPNs).

Since subplate neurons help provide feedforward excitation to layer 4 from the thalamus, they have potential to influence synaptic plasticity at the thalamocortical synapse. Synaptic strengthening in the cortex is ruled by changes in synaptic scaling (Turrigiano, 1999). From this, subplate activity can influence strengthening of the thalamocortical synapses. Specifically, subplate input to layer 4 (L4) can strongly depolarize cells in L4 (Kanold, 2009; Zhao et al., 2009). Because SPNs are driven by thalamic activity, SP-mediated depolarization of L4 cells occurs at the same time as direct thalamocortical (TC) input to L4 which might lead to a strengthening of thalamocortical synapses. Subplate neurons help strengthen the thalamic innervation to layer 4 of the cortex. Over development, subplate neurons are required for the maturation of inhibitory GABAergic activity (Kanold and Shatz, 2006; Kanold, 2009).

1.1a) The role of subplate neurons in the maturation of inhibition in layer 4

The nature of whether the GABAergic activity is either inhibitory or excitatory depends on the chloride (Cl) reversal potential (E_{Cl}) (Blaesse et al., 2009). Specifically, the chloride reversal potential is mediated by KCC2 and NKCC1, which control cytosolic chloride levels (Shimizu-Okabe et al., 2002). Early in development, KCC2 levels are low (thus E_{Cl} is high), therefore GABA is depolarizing (Rivera et al., 1999; Ganguly et al., 2001; Kanold and Shatz, 2006; Blaesse et al., 2009; Kanold, 2009). NKCC1 is a transporter of sodium, potassium, and chloride, and it is involved

in chloride influx (Ganguly et al., 2001). The expression of NKCC1 is reduced within the same time window that KCC2 expression increases and therefore could suggest a mechanism for chloride influx reduction as chloride efflux is increased (Ganguly et al., 2001). Thus, depending on the amount of depolarization and the membrane potential of the cells, depolarizing GABA can turn GABAergic activity excitatory, or have a shunting inhibitory nature (Kanold and Shatz, 2006; Blaesse et al., 2009; Kanold, 2009). Therefore over development, as KCC2 expression levels increase (which decreases E_{Cl}), GABA becomes inhibitory (Rivera et al., 1999; Kanold and Shatz, 2006; Kanold, 2009).

In addition, glutamatergic activity early in development may be necessary for inhibitory GABAergic maturation of layer 4 neurons (Kanold and Shatz, 2006; Kanold, 2009). Thus GABAergic activity is also involved in the maturation of excitatory glutamatergic circuits. Over the course of development, glutamatergic synapses emerge and therefore depolarize neurons further. As glutamatergic synapses strengthen, and reach a critical threshold of depolarization, there is an upregulation in the expression level of KCC2 mentioned above (Rivera et al., 1999; Ganguly et al., 2001; Kanold and Shatz, 2006; Kanold, 2009). If one blocks glutamatergic activity early in development *in vivo*, then there is a prevention of the developmental increase of the level of KCC2 (Kanold and Shatz, 2006; Kanold, 2009). There are three sources for glutamatergic inputs to layer 4 of the cortex: thalamic, intracortical, and subplate neurons (Kanold, 2009). Thus removal of SPNs when inhibition is immature prevents the increase in KCC2 expression level (Ganguly et al., 2001; Kanold and Shatz, 2006; Kanold, 2009).

1.2) *Cortical development and the thalamus*

The mammalian cortex is comprised of six cortical layers, and over development there is the inclusion of the transient subplate layer in the developing cortical white matter. There is a computational advantage of having many cortical layers in that it allows for a greater degree of complex information processing (Harris and Shepherd, 2015). The fact that there is a general similarity of neocortical structure across the entire cerebrum suggests that there is a common circuit factor in cortical operation that allows for potential interlayer communication, circuit processing, and plasticity (Douglas and Martin, 2004; Harris and Shepherd, 2015).

For cortical development, cortical neurons are generated in the ventricular zone (VZ) which then make up the preplate, which becomes divided into the marginal zone (MZ) and the deep subplate (SP) (Aboitiz, 2009; Hoerder-Suabedissen and Molnar, 2012). The cells between these layers make up the cortical plate (CP) (Aboitiz, 2009; Hoerder-Suabedissen and Molnar, 2012). The subplate is a transient population of neurons from the developing cortical white matter that help secure the connection between the thalamus and the cortex. Layer 5 and lesser layer 6 contain pyramidal neurons whose axons leave the cortex. The smaller pyramidal neurons are in layers 2 and 3 (the supragranular layer), which have primarily corticocortical connections, while the marginal zone (layer 1) contains mostly neuropil (Purves, 2008). Cortical layers are generated in an inside-out fashion in which the earlier produced neurons are located above the later producing ones. Inhibitory interneurons are generated from the ganglionic eminence, and migrate tangentially within the subplate and marginal zone (Hoerder-Suabedissen and Molnar, 2015). The

implication being that later produced neurons have to cross the layers of early-produced neurons, therefore this allows for modification of cortical processing and possible activation of homeostatic mechanisms in order to conserve the functioning of smaller circuits across a wider range of cortical processing and complex integration.

Neural circuits are vulnerable to destabilization by changes in synaptic strengths through changes in synaptic scaling. However this does not just pertain to cortical processing, but also thalamocortical communication and integration of circuit processing. Thalamic inputs enter into cortical layer 4 through the subplate, but the thalamic terminals are the minority of inputs on layer 4 neurons. Therefore an issue arises as to how the thalamus reliably drives layer 4 neurons.

Generally, subplate neurons are first to receive input from the thalamus and project up to L4 (Friauf and Shatz, 1991; Allendoerfer and Shatz, 1994; Hanganu et al., 2002; Zhao et al., 2009). From L4, feedforward connections project up to L2/3 where there are lateral connections within L2/3. After about a week in development, feedback connections return from L2/3 to L5/6 and ultimately the subplate (Viswanathan et al., 2012) (Fig. 1.1).

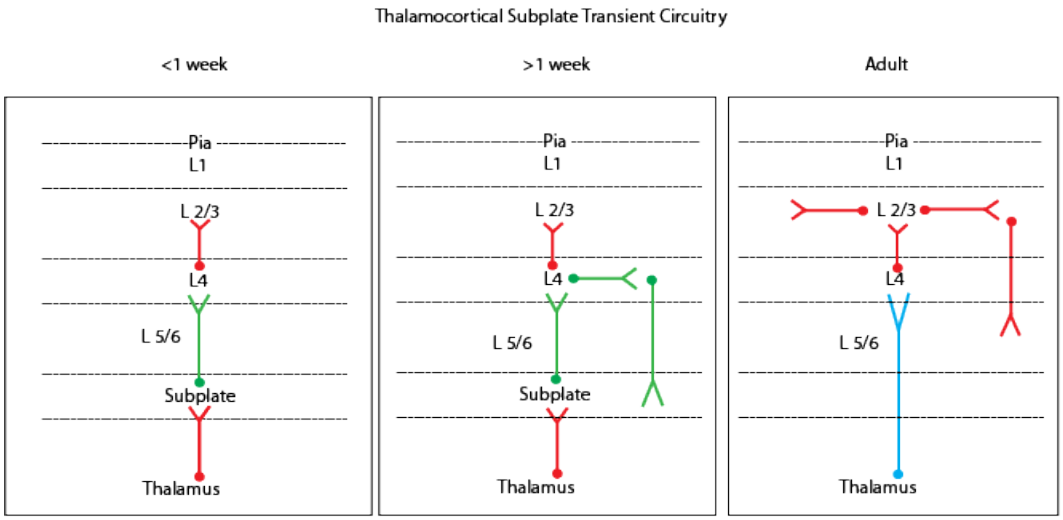

Figure 1.1: Thalamocortical Subplate Transient Circuitry. Feed-forward neural connections start from thalamus and project toward layer 4 via the subplate (green). As the cortex matures, the subplate neurons die off and connections between the thalamus and layer 4 become secure (blue). There are also lateral connections across cortical columns within layer 2/3 and these project back toward layer 5/6 (Viswanathan et al., 2012).

1.2a) Primary somatosensory cortex and the thalamus

Subplate neurons (SPNs) are among the first born cortical neurons in mammals (Luskin and Shatz, 1985; Valverde and Facal-Valverde, 1987; Kostovic and Rakic, 1990; Allendoerfer and Shatz, 1994; Kanold and Luhmann, 2010) and a subset of these SPNs reside among adult layer 6b (Viswanathan et al., 2016). SPNs are crucial in the establishment and functional maturation of thalamocortical circuits, including the whisker barrels of rodent S1 (Tolner et al., 2012). Within L4 of S1, thalamic afferents separate into barrels and are separate by spaces between barrels referred to as septa (Agmon et al., 1995;Viswanathan et al., 2016). Primary somatosensory cortex (S1) receives thalamic projections through three distinct pathways which originate at the whisker follicle and are relayed by the trigeminal

ganglion for encoding different stimulus properties (Koralek et al., 1988; Lu and Lin, 1993; Bureau et al., 2006; Urbain and Deschenes, 2007; Diamond et al., 2008; Meyer et al., 2010; Wimmer et al., 2010; Viswanathan et al., 2016). The lemniscal pathway, through the trigeminal ganglion, passes through the dorsomedial section of the thalamic ventral posterior medial nucleus (VPMdm) and then projects to the barrels of L4 (Hoogland et al., 1987; Pierret et al., 2000; Haidarliu and Ahissar, 2001; Varga et al., 2002; Land and Erickson, 2005; Viswanathan et al., 2016). However another pathway, the extra-lemniscal pathway, passes through the ventrolateral VPM (VPMvl) and projects to the septa between the barrels of secondary somatosensory cortex (S2) (Pierret et al., 2000; Bokor et al., 2008; Viswanathan et al., 2016). A third pathway, the paralemniscal pathway, passes through the POm and projects to layer 5a of S1 and S2 (Herkenham, 1980; Chmielowska et al., 1989; Lu and Lin, 1993; Bureau et al., 2006; Wimmer et al., 2010). Complexin-3 protein (Cplx-3) is expressed in the subplate of all cortical areas in around P7 and P21, with very few neurons labeled in the cortical plate (Viswanathan et al., 2016). Complexin-3 is a member of the complexin family, which regulates neurotransmitter release through the SNARE complex machinery (Hu et al., 2002; Xue et al., 2008; Vaithianathan et al., 2015). Complexin-3 was primarily functionally characterized in the retina, and is involved in ribbon bipolar synapses. Knock-out desynchronization of vesicle release leads to malformation of ribbon synapses and worsened the ability of sight for mice (Reim et al., 2005; Reim et al., 2009; Viswanathan et al., 2016). In the cortex paralemniscal pathway, the presence of complexin-3 is thought to encode for dynamic whisker information and this is consistent with synaptic specialization for temporal processing

(Diamond et al., 2008; Viswanathan et al., 2016). Therefore it is possible that complexin-3 early in development is functionally relevant and may aid in thalamocortical and corticothalamic circuit maturation(Viswanathan et al., 2016). Complexin-3-expressing SPN axons project to thalamorecipient layers L4, L5a, and L1 (Viswanathan et al., 2016). However by the second postnatal week, the L4 projections are biased towards the septa between the barrels (Viswanathan et al., 2016).

In previous work, we found that S1 complexin-3-SPNs targets localize with eventual projections of the medial posterior thalamic nucleus (POm) (Viswanathan et al., 2016). Thus while SPNs project to cortex, they also project long-distance axons back to the thalamus (Viswanathan et al., 2016). Therefore complexin-3-SPNs/L6b neurons are involved with the paralemniscal pathways and can possibly directly link corticothalamic and thalamocortical circuits (Viswanathan et al., 2016). Thus Cplx3-SPNs in the whisker barrel cortex project to regions (septa) and layers in barrel cortex which receive paralemniscal input after P8, and SPNs project back to the thalamus (Viswanathan et al., 2016). Therefore SPNs are in the optimal position to provide feedforward and feedback connections to connect the POm of the thalamus and its cortical projections (Viswanathan et al., 2016).

1.2b) Primary auditory cortex and the thalamus

SPNs have complex dendritic trees that integrate local inhibitory inputs and excitatory input from the medial geniculate nucleus (MG) of the thalamus and (Kanold and Shatz, 2006; Zhao et al., 2009; Viswanathan et al., 2012; Polley et al.,

2013; Meng et al., 2014). Specifically, there are two classes of SPNs: the first class which receives input form deep cortical layers only and the second class which receives inputs from deep and superficial layers including layer 4 (Viswanathan et al., 2012). Additionally, the superficial cortical input to SPNs emerges in the second postnatal week (Viswanathan et al., 2012). SPN axon terminals branch out extensively in the same layers of the cortex that receive the majority of direct axonal input from the MG of the thalamus (Kanold and Luhmann, 2010). MG axons innervate the subplate before birth and wait there before innervating middle cortical layers (Kanold and Luhmann, 2010; Polley et al., 2013). During the waiting period, SPNs make excitatory projections to excitatory and inhibitory neuron subtypes within auditory cortex (Luskin and Shatz, 1985; Ghosh and Shatz, 1993; Kanold and Luhmann, 2010; Polley et al., 2013). The auditory cortex has a rostral-caudal gradient of frequencies where the rostral end responds to higher frequencies and the caudal end responds to lower frequencies (Stiebler et al., 1997; Hackett et al., 2011). On a global scale, the auditory cortex has organized tonotopy but on a smaller scale in L2/3, there is heterogeneity and lack of an organized tonotopic gradient (Winkowski and Kanold, 2013).

1.3) *Hypoxia-Ischemia and abnormal brain development*

Normal embryonic brain development requires the proper maturation of neural circuits, which leads to normal cognitive functioning. While in-utero, the embryo is very vulnerable to injuries and insults that have potential to cause long-term health problems and disorders such as cerebral palsy and epilepsy (Jantzie et al.,

2014). The most common cause of many pediatric neurological disorders that is very costly to society is perinatal hypoxia-ischemia (HI). Hypoxia-Ischemia is a disorder in which the preterm infant undergoes a lack of oxygen and blood flow to the brain. Specifically, injury to the premature white matter of the brain results in disruption of the normal maturation of the brain and consequently increases risk of developing cerebral palsy and epilepsy in infants. According to the American Family Physician as of 2011, there are more than 4 million infants born a year that need breathing assistance at the time of birth and about 0.2-0.3% of this population end up developing moderate to severe HI (Raghuveer and Cox, 2011). Using a rodent stroke model of hypoxia-ischemia (HI), one can induce selective injury to developing neurons in the subcortical white matter region of the brain, the subplate neurons (McQuillen et al., 2003). Lesion studies, including those from our laboratory (Kanold et al., 2003; Kanold and Shatz, 2006; Tolner et al., 2012), have shown that subplate neurons are necessary for proper development of the cerebral cortex. Hypoxia-Ischemia results in brain damage that suggests that there are differences between developing brain and mature brain pathology. While HI causes brain damage selective to different brain structures over development, HI in the preterm human results in damage to the subcortical developing white matter, a condition referred to as periventricular leukomalacia (PVL) (Ferriero, 2004). Therefore, while it is clear that subplate neurons play a major role in the maturation of the developing circuitry of the brain, the mechanism by which damage to the subplate (SP) leads to altered development is unclear. Therefore understanding mechanisms that underlie hypoxia-ischemia brain injury and other abnormal brain injuries in the developing brain of

neonates is important for establishing more effective treatments for neurodevelopmental disorders.

1.4) Gestational to postnatal development of subplate neurons, and translation to humans

At around embryonic day 13 in rodents, axons begin to grow out of the thalamus and meet subplate axons coming from the preplate (Fig. 1.2) (Hoerder-Suabedissen and Molnar, 2015). A couple days later, the density of thalamocortical axons increases in the subplate region and inhibitory GABAergic interneurons start to migrate within the subplate (Fig. 1.2B) (Hoerder-Suabedissen and Molnar, 2015). At around embryonic day 18, the thalamocortical axons begin to enter the cortical plate for glutamatergic signaling (Fig. 1.2C) (Hoerder-Suabedissen and Molnar, 2015). At around postnatal day (P) 0, the thalamocortical axons reach cortical layer 4 and being to grow neurites to form a circuit involving the subplate and layer 4 for primary somatosensory cortex (Fig. 1.2E). At this time, subplate neurons start to undergo cell apoptosis and a portion of subplate neurons die off. Therefore, subplate neurons are a part of a transient developmental circuitry helping to establish secure connections between the thalamus and layer 4 of the cortex.

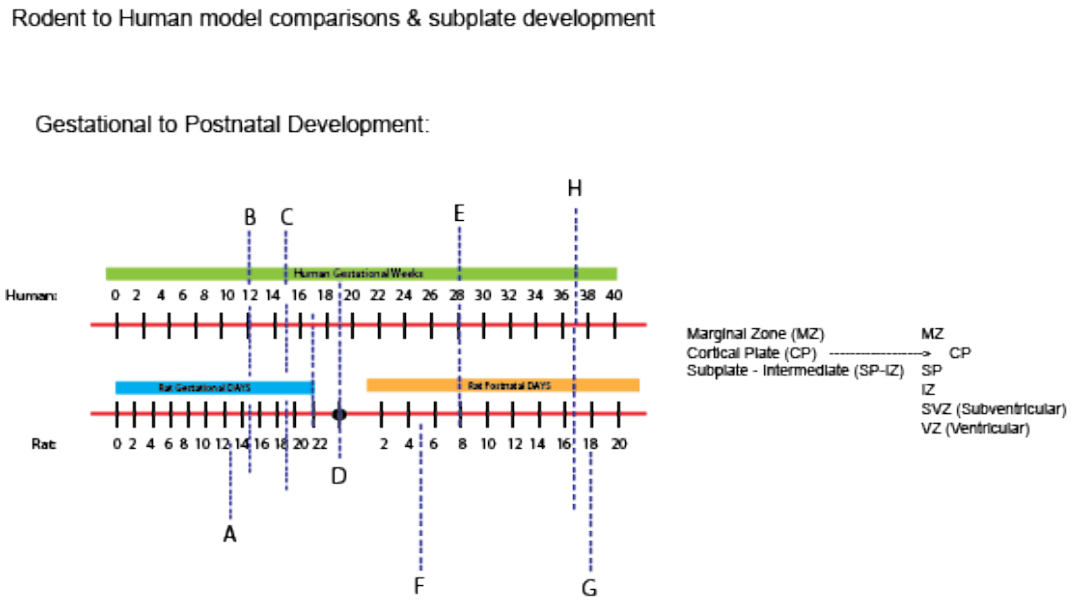

Figure 1.2: Comparison on human and rat brain development in terms of gestational and postnatal ages. Timelines comparing human gestational weeks to rat gestational days and rat postnatal days. Human gestational period is 40 weeks, whereas rat gestational period is about 22 days (Howdeshell, 2002).

In humans, SPNs make up about half of the cortical neurons in the second trimester and are present in the first few years of life (Luskin and Shatz, 1985; Valverde and Facal-Valverde, 1987; Kostovic and Rakic, 1990; Allendoerfer and Shatz, 1994; Kostovic et al., 2002; Kanold, 2009). For humans, the subplate is most prevalent at about 25 gestational weeks (GW) and begins to diminish and die off by about 6 months postnatal (Jantzie et al., 2014). Thalamocortical development in humans begins at around 25 GW, and in rodents the thalamocortical afferents of somatosensory cortex reaches the cortex at around P0 and innervate layer 4 shortly thereafter (McQuillen et al., 2003). For purposes of translational research into human

models, it is important to remember that P0 in the rat is about 20 GW in the human (Howdeshell, 2002). The critical period for brain development in rodents begins around P8 and this is comparable to 28 GW in humans (Howdeshell, 2002). In humans, SPNs make up about half of the cortical neurons in the second trimester (Luskin and Shatz, 1985; Valverde and Facal-Valverde, 1987; Kostovic and Rakic, 1990; Allendoerfer and Shatz, 1994; Kostovic et al., 2002; Kanold, 2009; Jantzie et al., 2014). This is around the time where premature infants are vulnerable to central nervous system injuries from late gestation, and other neonatal complications (Volpe, 1996) (Jantzie et al., 2014).

1.5) Homeostatic plasticity

There is a strong relation between excitation and inhibition in a form of a ratio referred to as the excitation-inhibition balance (E-I balance), which results in the proportionality of these two feedback signals. This proportionality can result in a fairly stable *network* in which large swings in neuronal activity such as seizures, are prevented.

Homeostatic mechanisms are activated on both local and global levels in order to help maintain this E-I balance on a network level. Networks and neurons use a combination of "homeostatic synaptic plasticity mechanisms to stabilize firing rates" during "developmental or learning-induced changes" in synaptic drive (Turrigiano, 2012). Overall, this contributes to the ability of central neuronal networks to maintain stable functioning, and at the same time maintain specificity of synaptic changes that encode information (Turrigiano, 2012).

On a network level, the activation of homeostatic synaptic plasticity can induce a network-wide adjustment that can help maintain the balance between excitation and inhibition. Homeostatic synaptic plasticity differs from Hebbian plasticity by the way that all of the neurons' excitatory synapses are scaled up or down proportionally, by the same multiplicative factor (Turrigiano, 1999; Turrigiano, 2011). This multiplicative scaling of synaptic strengths has the appropriate characteristics for allowing the preservation of relative differences between inputs, while allowing the neuron to adjust to the total amount of synaptic excitation it receives (Hensch and Fagiolini, 2004). Therefore cortical networks adapt to altered drive by scaling the strength of all excitatory connections onto excitatory cells up or down as a function of how active they are (Turrigiano and Nelson, 2004).

In cortical networks, there is a multitude of complex recurrent networks such as from subplate to layer 4 and back down to subplate. From this, homeostatic synaptic plasticity needs to function in order to independently adjust excitatory and inhibitory feedback loops within these recurrent networks for the preservation of activity, despite changes in synaptic drives. For example, when activity decreases too low, such as when sensory drive is reduced, excitation between pyramidal neurons is boosted, while feedback inhibition is reduced (Hensch and Fagiolini, 2004). However this action cannot cause such a global effect because cortical interneurons are very heterogeneous, therefore a network-wide reduction in inhibition would then have different consequences than selective changes for cortical functioning.

On a global level, raising network-wide firing rates activates a multitude of calcium-dependent signaling pathways, each with elements that are needed for the

expression of scaling down. However these calcium signals tend to converge at some point in the scaling pathway in order to coordinately regulate the important step in synaptic AMPA receptor reduction (Turrigiano and Nelson, 2004). Mechanistically, the cell-autonomous induced synaptic scaling operates over a long temporal scale of hours, a more global spatial scale, and uses distinct trafficking steps to enhance or reduce synaptic accumulation of glutamatergic-containing AMPA receptors onto most neurons (Turrigiano, 2011).

As there are network-wide adjustments, homeostatic synaptic plasticity needs to adjust in manner that maintains the network's set point of optimal functioning. Therefore, there is a relationship between increasing synaptic drive and the resultant increase in firing rate that is constrained. Essentially, if synaptic drive increases too much and the firing rates rise, all excitatory synaptic strengths are decreased until firing rates begin to fall again (Hensch and Fagiolini, 2004). Therefore these distinct plasticity rules operating on different classes of inhibitory and excitatory synapses should be consistent with the homeostatic shift in the E-I balance. Thus the net effect of changes induced by blocking of activity act to reduce inhibition, and enhance excitation to produce the restoration of stable network excitability. Ultimately, synaptic scaling acts to adjust the gain of the input, rather than the gain of the output, in order to reciprocally change excitation and inhibition, which in turn alters the E-I balance (Turrigiano and Nelson, 2004).

In contrast to the synaptic scaling mentioned, intrinsic homeostasis, in which changes in intrinsic excitability can alter a neuron's input/output function, acts to affect a network's behavior overall (Turrigiano, 2011). Changes in intrinsic plasticity

have been demonstrated in invertebrate central pattern generators. Here, neurons can compensate intrinsically for changes in modulatory drive and maintain their ability to fire in bursts (Turrigiano, 2011). Therefore intrinsic excitability alters the contribution of a neuron to large circuit formation without changing synaptic currents, however the functional effects of this type of modulation depend on how this excitability is modified. For example, if intrinsic plasticity affects the slope of the neuron input/output function without affecting threshold, then the neuron becomes sensitive to both excitation and inhibition, and this type of gain control will not involve changes in the E-I ratio (Turrigiano, 2011). However if the input/output function is modified to regulate excitability and modify firing threshold, then the relative effectiveness of excitation to inhibition may be altered by intrinsic plasticity (Turrigiano, 2011).

All in all, networks use a complex mix of synaptic and intrinsic mechanisms to optimize their function or adapt to a changing environment. Thus one must understand these rules behind network homeostasis in order to better understand diseases involving E-I imbalance such as epilepsy, autism, and schizophrenia.

Chapter 2: Methods

2.1) Animals:

Time pregnant Sprague Dawley rats were obtained from Charles River. Time of birth was marked P0 (±0.5 day).

2.2) Surgical methods for Subplate ablations:

At P0-1 (within 36 hours after the time of birth), animals were anesthetized with isoflurane and maintained at 1-1.5% during surgery. Body temperature was kept constant using a heating pad set at 35 °C. Small craniotomies were made overlying the primary somatosensory (S1) cortex (limb region: 0.5 posterior to 0.5 mm anterior from bregma; 1.7-2.3 mm from midline; barrel region: 0.4 to 0.8 mm posterior from bregma; 2.65-2.85 mm from midline) using a needle. Stereotaxic coordinates were confirmed histologically for the barrel region and electrophysiologically for the S1 limb region (see below and Results). Anti-rat p75-immunotoxin (192-IgG-saporin, MAB390, Chemicon; 400 nl, 1 μg/μl) or control toxin (anti-mouse p75-saporin 'mu-toxin', or IgG-saporin 'blank toxin'; both from Advanced Targeting Systems; 1 μg/μl) were dissolved in sterile physiological saline or 0.9% NaCl. The selectivity of p75-immunotoxin for SPNs is based on the expression of the p75 neurotrophin receptor, which is localized to subplate neurons (SPN) in rats at P0-1 (see fig.1A and also (Koh and Loy, 1989). There are many potential caveats related to injections into neonates, thus our primary controls were anti-mouse p75-saporin and IgG-saporin injections. However, we also examined non-injected animals and vehicle injected animals to gain insight into the potential sources of variability in the responses studied.

Toxin solutions or vehicle (physiological saline) were injected using a glass pipette (tip diameter 8-15 μm). The specificity of the p75 antibody (192-IgG) to the subplate in P0-1 rats was confirmed by immunostaining (Fig.1A). Fluorescent microspheres (Lumafluor Inc; 5-10% by volume) were coinjected for visualization of injection

sites. Multiple injections (2 for limb area, 3-5 for barrel area) distributed over an area within 1 mm were performed at ~300-700 μm depth. Littermates were sham-operated. After recovery in a warm (35 ºC) environment together with a sham-operated animal, pups were placed back into their nests. All pups survived the procedure and were monitored daily for weight, feeding and general behavior. After SPN removal, freely behaving animals showed normal sleep-wake cycles similar to those in non-injected control and toxin control rats (Fig. 3.1E).

Injection locations were validated (Fig. 3.1) by the coinjected fluorescent beads, and were localized at the level of the subplate and at the edge with the underlying white matter in the S1 cortex hindlimb/forelimb area. Loss of SPNs was evident near the injection sites in an area of approximately 0.75-1.5 mm width rostro-caudally and medio-laterally, while no neuronal loss was observed in overlaying cortical layers and in adjacent cortical areas. Control toxin (mu-toxin, n=4 or blank toxin, n=8) or vehicle injections (n=4) in the subplate did not cause observable SPN damage. Apart from the trajectory of the glass electrode used for injections or the electrode track from recordings, no further damage was observed within the cortex of toxin or vehicle-injected animals. Anti-rat p75-toxin and control toxin injections in overlaying cortical layers that did not reach the subplate (n=2 anti-rat p75-toxin, n=4 blank toxin) did not result in visible neuronal damage. In recordings from these animals, EEG signals appeared similar to those of non-injected controls.

A total of 149 rat pups from 57 litters were used in this study. Typically multiple animals in each litter were used for each experimental group and multiple litters were used for each experimental group. 22 litters were used for EEG studies.

30 litters were used for barrel cortex and thalamic histology. Since only one hemisphere was injected, we used the other hemisphere as within animal control. 5 litters were used for in vitro physiology.

2.3) In vitro slice preparation and solutions for electrophysiology of somatosensory cortex neurons:

Brains were sliced in thalamocortical orientation as prepared in previous publication (Zhao et al., 2009; Viswanathan et al., 2012). All procedures were approved by the University of Maryland Institutional Animal Care and Use Committee. Rats of both sexes were used and deeply anesthetized with isoflurane before decapitation and brain removal. Acute 500 um thalamocortical slices were prepared using a vibrating microtome (Leica) in ice-cold artificial cerebral spinal fluid (ACSF). ACSF consisted of (in mM): 130 NaCl, 3 KCl, 1.25 NaH_2PO_4, 20 $NaHCO_3$, 10 glucose, 1.3 $MgSO_4$, 2.5 CaCl, pH 7.35-7.4, equilibrated with 95% O_2-5% CO_2. The slices were incubated in ACSF for 1 hour at 30°C and then kept at room temperature.

2.4) Identification of layer 4 and subplate:

Layer 4 was identified with Nissl staining and in in vitro slices, being about less than 50% the width from pia to ventricle. Layer 4 is the granular layer between Layer 2/3 and Layer 5/6. Layer 4 boundaries are visible when the high density of large pyramidal cells decreases significantly (for lower L2/3, upper L4 boundary), and when the density of large pyramidal cells increases again in L5/6 (for lower L4, upper L5/6 boundary). Subplate was identified as a relatively cell sparse area between the

large layer 6 pyramidal cells and the ventricular zone was identified as the subplate zone (Viswanathan et al., 2012).

2.5) Electrophysiology for intrinsic properties of somatosensory cortex neurons:

Whole-cell recordings were performed with a patch-clamp amplifier as done in our previous publication (Tolner et al., 2012). Rat pups were deeply anesthetized with isoflurane (Halocarbon). A block of brain containing S1 and the thalamus was removed and thalamocortical slices (500 μm thick; (Agmon and Connors, 1991) were cut on a vibrating microtome (Leica) in ice-cold physiological solution containing (in mM): 130 NaCl, 3 KCl, 1.25 KH_2PO_4, 20 $NaHCO_3$, 10 glucose, 1.3 $MgSO_4$, 2.5 $CaCl_2$ (pH 7.35-7.4, in 95%O_2-5%CO_2). Slices were incubated for 1 hour at 30°C and then kept at room temperature. For recording, slices were held in a chamber on a fixed stage microscope (Nikon FN1) and superfused (2-4 ml/min) with 127 NaCl, 3 KCl, 1.25 KH_2PO_4, 20 $NaHCO_3$, 10 glucose, 4.5 $MgSO_4$, 2.5 $CaCl_2$ (pH 7.35-7.4, in 95%O_2-5%CO_2) at room temperature to reduce spontaneous activity in the slice. The location of the recording site in S1 was identified by appearance of barrels under DIC. Whole-cell recordings were performed with a patch clamp amplifier (Multiclamp 700B, Axon Instruments, CA) using pipettes with input resistance of 4-8 MΩ. Data were acquired with a Digidata AD board (Axon Instruments) under pClamp (v9 and v10) and analyzed offline using MATLAB (Mathworks, MA). Electrodes were filled with (in mM) 110 K-gluconate, 4 KCl, 4 NaCl, 0.2 $CaCl_2$, 10 HEPES, 1.1 EGTA, 2 Mg-ATP, 1 $MgCl_2$ and 5 glutathione (pH 7.2, 300 mOsm) for spiking patterns or with (in mM) 115 cesium methanesulfonate ($CsCH_3SO_3$), 5 NaF,

10 EGTA, 10 HEPES, 15 CsCl, 3.5 MgATP, 3 QX-314 (pH 7.25, 300 mOsm) for EPSC measurements. Biocytin or Neurobiotin (0.5%) was added to the electrode solution as needed. Membrane voltages were corrected for an estimated liquid junction potential of 14 or 10 mV respectively. For electrical stimulation we use a bipolar electrode (Microprobe, MD, biphasic, 0.2 ms, at 0.03 Hz) coupled to a stimulus isolator (Cygnus). The electrode was placed into the thalamocortical projections at a position that maximized the EPSC for each cell.

2.6) Histology of flattened barrel cortex and cytochrome oxidase staining:

Rat pups were perfused as described above and the two hemispheres were postfixed for 2h between 2 glass coverslips (spaced 1500 μm) to flatten the cortex. After cryoprotection 50 μm horizontal slices were cut on a freezing microtome or cryostat spanning the entire range of the cortex. Slices were incubated at 37 ºC with 20 mg diaminobenzidine (DAB), 25.0 mg cytochrome C (from horse heart, Sigma-Aldrich), 2.0 g solid sucrose in 50.0 ml PBS for 30-45min, washed 1x in PBS, dehydrated, mounted and coverslipped. Pictures were taken from multiple sections (up to 6) covering the entire depth extent of the barrel field. The presence of each barrel in each hemisphere was confirmed by aligning and merging the images using Photoshop (CS5, Adobe; see Fig. 3.5). The location of the injection site was determined from fluorescent beads contained in sections through the white matter or from evidence of the pipette track. Due to the number of washes and incubation steps, beads were not detectable in all sections. The presence of the full barrel pattern in different animals was performed qualitatively by judging on a scale from 0 to 4 the presence of a

complete barrel field. Scores of 0 indicated the presence of complete barrel field while scores of 1-4 indicated small (1, indicating a change in barrel shape), mild (2, indicating some missing barrels), medium (3, indicating missing rows or columns), or large (4, missing large parts) disruptions of the barrel field respectively. For judgment we used 4 independent observers blind to manipulation and animal ID. The scores of the observers for each animal were averaged.

2.7) Hypoxia-Ischemia surgery:

Sprague-Dawley pups postnatal day (P) 1-2 were anesthetized with 2-4% isoflurane for the Rice-Vannucci procedure (McQuillen et al., 2003; Failor et al., 2010; Ranasinghe et al., 2015). A small incision was made in the midline of the neck just above the sternal notch. The common carotid artery (CCA) was exposed and coagulated. Care was taken to not damage the sympathetic ganglion chain in order to avoid Horner's Syndrome, which results in a squinty-eye phenotype in animals. To induce either Mild HI or Moderate HI (Mod HI), different surgical techniques were used to cause ischemia. Cauterization of the CCA was done to cause temporary ischemia (Mild HI), or one suture was tied to ligate the CCA for a more severe ischemia (Mod HI). Sham surgeries exposing the CCA were performed as a control.

After ischemia surgery recovery, the pups were returned to the dam in normal room air for two hours. Following recovery, the pups were placed in humidified chambers at 34 degrees Celsius and exposed to 5% oxygen, balanced nitrogen for 2-3 hours and then returned to the dam. During hypoxia, one pup from each litter was monitored for skin temperature. Skin temperature was kept constant at 35 degrees

Celsius. Water bath temperature was kept constant at around 36 degrees Celsius. One of the chambers was modified to record the oxygen concentration in the chamber. The oxygen monitoring device, UV Flux 25% Oxygen Sensor Module (CM-0201, co2meter.com), embedded and sealed into one of the chambers, and connected to a computer where the oxygen concentration was recorded by GasLab® software. Pups were exposed to constant 5% oxygen during the entire duration of the hypoxia procedure. Surviving pups were removed if the total mortality rate for the entire litter reached on average 30-50%. None of the chambers were opened until the end of the hypoxia procedure, which is reflected in the graph of oxygen concentration returning to about room air 21% oxygen (Fig. 2.2). Metal chamber bases and a metal plate covering the bottom of the inside of the tank, with a larger water tank allowed for more stable heat distribution across all chambers. Chambers and tank were made of Lexan and manufactured at the UMD Physics Shop.

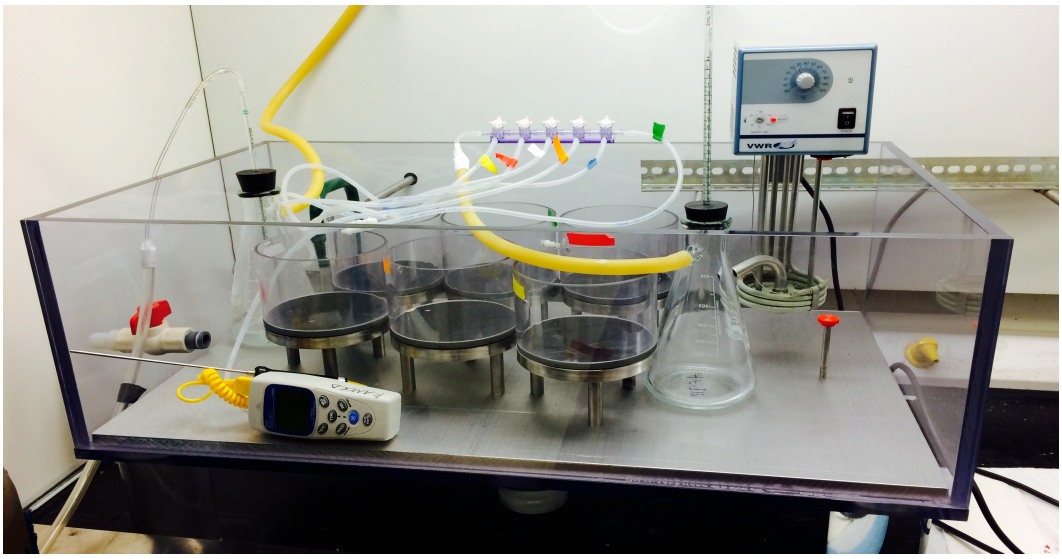

Figure 2.1: Hypoxia chamber setup. One of the chambers was modified to record the oxygen concentration in the chamber. The oxygen monitoring device, UV Flux 25% Oxygen Sensor Module (CM-0201) was supplied by co2meter.com, embedded and sealed into the chamber, and connected to a computer where the oxygen concentration was recorded by GasLab® software. Pups were exposed to a constant 5% oxygen during the entire duration of the hypoxia procedure. Metal bases and a metal plate, with a larger water tank allowed for more stable heat distribution across all chambers. Chamber was made of Lexan and manufactured at the UMD Physics Shop.

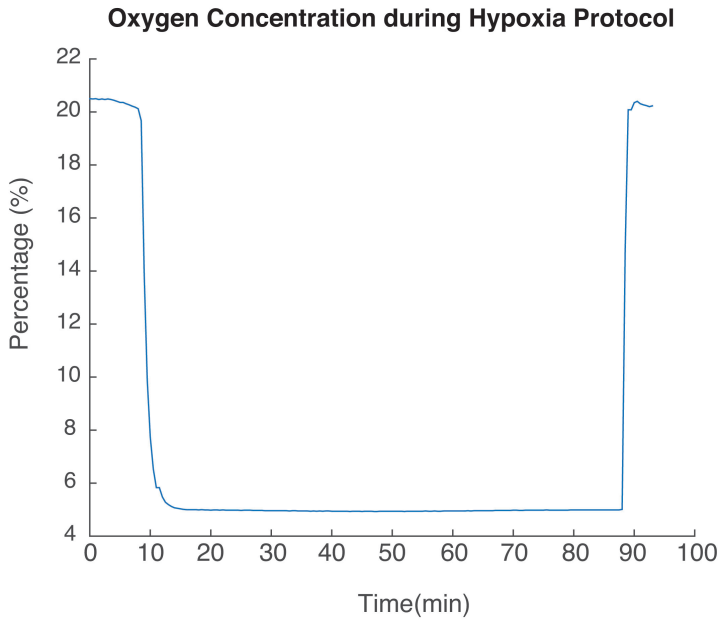

Figure 2.2: Oxygen percentage during hypoxia procedure. Oxygen concentration for the entire duration of the hypoxia exposure was consistent at 5% oxygen.

2.8) Slice preparation and solutions for auditory cortex neurons:

Thalamocortical brain slices were prepared as previously described (Zhao et al., 2009; Viswanathan et al., 2012; Meng et al., 2014). All procedures were approved by the University of Maryland Institutional Animal Care and Use Committee. Rats of either sex from were used. Rats were deeply anesthetized with isoflurane prior to decapitation and removal of the brain. Acute thalamocortical slices (500 μm) were prepared using a vibrating microtome (Leica) in ice-cold artificial cerebral spinal fluid (ACSF) consisting of (in mM): 130 NaCl, 3 KCl, 1.25 NaH_2PO_4, 20 $NaHCO_3$, 10 glucose, 1.3 $MgSO_4$, 2.5 CaCl, pH 7.35-7.4, equilibrated with 95% O_2-5% CO_2. The slices were incubated in ACSF for 1 hour at 30°C and then kept at room temperature.

2.9) Laser-scanning photostimulation (LSPS):

LSPS was performed as previously described (Viswanathan et al., 2012; Meng et al., 2014). 0.5-1mM caged glutamate (Ncm-Glu [*N*-(6-nitro-7-coumarylmethyl-L-glutamate]) (Kao, 2006; Muralidharan et al., 2016) was added to the ACSF. We typically stimulated an array of up to 30×30 sites with 40 μm spacing to enable us to probe areas of ~1mm x 1mm. Stimuli were applied at 1 Hz. Laser power (<25mW) was adjusted to achieve reliable neuron activation and repeatable maps. The same settings were used through all experiments. To detect monosynaptically evoked EPSCs, we measured peak EPSC amplitudes in a 50 ms time window after the stimulation. AMPAR-mediated responses were recorded by holding cells at -70mV, while GABA-mediated responses were recorded at a 0 mV holding potential. Traces containing a short-latency response (about 8 ms) were considered to reflect direct activation of receptors on the patched cell and were discarded from the analysis. Traces with latencies longer than 50 ms were discarded due to potential involvement of polysynaptic components. Analysis was performed essentially as previously described with custom software written in MATLAB (Meng et al., 2014). Layer boundaries were determined from infrared images as previously described (Meng et al., 2014).

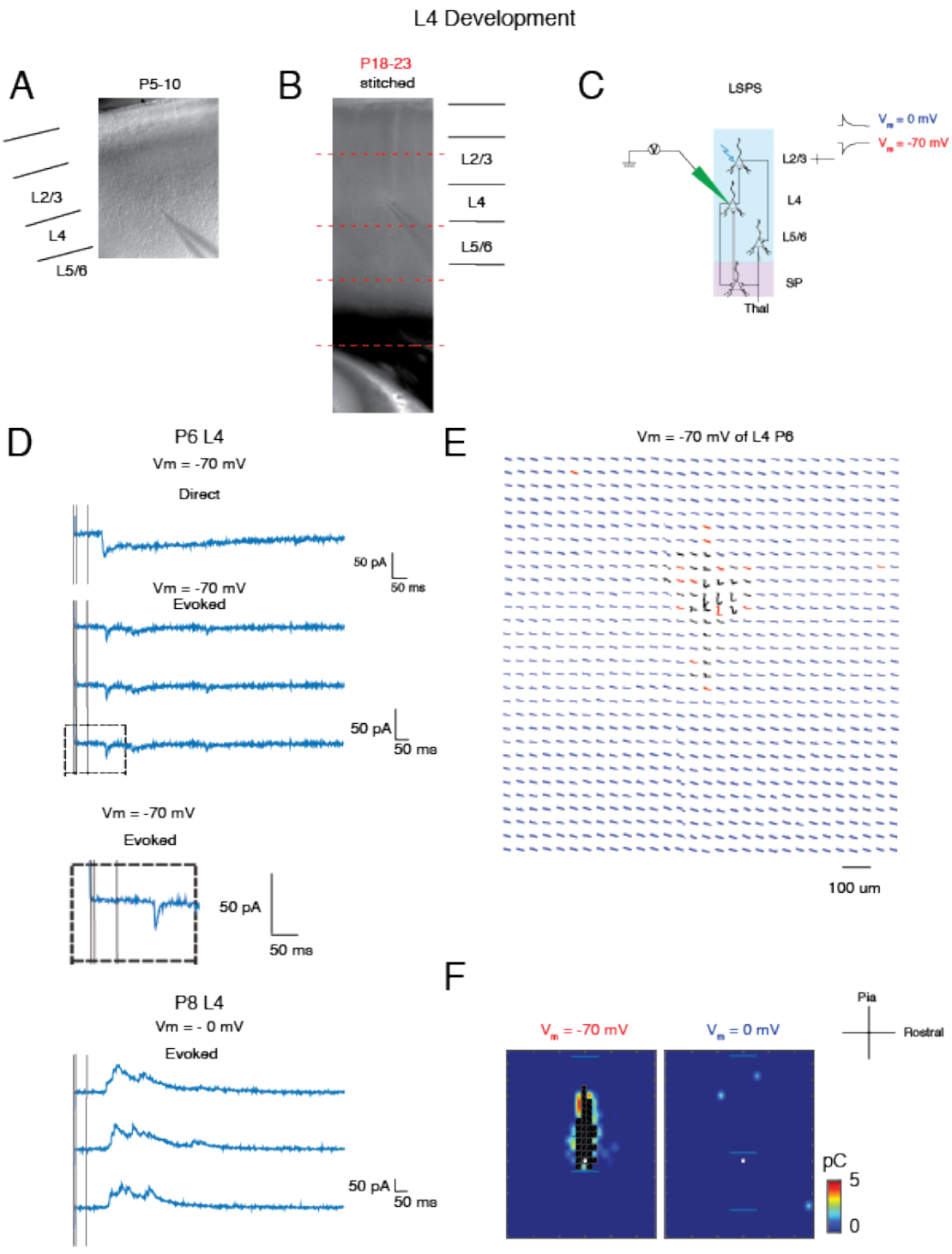
L4 Development
A
P5-10
L2/3
L4
L5/6
B
P18-23
stitched
L2/3
L4
L5/6
C
LSPS
Vm = 0 mV
Vm = -70 mV
L2/3
L4
L5/6
SP
Thal
D
P6 L4
Vm = -70 mV
Direct
50 pA
50 ms
Vm = -70 mV
Evoked
50 pA
50 ms
Vm = -70 mV
Evoked
50 pA
50 ms
P8 L4
Vm = - 0 mV
Evoked
50 pA
50 ms
E
Vm = -70 mV of L4 P6
100 um
F
Vm = -70 mV
Vm = 0 mV
Pia
Rostral
pC
5
0

Figure 2.3: LSPS and mapping method of intracortical connections over development of layer 4 neurons. A. Infrared DIC image of a thalamocortical brain slice of a P5-10 rat with a patch pipette on a layer 4 neuron. **B.** Infrared DIC image of a thalamocortical brain slice of a P18-23 rat with a patch pipette on a layer 4 neuron. Because the 10X magnification field of view was smaller than the entire brain slice, multiple images were taken along the entire cortical extent into the hippocampal region in order to show the location of the pipette along the rostral-caudal axis with respect to the hippocampus. **C.** Reference view of electrode positioning in the layer recorded and example laser photostimulation location (photostimulation from pia to L4- see methods for more details). **D.** Whole-cell voltage clamp recordings at holding potentials of -70 mV (top) and 0 mV (bottom) of a P6 L4 neuron distinguish between photostimulation-evoked excitatory and inhibitory currents. Shown are example traces obtained with photostimulation at different locations. The solid black lines on the blue traces indicate the time of the photostimulation; far left marks time 0 ms, next to it marks 8-ms, and left of that marks 50-ms post stimulus. 8 ms is the minimum latency for synaptic responses, and 50 ms marks the end of the analysis window. **E.** These are traces obtained by LSPS when hold one P6 L4 neuron at -70 mV. Traces in black show large-amplitude direct responses. Postsynaptic responses from 8 to 50 ms are the red traces, and the rest of the traces are in blue. **F.** Pseudocolor maps of a P6 L4 neuron show postsynaptic current (PSC) charge at each stimulus location for 1 example layer 4 neuron. Direct responses in black were set to zero pC. The white filled circle indicates the location of the soma and the horizontal bars indicate the layer boundaries and serve as scale bars of 200 μm.

2.10) LSPS synaptic electrophysiology of auditory cortex neurons:

Whole-cell recordings were performed with a patch-clamp amplifier (Multiclamp 700B; Molecular Devices). Electrodes were filled with (in mM): 115 cesium methanesulfonate ($CsCH_3SO_3$), 5 NaF, 10 EGTA, 15 CsCl, 3.5 MgATP, 3 QX-314, pH 7.25, 300 mOsm. Biocytin (0.5%) was added to the electrode solution as needed. To reduce the probability of multi-synaptic events, all slices are perfused with a high Mg^{2+} ACSF solution during recordings: 124 NaCl, 5 KCl, 1.23 NaH2PO4, 26 NaHCO3, 10 glucose, 4 $MgCl_2$, 4 $CaCl_2$. The electrode resistance in the bath was 4-10 MΩ. Data were acquired with a National Instruments AD board and software EPHUS (Suter et al., 2010). Membrane voltages were corrected for an estimated liquid junction potential of 10mV.

2.11) Electrophysiology of auditory cortex neurons:

Whole-cell recordings were performed from P5-10 in subplate and in layer 4 with a patch-clamp amplifier (Multiclamp 700B; Molecular Devices). Electrodes were filled with (in mM): 115 cesium methanesulfonate ($CsCH_3SO_3$), 5 NaF, 10 EGTA, 15 CsCl, 3.5 MgATP, 3 QX-314, pH 7.25, 300 mOsm. Biocytin or Neurobiotin (0.5%) was added to the electrode solution as needed. To reduce the probability of multi-synaptic events, all slices are perfused with a high Mg^{2+} ACSF solution during recording: 124 NaCl, 5 KCl, 1.23 NaH2PO4, 26 NaHCO3, 10 glucose, 4 $MgCl_2$, 4 $CaCl_2$. The electrode resistance in the bath was 4-10 MΩ. Data were acquired with a National Instruments AD board and software EPHUS (Suter et al., 2010). Membrane voltages were corrected for an estimated liquid junction potential of 10mV. Soma activation

profiles of neurons were created by recording in loose-patch mode while mapping the same area and recording action potentials.

2.12) Perfusion and sectioning for histology:

Animals were deeply anesthetized with isoflurane and were perfused transcardially with 4% PFA. When brains were removed, the right hemisphere of the brain was cut below the rhinal fissure to retain the identity of the ischemic hemisphere throughout histology experiments. Brains were post-fixed overnight in 4% PFA at 4° C. Brains were then transferred to 30% sucrose in PBS until ready to be stained. Brains were cut as 50 μm coronal sections on a freezing microtome in a bed of 30% sucrose in PBS. Slices were collected in room temperature PBS, and stored at 4° C.

2.13) Nissl staining and histological analysis:

Nissl staining allowed for identification of cortical layers including the subplate and the ventricular boundaries. For Nissl staining, free floating 50 μm coronal sections were rinsed in PBS, and mounted on glass slides. Then slides were dipped in Cresyl violet until they reached the appropriate darkness and contrast before being transferred to double distilled water. Then slices were dehydrated in an alcohol series of increasing alcohol concentration. Slices were then transferred to xylene and coverslipped in Permount (Fisher). Slides were air dried then scanned at 1X by Nikon Super Coolscan 9000ED.

We used custom routines in MATLAB to measure cortical thickness. Measurements were taken from pia to ventricle (also the lower subplate boundary). We calculated the ratio of the extent of ACX in both the hemispheres. We then averaged the ratios from all slices from each brain. Brains from each condition (Control, Mild HI, and Mod HI) were measured for cortical shrinkage. (N = Control = 5 brains, 24 slices total; Mild HI = 14 brains, 36 slices total; Mod HI = 5 brains, 19 brains total)

2.14) Statistics for LSPS mapping & electrophysiology:

Results are plotted by using the Multiple Comparison test. To perform multiple comparison of group means, we used one-way ANOVA or Kruskal-Wallis test based upon if group is normalized. Histology analysis results are plotted as boxplots using two-sided Student's t-test or one-way ANOVA (normally distributed).

2.15) Auditory startle threshold experiments:

For the Sensitivity (Level) Test: Brief startle sounds (20 ms, Gaussian white noise bursts) were presented from a calibrated speaker (Fostex T90A) positioned above the animal. To avoid temporal predictability of the startle sound event, noise bursts occurred at a random time (selected from a distribution ranging from 3000 to 9000 msec). To measure the startle-metric (i.e., input-output) function of the animal, startle sounds were presented in random order at a range of sound intensities extending from 55dB to 105dB SPL in 10dB step-wise increments and repeated 10 times. To measure the behavioral response, the animal was placed inside an acoustically transparent plastic container resting on a piezo-

electric sensor beneath the speaker. To calculate response amplitude on each trial, the root-mean-square (RMS) amplitude of the output of the piezo sensor was determined then averaged. The time window for calculating RMS amplitude extended from startle sound onset to 50 ms after onset.

Chapter 3: Subplate neurons promote spindle bursts and thalamocortical patterning in the neonatal rat somatosensory cortex

**This manuscript was published in Journal of Neuroscience: (Tolner* Sheikh* et al., 2012).

The effects of subplate neuron removal or ablation can result in neurological disorders such as pediatric neuropathologies (Kanold et al., 2003; Kanold, 2009). For example, subplate ablation in animals results in a period of seizures indicating hyperexcitability in developing neural circuits (Kanold, 2009). While the origin of seizures is unclear, these seizures could be generated by the depolarization of GABAergic activity or the unbalancing of glutamatergic activity by GABAergic circuits (Kanold, 2009). Previous experiments have shown the importance of subplate neurons for the proper development of the somatosensory cortex via SPN lesions/removal of SPNs prior to the onset of the critical period (Ghosh and Shatz, 1993; Kanold et al., 2003; Tolner et al., 2012).

By removing subplate neurons, I was able to disrupt the anatomical barrel patterning in layer 4 of the cortex (Tolner et al., 2012). In addition, the removal of subplate neurons caused a lack of strengthening of thalamocortical connections as observed by a reduction in recorded excitatory postsynaptic currents (EPSCs) of layer 4 (Tolner et al., 2012). Not only was there an anatomical deficit from removing subplate neurons from the developing thalamocortical circuitry, but there was also a functional physiological deficit.

Abstract:

Patterned neuronal activity such as spindle bursts in the neonatal cortex is likely to promote the maturation of cortical synapses and neuronal circuits. Previous work on cats has shown that removal of subplate neurons, a transient neuronal population in the immature cortex, prevents the functional maturation of thalamocortical and intracortical connectivity. Here we studied the effect of subplate removal in the neonatal rat somatosensory cortex (S1). Using intracortical EEG we show that after selective removal of subplate neurons in the limb region of S1 endogenous and sensory evoked spindle burst activity is largely abolished. Consistent with the reduced in vivo activity in the S1 limb region, we find by in vitro recordings that thalamocortical inputs to layer 4 neurons are weak. In addition, we find that removal of subplate neurons in the S1 barrel region prevents the development of the characteristic histological barrel-like appearance. Thus, subplate neurons are crucially involved in the generation of particular types of early network activity in the neonatal cortex, which are an important feature of cortical development. The altered EEG pattern following subplate damage could be applicable in the neurological assessment of human neonates.

Introduction

Neuronal activity influences circuit development (Katz and Shatz, 1996; Erzurumlu and Kind, 2001; Zhang and Poo, 2001; Feldman and Brecht, 2005; Gonzalez-Islas and Wenner, 2006; Inan and Crair, 2007; Xu et al., 2011). A characteristic feature of neuronal activity in the immature mammalian nervous system

are spontaneous, recurring network events that are present before the development of sensory driven activity (Yuste and Denk, 1995; Garaschuk et al., 2000; Ben Ari, 2001; Adelsberger et al., 2005; Calderon et al., 2005; Vanhatalo et al., 2005). In preterm babies, the most prominent cortical EEG features are spontaneous activity transients characterized by slow waves nesting higher frequency oscillations (Vanhatalo et al., 2002). In the immature rodent somatosensory and visual cortex, around the end of the first postnatal week, endogenous patterned activity is characterized mainly as recurrent spindle bursts (Khazipov et al., 2004; Bernard et al., 2005; Hanganu et al., 2006; Minlebaev et al., 2009; Yang et al., 2009; Colonnese and Khazipov, 2010; Mohns and Blumberg, 2010; Seelke and Blumberg, 2010). The shared characteristics of human preterm activity transients and rodent spindle bursts suggest that they are homologous functional features of the immature cortex (Milh et al., 2007; Minlebaev et al., 2009; Vanhatalo and Kaila, 2010). GABAergic and glutamatergic signaling underlies cortical spindle bursts (Khazipov et al., 2004; Minlebaev et al., 2007; Yang et al., 2009), but the circuitry that drives and controls them is unknown.

Subplate neurons (SPNs) are a transient population of neurons of the immature neocortex, located in the developing white matter (Kostovic and Rakic, 1980; Kanold and Luhmann, 2010). SPNs are innervated by thalamic axons before these grow into cortical layer 4, while SPNs provide excitatory input to layer 4 (Pinon et al., 2009; Zhao et al., 2009; Kanold and Luhmann, 2010). Thus SPNs are a transient relay and processing station for thalamic input and might be involved in the generation of cortical spindle bursts. Firstly, SPNs have intrinsic oscillatory

properties (Hirsch and Luhmann, 2008), are thought to support the propagation of pharmacologically evoked intra-cortical activity waves (Dupont et al., 2006), and might be active during spindle bursts (Yang et al., 2009). Secondly, SPNs are intimately associated with thalamocortical circuits, which might be involved in the generation of spindle bursts. Because spontaneous activity in the S1 limb region is characterized mainly by spindle bursts (Khazipov et al., 2004; Yang et al., 2009) we first investigated the effect of SPN removal in the limb region. We show that focal removal of SPNs in rats shortly after birth prevents spindle bursts, while having little effect on the occurrence of sharp potentials. The role of neuronal activity in cortical development in rodent has been investigated in the S1 barrel region (Katz and Shatz, 1996; Erzurumlu and Kind, 2001; Zhang and Poo, 2001; Feldman and Brecht, 2005; Gonzalez-Islas and Wenner, 2006; Inan and Crair, 2007). We thus investigated the effects of SPN removal in the barrel region. We find that SPN removal prevents the developmental strengthening of thalamocortical inputs to layer 4 neurons and impairs the development of the characteristic barrel pattern. Thus, SPNs are a key element in the development of the patterned organization of S1, and in the functional development of its endogenous activity patterns.

Methods:

We used rat pups of both sexes aged P0-P14 that were kept together with their parents and littermates. Postnatal day (P) 0 refers to the day of birth.

Statistics:

Statistical analysis between groups was performed using the Mann-Whitney U-test or Students T-test, with 2-tailed distribution. Average values are expressed as mean ± standard error unless stated. Statistical significance was taken at $p< 0.05$.

Results:

Local removal of subplate neurons in neonatal rats using p75-immunotoxin

Expression of the p75 neurotrophin receptor is localized to subplate neurons (SPN) in rats at P0-1 (see also (Koh and Loy, 1989). We used immunotoxins against p75 neurotrophin receptor-expressing cells to selectively remove SPNs (Kanold et al., 2003; Kanold and Shatz, 2006). We confirmed the specificity of the p75 antibody used for SPN ablations in rat by immunostaining (Fig. 3.1A). Since the neurodegenerative effect of p75-immunotoxin has been reported to become evident histologically after about 2-4 days (Book et al., 1995), and since EEG recordings (see below) are technically difficult to carry out in very young rat pups due to their weak skull, we studied the effects of SPN damage in rats about 1 week after the immunotoxin injections. The localized immunotoxin injections in the subplate (barrel or limb region) caused loss of SPNs near the injections in an area of approximately 0.75-1.5 mm width rostro-caudally and medio-laterally while leaving the overlying cortical plate intact (Fig. 3.1C, D; n= 7 ablated rats, limb region). Injections of control toxin or vehicle into the subplate did not cause loss of SPNs (Fig. 3.1C, D; n=4 mu toxin, n=8 blank toxin, n=4 vehicle-injected rats, limb region). Behaviorally, animals with local SPN ablation were indistinguishable from control non-injected, vehicle

injected or control toxin injected rats and showed normal sleep-wake cycles as judged by their mobility patterns (Fig. 3.1E).

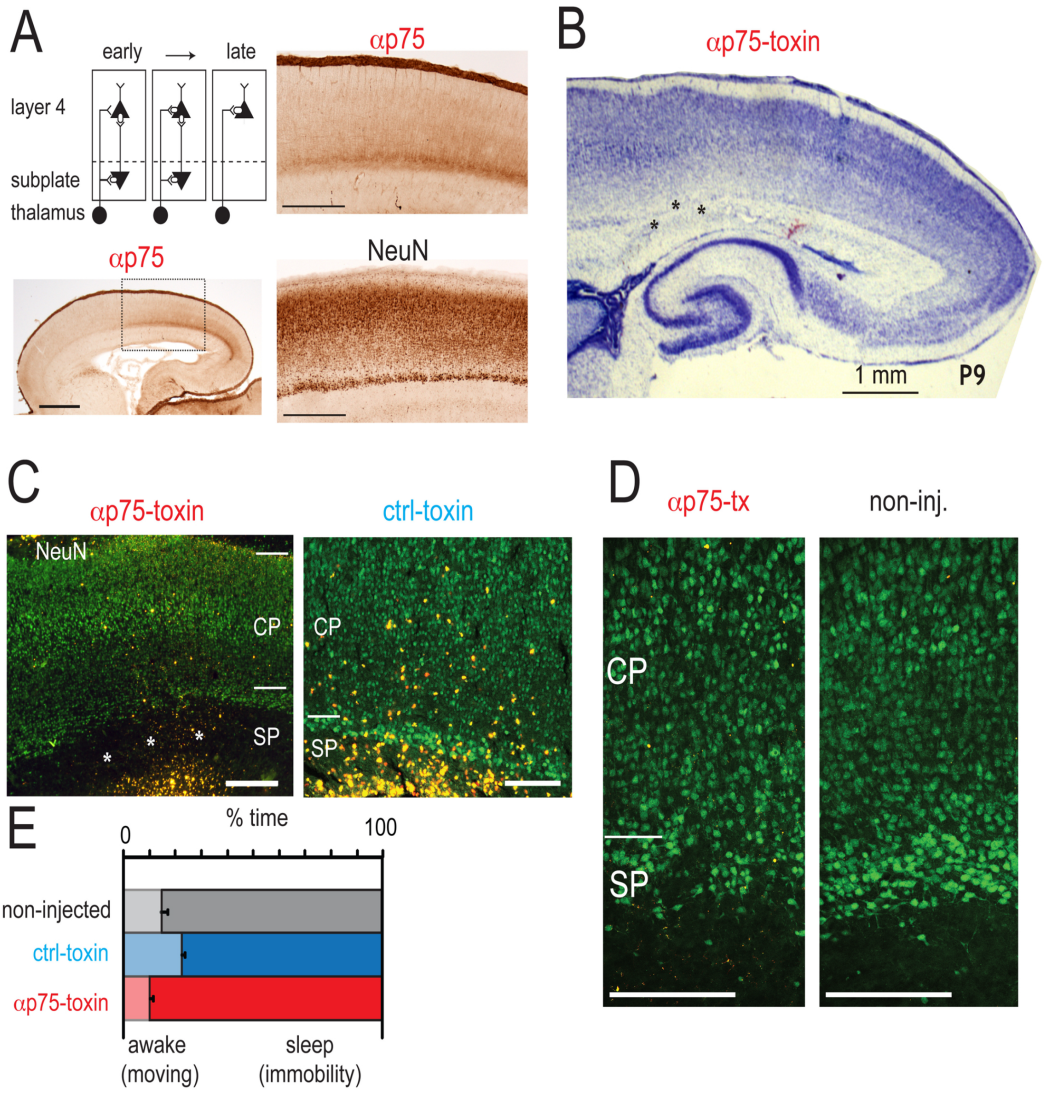

Figure 3.1: Selective removal of SPNs in rat S1. A. Schematic of subplate circuits (top left) and location of the subplate in rat. Distribution of p75 in P0 rat brain as shown by immunolabelling using the antibody 192-IgG (α-p75) that is part of the immunotoxin used for subplate neuron (SPN) targeting. Bottom left: Low power image. S1 marked by rectangle. Scale bar 1 mm. Top right: Detail of the S1/parietal cortex region depicted by the rectangle in low power image. Scale bar 500 μm Bottom right: NeuN-stained adjacent brain section showing the subplate zone below the cortical plate. Deep white matter SPNs are poorly labeled by NeuN. Scale bar 500 μm **B-D:** Focal injections of anti-rat p75-immunotoxin at the level of SPN in P0-1 rats cause a highly selective ablation, leaving neurons in the overlying cortical plate intact. Nissl (B) and NeuN (C, D labeled in green) stained sections from a rat that received focal injections of anti-rat p75-immunotoxin (B and left in C) in the S1 cortex limb region at P1. The area of SPN ablation, marked by ***, covers an area of about 1-1.5 mm in the mediolateral and anterioposterior extent in the S1 hindlimb/forelimb region, while leaving the subplate in adjacent anterior and posterior cortical regions intact. Fluorescent microspheres coinjected with the immunotoxin are visible as a cluster of pink (in **B**) or yellow (in **C**) spots in the white matter near the damaged subplate. Scale bars **1 mm (B)** and 400 μm (C). **C**, right**:** Injections of anti-mouse-p75-immunotoxin (mu-toxin) do not cause SPN ablation. NeuN stained section from a P5 rat that was injected with mu-toxin at P0. Scale bar **400 μm D**: left: Higher magnification image of the ablated S1 region with damaged SPN layer from the anti-rat p75-immunotoxin injected animal shown on the left in C. Note the normal presence of neurons in the overlaying cortical plate above the ablated SPN layer. **D**, middle: unaffected S1 region with intact SPN layer from a non-injected control animal. **Right:** Higher magnification image of the unaffected S1 region with intact SPN layer from the mu-toxin injected animal shown on the right in C. Scale bars in D **50** μm. **E:** SPN removal did not influence the behavior of animals as evident from sleep-wake cycles (measured from animal motility using piezo sensors; see Methods for details). (Experiment done by Dr. Else A. Tolner.)

Subplate removal prevents spontaneous spindle bursts in the S1 limb region

To identify the functional consequences of SPN removal on spindle bursts, we used chronic full-band (Fb) EEG-recordings (labeled 'chronic' in Fig. 3.2) from freely moving P7-P10 rats (Sipila et al., 2006) to investigate spindle bursts (Fig. 3.2A, C and D). Because spindle bursts have been well characterized in the S1 limb region (Khazipov et al., 2004; Yang et al., 2009) and since the limb allows selective sensory stimulation we recorded EEG activity from the S1 limb region. We used Fb-EEG, since the low frequency component of spindle bursts in rats is attenuated and distorted by high-pass filtering in standard AC recordings (Minlebaev et al., 2009). Since it is technically challenging (and possibly damaging) to chronically implant electrodes in rat pups younger than P5, especially considering the subplate injections at P0-1, electrodes were implanted in subplate-targeted pups at P6, after which we studied the functional effect of subplate ablation. In the chronic freely moving recordings, pups were recorded between P7 and P10 in daily sessions of about 30-45 minutes in a small pre-warmed recording chamber. Movements (including breathing) were monitored by a force transducer coupled to the recording platform as well as by a piezo element connected to the pup's body and video (see Methods for details). To constrain potential movement artifacts we recorded in a second cohort of animals using acute head-fixed preparations (labeled 'acute' in Fig. 3.2). We did not see any effects of head fixation on spindle burst activity; hence the acute and chronic EEG data were pooled.

Spindle bursts consisted of higher frequencies in the α to γ-range embedded in a δ wave (Fig. 2B; (Marcano-Reik and Blumberg, 2008; Minlebaev et al., 2009;

Mohns and Blumberg, 2010). Under control conditions (n=12 non-injected, n=8 blank toxin, n=2 mu-toxin, n=3 vehicle-injected rats), spindle bursts were observed regularly in acute or chronic recordings, typically occurring at a rate of about 0.5-3 events/min (Fig. 3.2C, E and G). Since chronic and acute experiments showed that injection per se did not influence SB occurrence, the data for blank toxin, mu-toxin and vehicle-injected controls were pooled and will be referred to as 'control-injected'. In contrast to the control-injected animals, following SPN removal spindle bursts were rarely observed (Fig. 3.2D, F). The rate of occurrence following subplate ablation was 0.09 +/-0.04 events/min (n=7) versus 1.48 +/- 0.31 events/min in control-injected animals (n=13; $p<0.0001$; Fig. 3.2G). The peak frequency of the spindle bursts in ablated rats (11.1±1.5 Hz; n=1 out of 3 chronically recorded pups; n=4 out of 4 acutely recorded pups) was slightly reduced compared to that of control-injected pups 15.5±0.8 Hz; $p=0.035$) but within the range of 8-20 Hz observed for non-injected animals (Fig. 3.2H). The duration of remaining spindle bursts in ablated rats (1.77 ±0.24 sec; n=1 out of 3 chronically recorded pups; n=4 out of 4 acutely recorded pups) was comparable to that of control-injected pups (1.60 ± 0.15; n=13; $p=0.6$) or non-injected animals (1.77±0.29 sec, n=10; Fig. 2I).

The cumulative root-mean-square (cRMS) of the EEG is an unbiased measure of total activity. A high rate of occurrence of spindle bursts leads to a high cRMS in the appropriate frequency band, while a reduction in the rate of spindle bursts has the opposite effect. Thus we investigated if the loss of spindle bursts in the S1 limb region is reflected in the cRMS of the EEG. We first measured the cRMS in the frequency band that comprises most spindle burst activity. The cRMS in the 10-45 Hz

band was reduced after ablation but not in control- injected animals (62.5 +/- 4.2% for ablated, n=7 versus 103.2 +/- 13.6 % for control-injected rats n=13; p=0.013; calculated as % of the mean value for non-injected controls; Fig. 3.2J). In addition, cRMS values for the 1-4 Hz and 4-10 Hz frequency bands – in which spindle bursts also contain energy- were also lower in ablated than in control-injected rats ([1-4 Hz]: 57.9 +/- 8.8% for ablated versus 95.9 +/- 12.7% control- injected, p=0.0449; [4-10 Hz]: 58.8 +/-8.6% for ablated vs 107.2+/- 18.2 %, control-injected; p=0.0556). In some ablated animals we observed conspicuous large amplitude DC shifts (up to 500uV) of several seconds duration and of unknown origin (see Fig. 3.2D).

In addition to spontaneous spindle bursts, sharp potentials are a second activity pattern that is regularly observed in neonatal rat cortex (Khazipov et al., 2004; Bernard et al., 2005; Seelke and Blumberg, 2010). We therefore investigated whether the presence of sharp potentials in the S1 limb region is affected by local subplate removal. In non-injected and control-injected animals, sharp potentials were present at rates that ranged between 1 and 6 events per minute (3.6±0.5 events/min, n=13 control-injected animals; Fig. 3.2K). After SPN ablation, sharp potentials were still present (1.8±0.3 events/min, n=7 ablated rats; p=0.056, Mann-Whitney; Fig. 3.2K). In chronic EEG recordings in freely moving rats, additional recordings from parietal and occipital regions also showed regular sharp potentials in ablated rats (n=3) as seen for animals in the control groups (n=6 non-injected; n=2 mu-toxin and n=2 blank toxin; data not shown). Thus, while SPNs are required for the generation of spontaneous spindle bursts they do not seem to play a role in the modulation of the frequency of cortical sharp potentials.

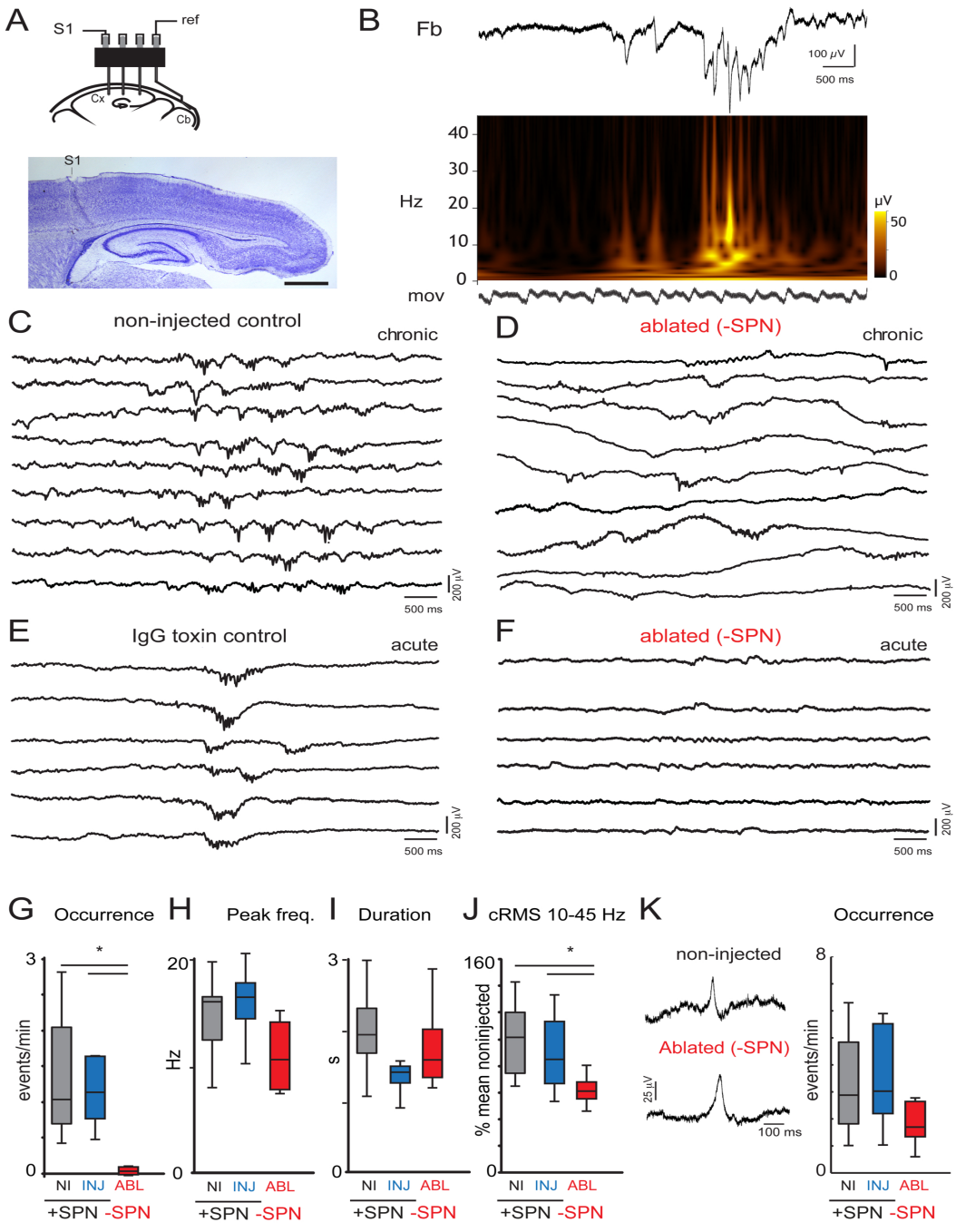
A
S1
ref
Cx
Cb
S1
B
Fb
100 μV
500 ms
40
30
Hz
20
10
0
μV
50
0
mov
C
non-injected control
chronic
200 μV
500 ms
D
ablated (-SPN)
chronic
200 μV
500 ms
E
IgG toxin control
acute
200 μV
500 ms
F
ablated (-SPN)
acute
200 μV
500 ms
G
Occurrence
events/min
3
0
*
NI INJ ABL
+SPN -SPN
H
Peak freq.
Hz
20
0
NI INJ ABL
+SPN -SPN
I
Duration
s
3
0
NI INJ ABL
+SPN -SPN
J
cRMS 10-45 Hz
% mean noninjected
160
0
*
NI INJ ABL
+SPN -SPN
K
non-injected
Ablated (-SPN)
25 μV
100 ms
Occurrence
events/min
8
0
NI INJ ABL
+SPN -SPN

Figure 3.2: SPN are required for the generation of spindle bursts in immature S1 limb region. A: Scheme depicting the electrode configuration used for chronic EEG recordings. Photomicrograph shows the location of the AgCl electrode track in deep cortical layers of the S1 limb region of a P9 non-injected control rat. Scale bar 1 mm. **B:** Sample trace from a P8 animal showing the frequency composition of a spindle burst. Top trace shows full-band (Fb) EEG, in the middle is the time-frequency plot showing the frequency composition. The lower trace (labelled 'mov') shows the signal from the movement sensor, indicating regular breathing. Note that spindle bursts can occur in the absence of limb and trunk movements. **C-F**: Segments of EEG traces under various conditions. Segments containing spindle bursts were aligned to facilitate visual inspection. **C:** Spindle burst activity is observed regularly in the S1 hindlimb/forelimb region of rats between P7-10. Multiple traces showing spontaneous spindle burst activity from a freely behaving non-injected control rat at P10. **D**: After SPN ablation at P0-1, spindle burst activity is largely absent and the figure shows the most salient events during the recording epoch. Example traces from a freely behaving P7 rat with local SPN ablation in S1. Sharp potentials are less affected and are regularly seen at a bit reduced frequency compared to injected control animals (see Fig. 3.1K for details). **E**. Control toxin injections (IgG toxin) at P0-1 do not impair the expression of spindle burst activity at P7-10. Example traces from a head-fixed P9 rat showing regular spindle burst activity recorded in the S1 hindlimb area. **F:** EEG recorded from the S1 hindlimb region of a head-fixed SPN ablated rat at P9, showing faint oscillations, most of which did not meet the spindle burst criterium with prominent activity in the 5-40 Hz range (see Methods). **G-I**: Box plots summarizing occurrence of spindle bursts (G), spindle burst peak frequency (H), and spindle burst duration (I). Asterisk '*' indicates a significant ($p<0.05$) reduction in spindle burst occurrence after ablation. Two of the 3 chronically recorded ablated rats did not show any spindle burst activity in the recording sessions, carried out at P7 and P8. Box plots show the median +/- quartile values from the pooled acute and chronic values from non-injected controls (n=10 for G; n=9 for H), control-injected controls (n=13) and ablated rats (n=7). **J**: Box plot shows cRMS values for the 10-45 Hz frequency range in spontaneous EEG recordings. Asterisk '*' indicates a significant ($p<0.05$) reduction in cRMS after ablation. **K**: Left: Sample EEG traces of sharp potentials from a freely behaving (chronic) non-injected control animal with (+SPN) or an ablated animal without SPN (-SPN). Right**:** Sharp potential frequency (events/minute) in the S1 limb region during periods of immobility from freely behaving (chronic) and head-fixed (acute) recordings, in P7-P10 rats with intact (+) and locally ablated (-) SPN. (Experiment done by Dr. Else A. Tolner.)

Subplate removal prevents sensory evoked spindle bursts in the S1 limb region

Evoked activity in the immature S1 is known to uniformly consist of spindle bursts (Khazipov et al., 2004; Minlebaev et al., 2007; Yang et al., 2009). To reliably activate all afferent projections, we electrically stimulated the forepaw or hindpaw. Electrical stimulation of the forepaw or hindpaw led to evoked spindle bursts in S1 in non-injected, vehicle-injected, and control-toxin injected animals (Fig. 3.3A). In ablated rats, evoked activity was markedly reduced and contained much less activity in the spindle burst range (Fig. 3.3B). This reduction in spindle burst activity in single trials was also visible in the average LFP (Fig. 3.3C). We quantified the impairment in evoked S1 activity by calculating the ratio of stimulation trials in which responses contained spindle burst activity, which was reduced by more than half for the ablated animals (0.30±0.06, n=4 ablated vs. 0.67±0.08, n=8 control-injected animals; p=0.0108; Fig. 3.3D). This indicates a reduction in the stimulus response relation in S1 following subplate removal. To further characterize the evoked responses, we computed the power in the 5-40 Hz 'spindle' frequency range of EEG in the first 500 ms following the stimulation. The power was reduced in ablated animals (6760±3019 $(\mu V)^2$/ms, n=4) compared to control-injected animals (22157±3775 $(\mu V)^2$/ms, n=8; p=0.0162; Fig. 3.3E). Thus, together these data suggest that SPNs are important not only for the generation of spontaneous spindle bursts but also for the development of early sensory evoked responses.

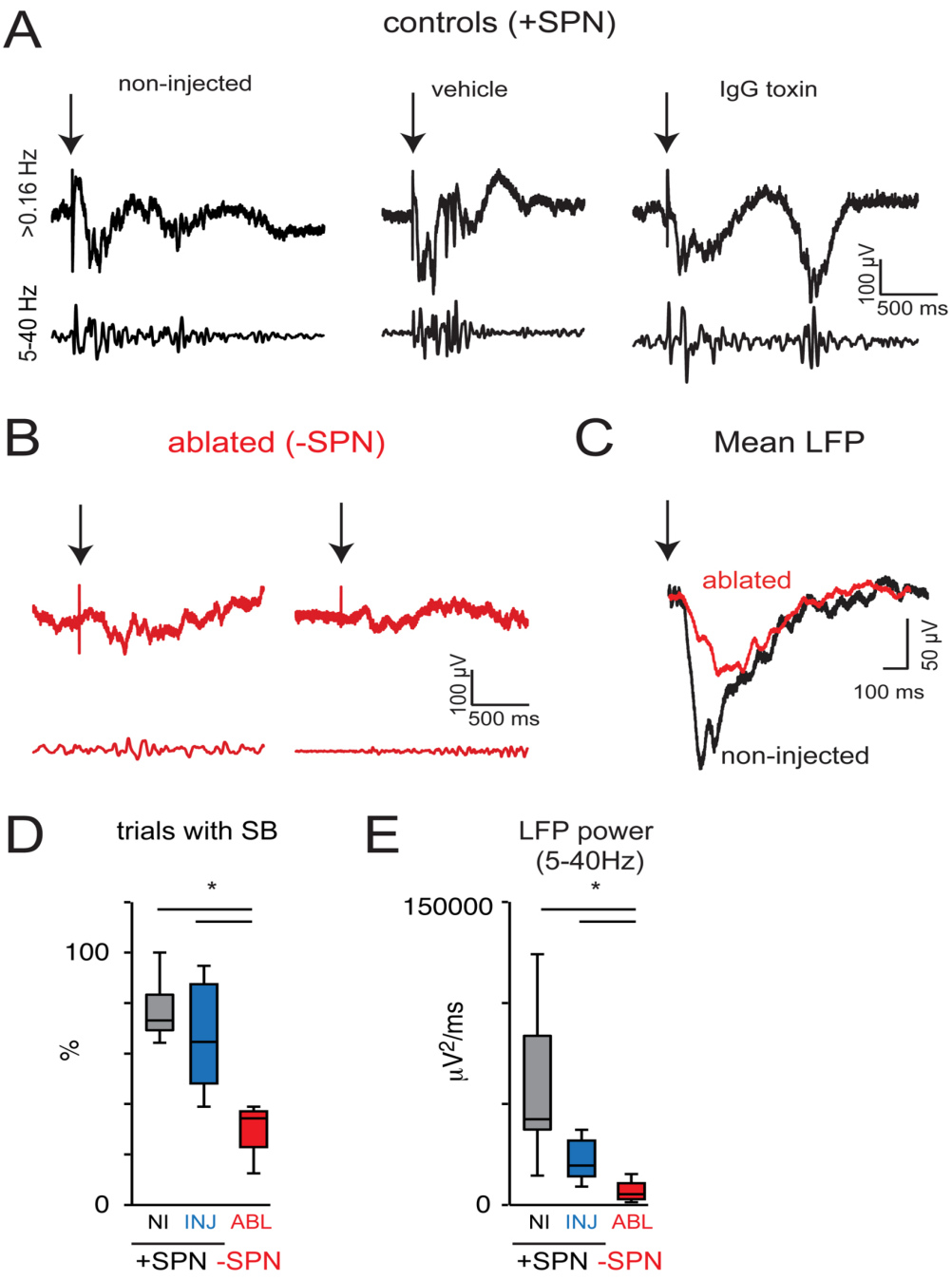
A
controls (+SPN)
non-injected
vehicle
IgG toxin
>0.16 Hz
5-40 Hz
100 µV
500 ms
B
ablated (-SPN)
100 µV
500 ms
C
Mean LFP
ablated
50 µV
100 ms
non-injected
D
trials with SB
*
100
%
0
NI INJ ABL
+SPN -SPN
E
LFP power
(5-40Hz)
*
150000
µV²/ms
0
NI INJ ABL
+SPN -SPN

Figure 3.3: SPNs are required for the expression of sensory evoked spindle burst activity in the rat S1 limb region. A: Single trial local field potential (LFP) responses in middle-deep layers of the S1 limb region to electrical stimulation of the hind- or forepaw for control animals (non-injected, vehicle injected, or control IgG toxin injected; +SPN). The 5-40 Hz band-pass filtered traces reveal evoked spindle burst activity. **B:** Single trial LFP responses to electrical stimulation of the hind- or forepaw in subplate ablated animals (-SPN). After local SPN ablation, evoked spindle burst activity in the S1 hindlimb/forelimb region is significantly reduced. **C**: Mean evoked LFP of a non-injected and ablated animal illustrates the lower amplitude of the LFP after local SPN ablation. **D**: The ratio of evoked responses with spindle burst activity (see Methods) is reduced in rats with local SPN ablation. * p **=** 0.0108 for comparison of control-injected (n=8) with ablated rats (n=4; 2-tailed Mann-Whitney U test). **E:** Evoked LFP power in the 5-40 Hz band is reduced for ablated animals (n=4; * p=0.0162 for comparison with injected controls [n=8]; 2-tailed Mann-Whitney U-test). Shown are responses to stimulation at 2x threshold intensity. Threshold stimulation levels were higher in ablated than in toxin control animals (2.0 mA for ablated rats vs 0.7+/- 0.2 mA for injected controls). (Experiment done by Dr. Else A. Tolner.)

Subplate removal prevents strengthening of thalamocortical connections

Our in vivo recordings showed a marked reduction in both spontaneous and sensory evoked activity in the S1 limb region. The reduced activity can arise from abnormal firing of cortical neurons or from altered synaptic connectivity, especially of thalamocortical synapses. Thalamocortical connectivity and patterning can be probed in vitro in the S1 barrel region (Katz and Shatz, 1996; Erzurumlu and Kind, 2001; Zhang and Poo, 2001; Feldman and Brecht, 2005; Gonzalez-Islas and Wenner, 2006; Inan and Crair, 2007). To investigate these possibilities we ablated SPNs in the S1 barrel region and about 10 days after subplate removal performed whole patch clamp recordings from layer 4 neurons (N=106) in slices of S1 (n=30 animals). We first investigated how SPN removal affects the intrinsic properties of cells in layer 4, the target layer of SPN projections (Zhao et al., 2009). Current injections in cells in control and ablated areas readily evoked action potentials in both sets of neurons (n=15 and n=20 cells respectively; Fig. 3.4A). By injecting currents of different

amplitudes we found that input resistance and resting potential of layer 4 neurons in control and ablated areas were similar (both $p>0.05$; Fig. 3.4B). These results suggest that removal of SPNs in rat pups does not grossly affect the intrinsic properties of cortical neurons. Since SPNs are implicated in the maturation of thalamocortical synapses in cat visual cortex (Kanold et al., 2003) we next investigated if these neurons play a similar role in rodent S1. We thus stimulated thalamocortical projections while recording from layer 4 neurons (Fig. 3.4C). In both populations of neurons, short latency EPSCs were observed (Fig. 3.4D, left). Increasing the stimulation level led to an increase in EPSC amplitude (Fig. 3.4D, right, showing example responses of two cells). We found that the maximum EPSC amplitude was significantly smaller for layer 4 cells from ablated animals (n=26 cells) than in layer 4 cells from non-injected (n=17), vehicle (n=14), or control-toxin (n=14) injected animals (Fig. 3.4E, $p<0.0001$). These results show that thalamocortical transmission is impaired after subplate removal.

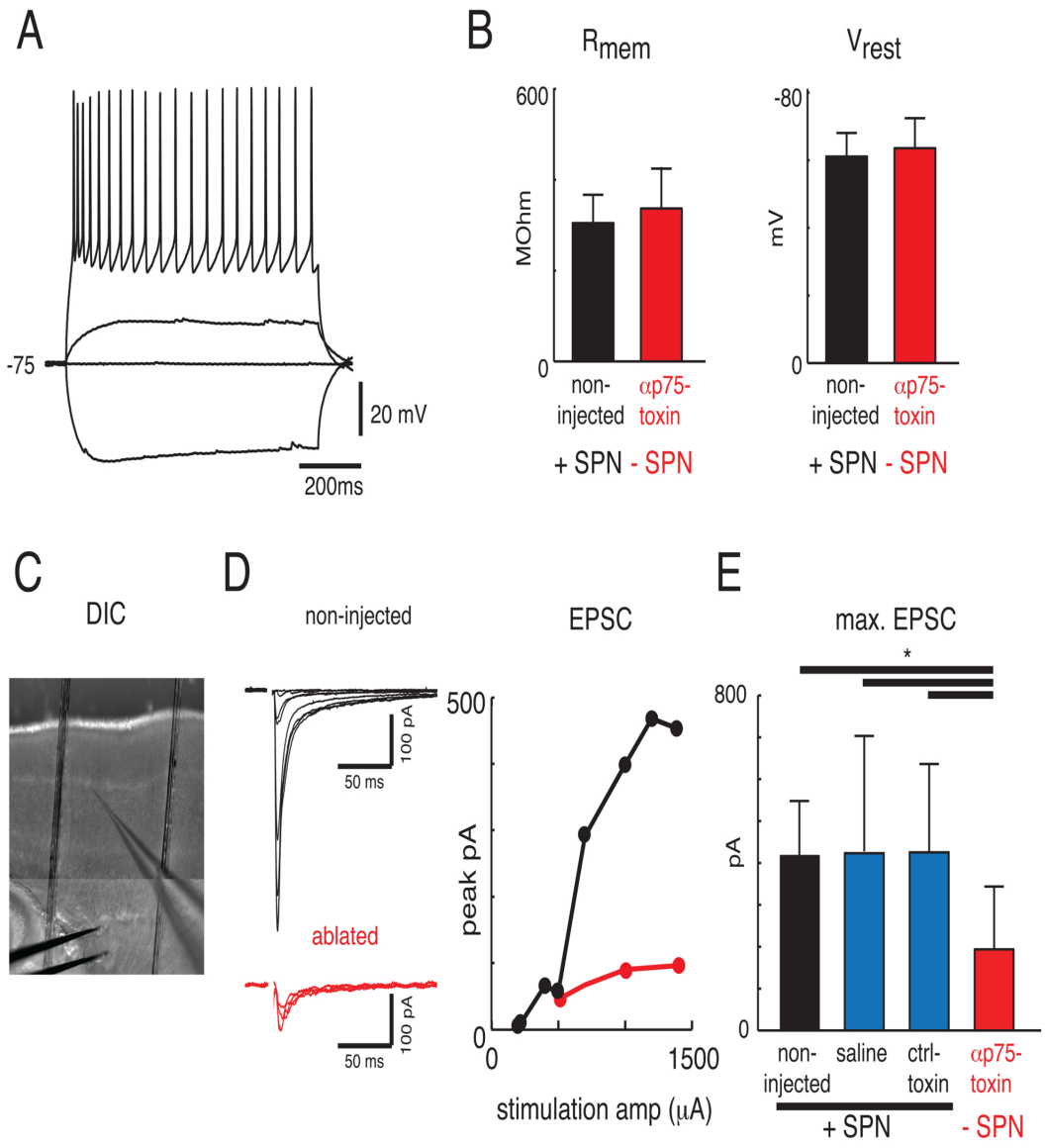
A
-75
20 mV
200ms
B
Rmem
600
MOhm
0
non-injected
αp75-toxin
+ SPN - SPN
Vrest
-80
mV
0
non-injected
αp75-toxin
+ SPN - SPN
C
DIC
D
non-injected
100 pA
50 ms
ablated
100 pA
50 ms
EPSC
500
peak pA
0
0
1500
stimulation amp (μA)
E
max. EPSC
*
800
pA
0
non-injected
saline
ctrl-toxin
αp75-toxin
+ SPN
- SPN

Figure 3.4: SPN ablation in the S1 barrel cortex in rats alters thalamocortical synaptic strength in layer 4 neurons. A: Whole-cell recording of layer 4 principal neuron in a thalamocortical slice from a subplate-ablated P10 rat. Traces show responses to multiple current injections. **B:** Neurons from control vs. ablated slices have similar input resistance (304.4±62 MW vs. 336.6±89.9 MW; mean ± std, P>0.1) and resting potential (-61.1±6.9 mV vs. –64.4±8.3 mV; mean ± std, P>0.1). Recordings were made in slices from P10 rats, after local SPN targeting at P0 for ablated or control-injected animals. **C:** Recording configuration showing the recording pipette in layer 4 and stimulation electrode in the thalamocortical projections. **D, left:** Traces show evoked EPSCs of a representative neuron from each population to stimulations with varying stimulation intensities. **Right:** Graph shows EPSC amplitude for the two neurons shown on the left as a function of stimulation strength. Note that the maximum EPSC is smaller in layer 4 cells from the SPN ablated region. **E:** Shown are the maximal EPSC's for all recorded SPNs in each group. The maximum evoked EPSC amplitude is ~50% smaller in slices from SPN ablated animals than in slices from non-injected, control-toxin, or saline injected animals (194.1±148.8 pA vs. 415.3±127.6 pA, 420.9±212.8 pA, 421.7±276.9 pA; mean ± std, P<0.0001, '*'; ANOVA). Evoked EPSC amplitudes from slices of saline and control-toxin injected animals are indistinguishable from control (P>0.1; ANOVA)**.** (Experiment done by Aminah Sheikh.)

Subplate removal prevents barrel patterning

An organizational hallmark of S1 are the whisker barrels where thalamic afferents representing the whiskers form a barrel pattern (Katz and Shatz, 1996; Erzurumlu and Kind, 2001; Zhang and Poo, 2001; Feldman and Brecht, 2005; Gonzalez-Islas and Wenner, 2006; Inan and Crair, 2007). The formation of this pattern has been shown to depend on glutamatergic activity (Fox et al., 1996; Iwasato et al., 2000). Spindle bursts have been suggested to be instructive in both the functional and structural development of barrel cortex (Minlebaev et al., 2007). In light of the disruption of spindle bursts following subplate removal we therefore hypothesized that the functional organization of S1 might be impaired. We thus tested if this organization depends on SPNs. We ablated SPNs at P0 and performed cytochrome oxidase staining about 10 days after subplate removal and quantified the presence of all barrels in the S1 whisker field. In non-injected (n=7), control-toxin

injected (n=19), and vehicle-injected hemispheres (n=5), we observed a normal pattern characterized by the presence of densely stained barrels in each row and position (Fig. 3.5A, C; each p>0.1 compared with non-injected control).

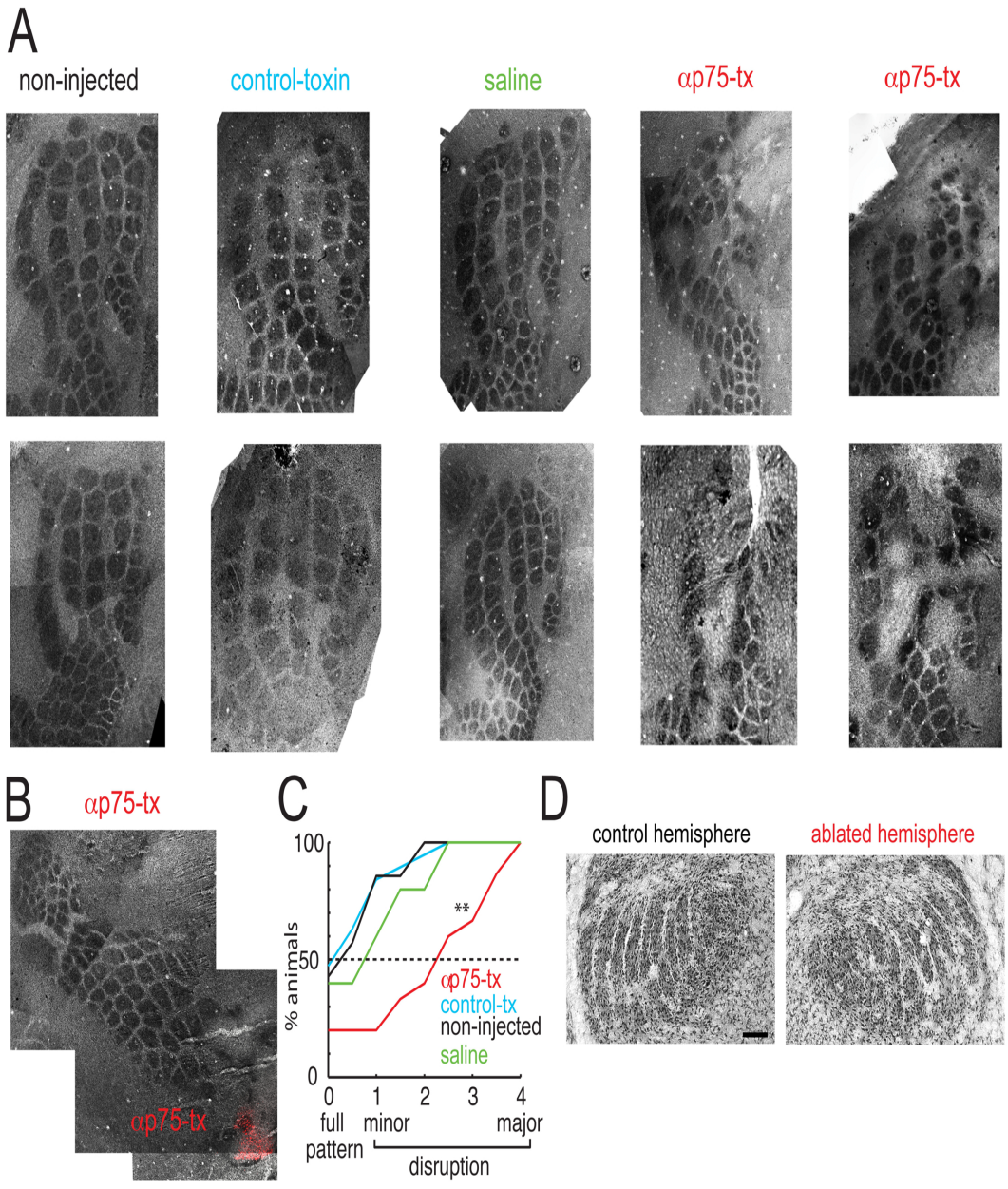

Figure 3.5: Subplate neurons are required for S1 barrel formation. A: Cytochrome oxidase stained sections from (from left-to-right): 2 control non-injected animals, 2 animals injected with control toxin (mu-toxin), 2 animals injected with saline, and 4 animals injected with anti-rat p75-immunotoxin. In anti-rat p75-immunotoxin injected animals clear gaps were present in the barrel field. **B:** Cytochrome oxidase stained sections from an anti-rat p75-immunotoxin injected animal in which fluorescent beads (red) were overlaid on the brightfield image. Note that barrels in vicinity to fluorescent beads were disrupted. **C**: Quantification of the ablation effect shown as a cumulative distribution of disruption scores for animals in the four experimental categories. A score of 0 indicates the presence of a full barrel field while scores from 1 to 4 indicate progressively more severe disruptions. Plotted is the fraction of animals for each manipulation category. Injections of p75-immunotoxin (red) caused a disruption of the barrel pattern compared to control toxin (black) or non-injected control (blue) (both $p<0.05$). Injections of saline (green) or control toxin (black) did not cause a significant disruption ($p>0.1$). **D:** Cytochrome oxidase stained thalamic sections from an ablated and non-injected control hemisphere showing the barreloids. No obvious differences are seen. Scale bar 100 μm. (Experiment done by Aminah Sheikh.)

In contrast, in hemispheres where SPNs had been removed the barrel pattern showed large gaps or complete absence of densely stained barrels depending on the size of the injected area (n=15, compared to control-toxin injected animals p=0.0012; compared to non-injected p=0.0168; Mann-Whitney; Fig. 3.5A, B, C). In animals in which fluorescent beads were recovered, the gaps in the barrel pattern were located superficial to the location of the beads in the deeper sections (Fig. 3.5B). The variability of the size of the gaps might be due to targeting variability and/or variability in the maturity of barrel cortex at the time of ablation (Fig. 3.5C). The effects of SPN removal were restricted to the cortex as barreloids in the thalamus were present after subplate removal (n=4 animals, Fig. 3.5D). Thus SPNs are required for the normal patterning of S1 barrel cortex in rodents. Together our data show that SPNs are required for normal activity patterns and for the development of functional organization of rodent S1.

Discussion

Our results show that the presence of SPNs in the newborn rat cortex is required for the generation of spindle bursts, a specific type of self-organized activity in the immature cortex (Khazipov et al., 2004). Consistent with our finding that removal of SPNs reduces spindle burst activity we find that thalamocortical transmission is impaired. In addition we observed a disruption of the development of the patterning of the barrel field. Prior work has implicated spindle bursts in the formation of barrels (Minlebaev et al., 2007). Although our data do not conclusively show a causal link between spindle burst activity and barrel formation, our observations are consistent with the idea that spindle bursts promote the development of thalamocortical organization.

What is the role of SPNs in the generation of spindle bursts? While spindle bursts can be triggered by peripheral sensory inputs (Khazipov et al., 2004; Marcano-Reik and Blumberg, 2008; Minlebaev et al., 2009; Colonnese et al., 2010; Mohns and Blumberg, 2010), they can also occur in the absence of such inputs (Khazipov et al., 2004; Hanganu et al., 2006). Therefore, while they can be triggered by external stimuli, the generation of spindle burst activity seems to rely to a large extent on circuits intrinsic to the central nervous system. Thus, what circuits underlie the generation of spindle bursts? The thalamus was shown to be active during spindle burst activity *in vivo* at earlier ages and has been suggested to actively contribute to spindle burst generation (Khazipov et al., 2004; Evrard and Ropert, 2009). Thalamic activity is relayed to the cortex. SPNs are located between thalamus and the thalamorecipient layer 4, receive thalamic inputs, and provide excitatory inputs to

layer 4 (Friauf and Shatz, 1991; Hanganu et al., 2002; Zhao et al., 2009). Thus, SPNs receive and relay thalamic inputs to layer 4. Therefore SPNs can mediate spindle burst activity. In line with such a role, we observed impaired sensory-evoked responses including abolishment of spindle bursts as well as impaired thalamocortical transmission in the absence of SPNs. These results mirror previous results in cat that were obtained after much longer post-ablation periods (Kanold et al., 2003) and show strong short-term effects of SPN removal. SPNs might play multiple roles in mediating spindle burst activity. The absence of both spontaneous and evoked cortical spindle burst activity after loss of SPNs could be a direct result of the missing relay in the subplate and/or of impaired maturation of thalamocortical connectivity. In this case SPNs might play a permissive role in promoting spindle bursts. In addition, SPNs might be directly involved in the generation of spindle bursts since they are active during these events (Yang et al., 2009) and tend to oscillate in the spindle-frequency range (Hirsch and Luhmann, 2008).

Since thalamocortical transmission is impaired in the absence of SPNs and since we still observed a large number of sharp potentials consequent to SPN removal, it is likely that circuits intrinsic to the cerebral cortex can generate sharp potentials. In agreement with this, *in vitro* work has shown that sharp potentials but not spindle bursts can be recorded in neocortical slices from immature mice, which lack thalamocortical circuits (Rheims et al., 2008).

The low level of remaining spindle burst activity that was observed in the ablated S1 region could originate from nearby unaffected regions of S1. Although spindle burst activity in vivo has been demonstrated to be spatially confined, spindle

bursts were shown to slowly spread within an area of at least a couple of mm across S1 (Khazipov et al., 2004). It was demonstrated in vitro that the intracolumnar synchronization of subplate-driven cholinergic oscillations in neonatal S1 is mediated by gap junctions (Dupont et al., 2006), and it has been indicated by other in vitro work that a similar mechanism could underlie the slow spread of early network activity across S1 (Sun and Luhmann, 2007).

Although substantial changes in spindle burst rate have been reported to occur towards the end of the first postnatal week in rats (Marcano-Reik et al., 2010), SPN ablation caused comparable low rates of spindle burst occurrence for the different animals in both acute and chronic recordings within the P7-10 time window studied. A fall in brain temperature below the physiological level of 37 °C is known to have strong effects on network activity. The brain temperature of about 34-35 °C during our acute and chronic experiments may have caused a generally lower level of spindle burst and sharp potential activity (Karlsson and Blumberg, 2004). Anesthesia can also affect spindle bursts (Colonnese et al., 2010). However, we find that the effects of SPN ablation are comparable for both the acute and chronic experiments, thus potential confounding effects in the acute experiments of recovery from anesthesia seem to be minimal.

The development of thalamocortical patterning in both rodent somatosensory barrel cortex and ocular dominance columns (ODCs) in cat visual cortex is thought to be dependent on neuronal activity (Chapman et al., 1986; Schlaggar et al., 1993; O'Leary et al., 1994; Shatz, 1996; Erzurumlu and Kind, 2001; Sengpiel and Kind, 2002; Feldman and Brecht, 2005; Inan and Crair, 2007) and mechanisms of synaptic

plasticity mediated by NMDA receptors (Fox et al., 1996; Iwasato et al., 2000). SPN removal in cat prevents the formation of ODCs (Ghosh and Shatz, 1992; Kanold et al., 2003), and our data here show that SPN removal in rodent prevents the formation and refinement of the barrel pattern. SPN neurites have also been shown to be dynamically integrated into the developing barrel cortex circuitry (Pinon et al., 2009). Thus SPNs seem to play functionally similar roles in cat and rodents and across cortical areas. The observed variability in the effect of subplate removal on the barrel pattern might be due to variability in the positioning of our injections and therefore the extent of the ablation. Moreover, we observed that in subplate ablated regions cells located in areas with a larger concentration of fluorescent beads (that were coinjected with the immunotoxin) tended to show smaller maximal EPSCs suggesting a graded effect of the ablation. In addition, the variability in the barrel pattern could be due to variability of the maturity of the barrel pattern at time of ablation. We performed our ablations at P0, which may coincide with the end of the time window for the role of the subplate in barrel formation. This notion is supported by the fact that subplate damage via neonatal hypoxia-ischemia at P1/P2 seems to not interfere with barrel formation (McQuillen et al., 2003), but rather with barrel plasticity (Failor et al., 2006; Quairiaux et al., 2010). Finally, the disruption in the barrel pattern that we observed using cytochrome oxidase staining could also at least partially reflect the decreased sensory driven activity in the cortex since cytochrome oxidase levels can be regulated by neuronal activity.

Our data suggest that SPNs play an important developmental role in the functional and structural development of the S1 cortex. However in all neuronal

ablation studies it is possible that some of the observed effects could be partially mediated by pathways other than the loss of the targeted neurons themselves or the loss of neural activity. SPN immunolesions may be accompanied by microglial or glial activation (Book et al., 1995) with possible consequent non-neural activity dependent effects on brain development and plasticity (Roumier et al., 2008; Tremblay et al., 2011). However, since layer 4 cells were physiologically normal consequent to SPN ablation, our results suggest that such possible effects did not spread to this layer. On the other hand, cortical activity itself can affect microglial activation thus effects of SPN removal on neuronal activity can change the status of glia (Fontainhas et al., 2011; Tremblay, 2011). In addition, SPNs selectively express connective tissue growth factor and are coupled via gap junctions (Heuer et al., 2003; Kanold and Luhmann 2010; Wang et al., 2011) suggesting that SPNs might signal to non-neuronal cells, and/or signal to other neurons not only via chemical synapses. Thus while the effects of SPN removal are consistent with a neural signaling role of SPNs via their excitatory synapses with layer 4, it is possible that some effects of SPN removal are mediated by other pathways, possibly involving non-neuronal cells. The fact that recent work (Hoerder-Suabedissen et al., 2009; Osheroff and Hatten 2009; Oeschger et al., 2011) identified a host of subplate specific genes might enable usage of neuronal silencing methods to dissect the role of SPN mediated neuronal activity and other potential signaling routes.

In newborn preterm and term babies, observation of spontaneous movements is used to assess neurological development, whereby abnormalities have been linked to damage of periventricular regions that include the subplate (Volpe, 1996; Bos et

al., 1998; Hadders-Algra, 2007). Functional data from human subplate are scarce, and direct information is available mostly from in vitro studies (Moore et al., 2011). Therefore the altered EEG pattern of local subplate damage in rodents, leading to a loss of the characteristic spindle burst activity, may help to identify EEG patterns indicative of local cortical or white matter damage in human babies. Thus the spontaneous and sensory evoked activity patterns in the EEG in human babies might be used for early neurological assessment (Vanhatalo et al., 2009; Vanhatalo and Kaila, 2010).

In summary, we show here that SPNs play an important role in the generation of spindle bursts. Neuronal activity is required for the normal development of cortical circuits, and the present work shows that the spindle burst network activity promoted by SPNs is in a key position to affect cortical development.

Chapter 4: Development of intracortical circuits in the rat auditory cortex

Abstract:

Subplate neurons (SPNs) are necessary for the proper development of the cerebral cortex (Ghosh and Shatz, 1993; Kanold et al., 2003; Kanold and Shatz, 2006; Kanold, 2009). They are amongst the earliest appearing neurons born at around E10.5-11.5 and disappear in the adult brain as thalamocortical connections become secure(Molyneaux et al., 2007). However it is not documented as to what the changes are in the functional synaptic circuitry of input to L4 in auditory cortex of the Sprague-Dawley rat over development with respect to the spatial distribution of connections and the strengths of those connections throughout the auditory critical period. Thus we used laser-scanning photostimulation (LSPS) in acute thalamocortical slices of rat auditory cortex during P5-10 and P18-23 to investigate the functional circuit changes over development of the auditory cortex of the rat. We find that development results in expansion and strengthening of excitatory inputs from L2/3 and within L4, but with more emphasis on L4 excitatory inputs of auditory cortex. We also find that development results in expansion and strengthening of inhibitory inputs from L2/3 and within L4, but with more emphasis on L2/3 inhibitory inputs.

Introduction:

Subplate neurons (SPNs) are necessary for the proper development of the cerebral cortex (Ghosh and Shatz, 1993; Kanold et al., 2003; Kanold and Shatz, 2006; Kanold, 2009). Subplate neurons play a universal role in thalamocortical development

of mammals. They are amongst the earliest appearing neurons born at around E10.5-11.5 and disappear in the adult brain as thalamocortical connections become secure (Molyneaux et al., 2007). The cell bodies of subplate neurons are located in the developing white matter of all cortical regions (Kostovic and Rakic, 1990; Kanold, 2009). Subplate neurons are a transient population of neurons in the developing white matter that help secure the connection and relay feedforward excitatory transmission from the thalamus to the cortex (Kanold et al., 2003; Kanold, 2009; Tolner et al., 2012). Over development, the subplate axons serve as a guide for growing thalamocortical axons, and eventually these subplate neurons die off as the species matures (Allendoerfer and Shatz, 1994; Kanold and Luhmann, 2010). Thus to investigate functional connectivity changes in auditory cortex for input to L4 neurons, we used a thalamocortical slice preparation of auditory cortex and mapped the differences in the spatial distributions of L4 input. We find that development results in expansion and strengthening of excitatory inputs from L2/3 and within L4, but with more emphasis on L4 excitatory inputs of auditory cortex. We also find that development results in expansion and strengthening of inhibitory inputs from L2/3 and within L4, but with more emphasis on L2/3 inhibitory inputs. We also find that expansion of excitation compared to inhibition within L4 and a strengthening of inhibition from L2/3 and within L4 as a result of development. Thus while basic intracortical circuitry is preserved throughout development, in the Sprague Dawley rat, we find subtle changes in the distribution of inputs to layer 4 as well as the strengths of excitatory and inhibitory inputs.

Results:

Development results in expansion and strengthening of excitatory inputs from L2/3 and within L4, but with more emphasis on L4 excitatory inputs

Because SPNs project to L4 and excite L4 (Zhao et al., 2009; Viswanathan et al., 2016), and SPNs are important for the maturation of L4 circuitry, we investigated if functional circuitry of L4 of the primary auditory cortex (A1) refined in the rat model. We recorded from L4 neurons (N = 76 cells, 40 from P5-10 and 36 from P18-23) and performed LSPS (Fig. 2.3) in A1. Since L4 cells in A1 receive most of their input from subplate, L4, and L2/3, we focused on mapping supragranular and granular layers. Over development from P5-10 to P18-23, we find that the total area of excitatory input to layer 4 expanded from L2/3 and within L4 (Fig. 4.1D). With respect to the mean EPSC charge to L4, (Fig. 4.1E) both layer 2/3 and L4 excitatory postsynaptic charge weakened, but it weakened significantly more within L4 compared to L2/3 as the brain matured. When examining the rostral-caudal extent along the tonotopic axis, the excitatory input to L4 expanded from both L2/3 and within L4 for EPSCs (Fig. 4.1G), but more so from within L4.

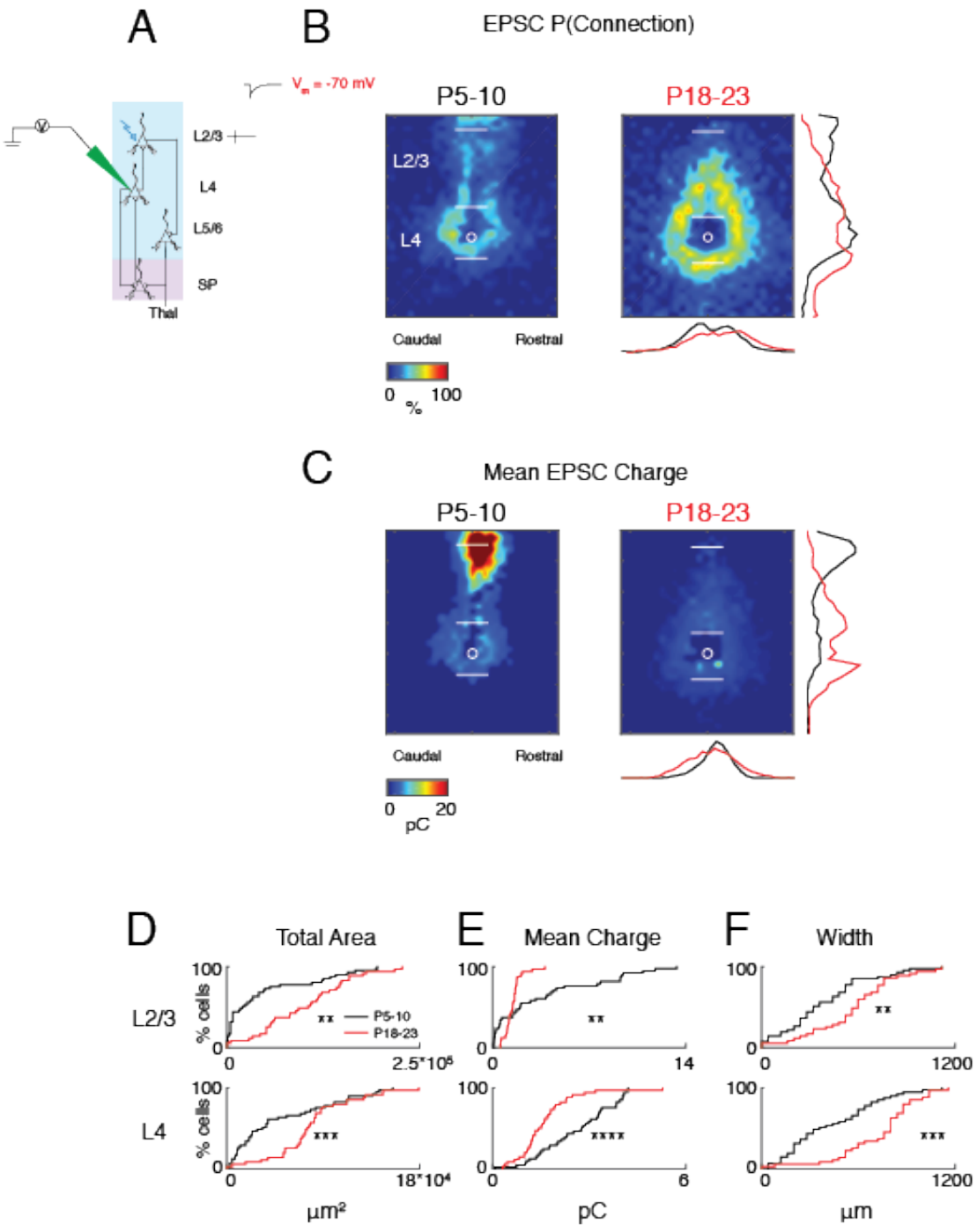
A
B
EPSC P(Connection)
V_m = -70 mV
L2/3
L4
L5/6
SP
Thal
P5-10
P18-23
L2/3
L4
Caudal
Rostral
0
100
%
C
Mean EPSC Charge
P5-10
P18-23
Caudal
Rostral
0
20
pC
D
Total Area
E
Mean Charge
F
Width
L2/3
L4
% cells
100
0
P5-10
P18-23
**
***
****
2.5*10^5
18*10^4
14
6
1200
µm²
pC
µm

Figure 4.1: Development results in expansion and strengthening of excitatory inputs from L2/3 and within L4, but with more emphasis on L4. A. Reference view of electrode positioning in the layer recorded and example laser photostimulation location (photostimulation from pia to L4- see methods for more details). **B.** Spatial distribution of sites of excitatory input to L4 neurons that alter as the circuitry matures from P5-10 to P18-23. Probability of connection occurrence P(Connection) for excitatory (-70 mV) activity. **C.** Spatial distribution of transferred charge (Mean EPSC Charge) for excitatory (-70 mV) activity. **D-F.** Cumulative distribution function (CDF) of excitatory input to L4 neurons. Layer totals for area (left), mean transferred charge (middle), and marginal width along rostral-caudal axis (right) for L2/3 and L4 input to the recorded L4 neuron. Horizontal bars indicate layer boundaries and serve as scale bar of 200 um. Black and red overlaying traces on the side of the maps indicate summed EPSC marginal distributions for each group. Total area L2/3: p=2.319427e-04; total area L4: p=1.184074e-04. Mean charge L2/3: p=4.029553e-03; mean charge L4.

Development results in expansion and strengthening of inhibitory inputs from L2/3 and within L4, but with more emphasis on L2/3 inhibitory inputs

Over development from P5-10 to P18-23, we find that the total area of inhibitory input to layer 4 expanded from L2/3 and within L4 (Fig. 4.2D), with most of the expansion of inhibitory input arising from L2/3. When looking at the mean IPSC charge within the layer for inhibitory GABAergic input to L4 neurons, (Fig. 4.2E) both layer 2/3 and L4 inhibitory postsynaptic charge strengthened, but it strengthened more significantly from L2/3 compared to L4 as the brain matured. When examining the rostral-caudal extent along the tonotopic axis with the rostral end for high frequencies and the caudal end of low frequencies, the inhibitory input to L4 expanded from both L2/3 and within L4 for EPSCs (Fig. 4.2G), but with more emphasis on expansion along that axis arising from L2/3.

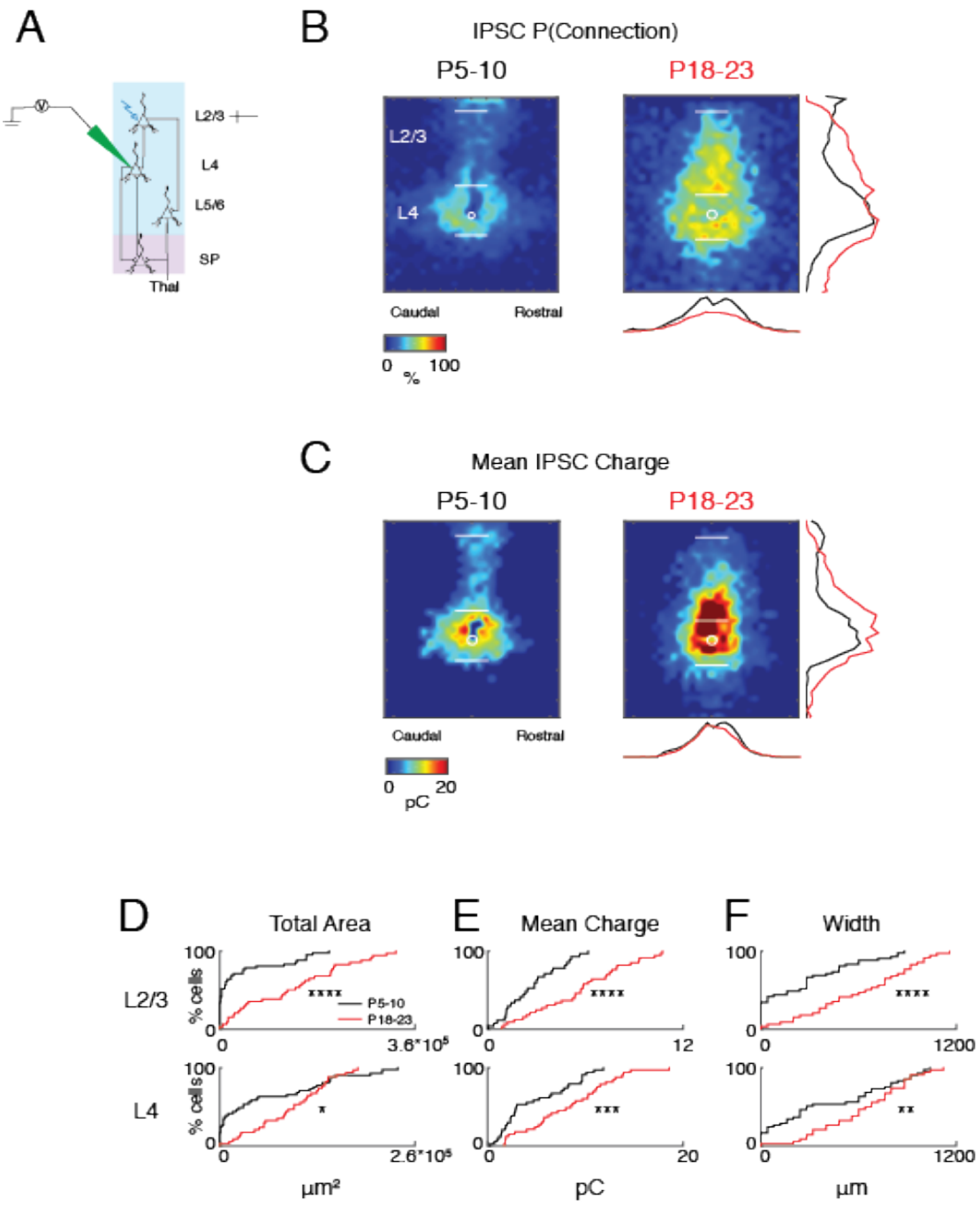
A
L2/3
L4
L5/6
SP
Thal
B
IPSC P(Connection)
P5-10
P18-23
L2/3
L4
Caudal
Rostral
0
100
%
C
Mean IPSC Charge
P5-10
P18-23
Caudal
Rostral
0
20
pC
D
Total Area
E
Mean Charge
F
Width
L2/3
L4
% cells
100
0
****
P5-10
P18-23
3.6*10⁵
2.6*10⁵
12
1200
*
***
**
µm²
pC
µm

Figure 4.2: Development results in expansion and strengthening of inhibitory inputs from L2/3 and within L4, but with more emphasis on L2/3 inhibitory inputs **A.** Reference view of electrode positioning in the layer recorded and example laser photostimulation location (photostimulation from pia to L4- see methods for more details). **B.** Spatial distribution of sites of inhibitory input to L4 neurons that alter as the circuitry matures from P5-10 to P18-23. Probability of connection occurrence P(Connection) for inhibitory (0 mV) activity. **C.** Spatial distribution of transferred charge (Mean IPSC Charge) for inhibitory (0 mV) activity. **D-F.** Cumulative distribution function (CDF) of inhibitory input to L4 neurons. Layer totals for area (left), mean transferred charge (middle), and marginal width along rostral-caudal axis (right) for L2/3 and L4 input to the recorded L4 neuron. Horizontal bars indicate layer boundaries and serve as scale bar of 200 μm. Black and red overlaying traces on the side of the maps indicate summed IPSC marginal distributions for each group. Total area L2/3: p=2.374118e-06; total area L4: p=3.976349e-02; mean charge L2/3:

For excitatory input to layer 4 neurons over development, by P18-23 the total amplitude of EPSCs within only L4 increased drastically (Fig. 4.3A). With respect to the mean EPSC amplitude over each separate layer, we see the same increase for EPSC input within only L4. When we consider the inhibitory input to L4, we see the same increase by the same factor within L4 for the total amplitude of IPSCs (Fig. 4.3B). For the total charge of IPSCs for input to L4, we see increases in both L2/3 and within L4, but more so from arising from L2/3 inputs. When we take the average of the IPSC amplitudes for input to L4, there is a drastic increase in the mean amplitude of IPSCs for P18-23 from L2/3 and L4.

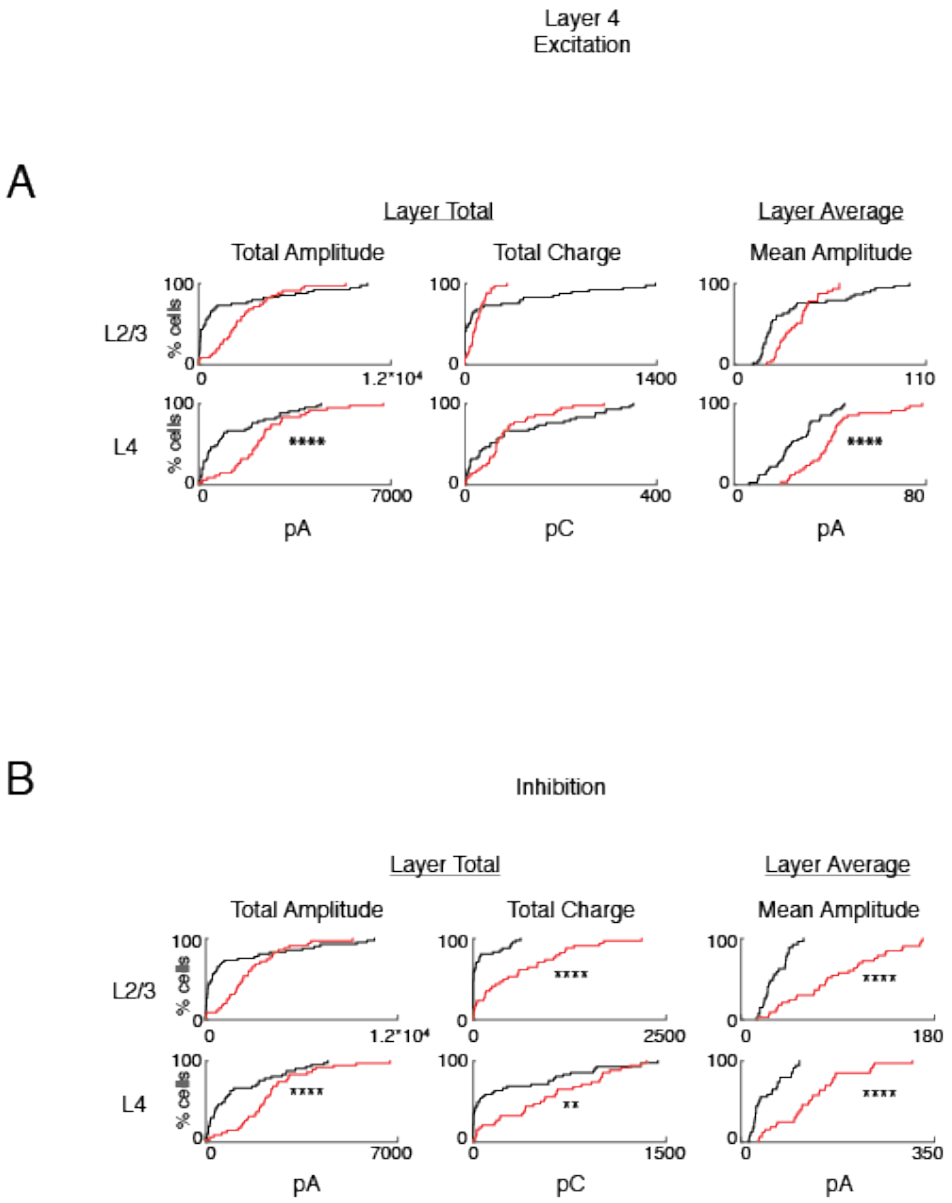

Figure 4.3: By P18-23, EPSC and IPSC amplitudes increase within L4 and total charge of IPSC increases from L2/3 and within L4. Cumulative distribution functions of layer totals and layer averages for excitatory input and inhibitory input to L4 neurons over development. Layer totals for amplitude of PSCs (left), transferred charge (middle), and mean amplitude (right) for L2/3 and L4 input to the recorded L4 neuron. **A.** For excitatory input (EPSC), total amplitude L2/3: p=1.332597e-01; total amplitude L4: p=4.397362e-05; total charge L2/3: p=5.477427e-02; total charge L4: p=1.994736e-01; mean amplitude L2/3: p=6.381987e-01; mean amplitude L4: p=1.824287e-06. **B.** For inhibitory input (IPSC), total amplitude L2/3: p=1.332597e-01; total amplitude L4: p=4.397362e-05; total charge L2/3: p=5.057224e-06; total charge L4: p=9.767643e-03; mean charge L2/3: p=5.967257e-08; mean charge L4: p=2.808682e-08.

Expansion of excitation compared to inhibition within L4 and a strengthening of inhibition from L2/3 and within L4 as a result of development

With respect to the distribution of excitatory input to inhibitory input over development, the input area to layer 4 resulted in an increased excitatory-inhibitory ratio (EI ratio) within L4 (Fig. 4.4A, B). This indicates an expansion in excitatory input area from within L4. With respect to the charge, development resulted in a decrease in the EI ratio, and thus a strengthening of the inhibition arising from L2/3 and from within L4. This indicates an increase in the inhibitory synaptic charge for both layers. However, there was considerably stronger inhibitory input arising from L2/3 compared to L4 (Fig. 4.4A, B).

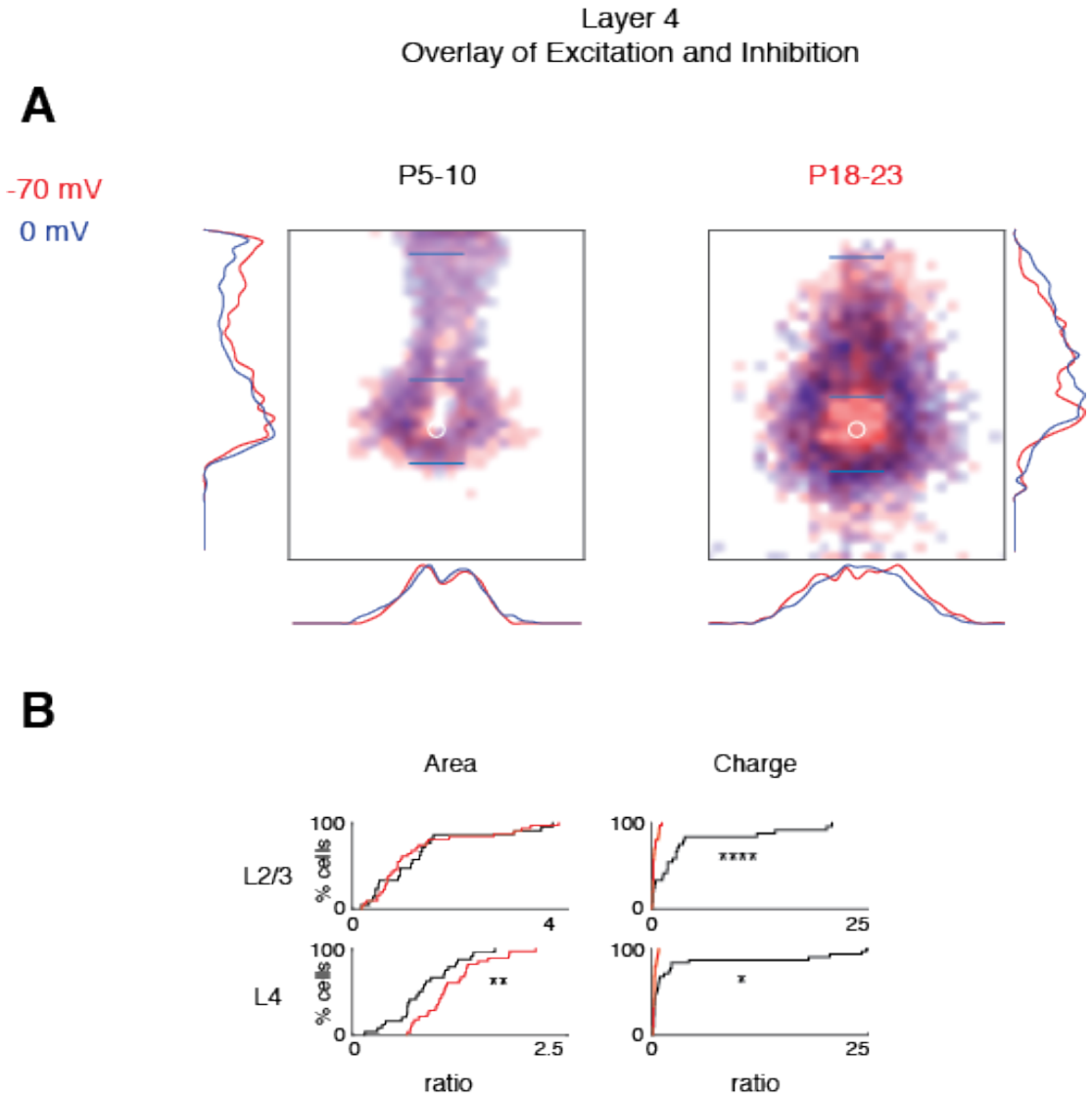

Figure 4.4: Expansion of excitation compared to inhibition within L4 and a strengthening of inhibition from L2/3 and within L4 as a result of development. A. Summary schematic of excitatory and inhibitory input to L4 neurons superimposed (P5-10 left, P18-23 right). Red color represents excitatory input, and blue color represents inhibitory input to L4. Red and blue overlaying traces on the sides of the maps indicate summed EPSC and IPSC marginal distributions. Blue scale bar denotes 200 μm. **B.** Cumulative distribution function (CDF) of the ratio of excitatory to inhibitory input as it changes over development for both area (left) and charge (right) for L2/3 and L4. Area L2/3: p=3.074280e-06; area L4: p=8.680023e-03; charge L2/3: p=5.271073e-06; charge L4: p=1.031183e-02.

Additionally, development causes an increase in the width along the rostral-caudal axis of excitatory and inhibitory charge. Over development by P18-23, there is an increase in the width of the EPSC charge extent arising from L2/3 and within L4 along the rostral-caudal axis of primary auditory cortex (Fig. 4.5A). However for inhibition, development by P18-23 results in an increase in the width of IPSC charge extent arising from L2/3 only (Fig. 4.5B). Thus development causes an increase in the width along the rostral-caudal axis of excitatory and inhibitory postsynaptic charges.

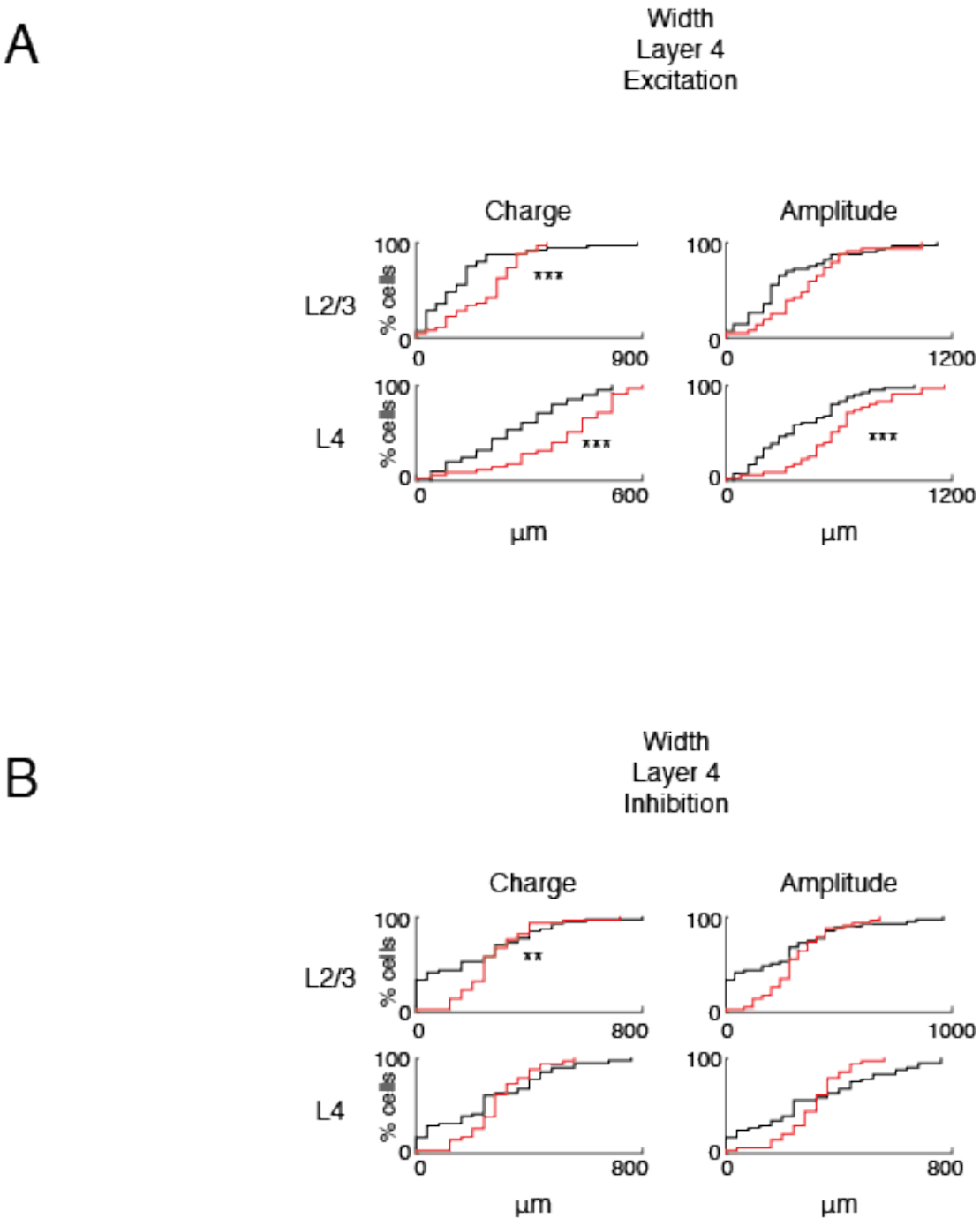

Figure 4.5: Development causes an increase in the width along the rostral-caudal axis of excitatory and inhibitory charge. Cumulative distribution functions for excitation (A) and inhibition (B) for input to L4. **A.** For excitatory input, charge L2/3: p=5.785724e-04; charge L4: p=2.951038e-04; amplitude L2/3: p=7.486126e-02; amplitude L4: p=5.356131e-04 **B.** For inhibitory input, charge L2/3: p=2.549075e-03; chargeL4: p=4.439721e-01; amplitude L2/3: p=1.360446e-01; amplitude L4: p=8.796482e- 01.

Discussion:

Here we show that over development form P5-23 rat, there are distinct laminar changes in the excitatory and inhibitory inputs to layer 4 neurons. From previous studies, we know that SPNs are the first to receive thalamic input and project that to L4 (Zhao et al., 2009). Thus we were interested in investigating the developmental differences in the functional circuitry of L4. The functional microcircuit changes we find were more pronounced within layer 4 with respect to excitatory input, and arising from L2/3 with respect to inhibitory input to L4. The rodent auditory critical period begins around P11-12 and does not extend beyond the first postnatal month (Zhang et al., 2001). Thus development reveals a hyperconnectivity of excitatory and inhibitory input from L2/3 and L4 as the circuits mature through the auditory critical period. Importantly, L4 neurons receive functional synaptic input from L2/3 and within L4 as early as P5, which is before the onset of hearing. In addition, the expansion along the rostral-caudal extent from P5-10 to P18-23 suggests broader tuning across the primary auditory cortex. However the different types of input, excitatory compared to inhibitory, are focused in a differential laminar manner. For excitatory input, there is expansion along the rostral-caudal axis, but even more concentrated within L4 along the laminar extent. However while there is maturation and strengthening of inhibitory input to L4, the expansion along the width of the auditory cortex is also columnar but the inhibitory input expands to a greater degree within the laminar L2/3 extent. From this study, we are able to show that while the basic circuitry of L2/3 to L4 is conserved through

development in the auditory cortex of the rat, excitation and inhibition adjust in similar manners but additionally extend their inputs distinctly along different laminae.

Over development, we observed differential changes in the excitatory and inhibitory circuits of L4 neurons. For proper brain function, it is important that there is a balance of excitation to inhibition otherwise imbalance can result in seizures. Thus we tested if development resulted in an imbalance of excitation to inhibition. Therefore we take the ratio of excitation to inhibition (EI ratio) to investigate if the balance of this activity shifted. We find that with respect to the input area from L2/3, the EI ratio was balanced, but the EI ratio within the laminar extent of L4 was imbalanced. Specifically, within L4, the EI ratio increased thus revealing an increase in the excitatory component within L4. We also find that the strength of these connections (charge) shifted the EI ratios in both layer 2/3 and L4. However the shift of the EI ratio for the charge revealed a lower EI ratio and thus a larger inhibitory component. Additionally, there was an even greater shift of the EI ratio from L2/3, thus there was more emphasis on the EI ratio shifting from the supragranular layer. This may be due to the increase in the lateral connections for inhibitory input from L2/3. Thus the lateral connectivity expansion focuses more on the increase in inhibition over development. Additionally, while the EI ratios are imbalanced, our results suggest that the increase in IPSC charge from L2/3 and L4 are what prevent the brain from developing seizures as the circuitry expands from P5. Also, our results show that spatially in the map of the EI ratios, the overlay of excitation to inhibition is equally distributed.

We also investigated the changes in the charge and amplitude of the EPSC and IPSC along the rostral-caudal axis over development. We find that while the average charge of the EPSCs decreased in L2/3 and L4 through development, the width of the charge expanded along L2/3 and L4. Averaging the charge in L2/3 and in L4 separately reduces the emphasis of hot spots of sparse localized input, however the width CDFs provide us information on the lateral expansion of connections regardless of hot spots. Thus this widening of the charge across the lateral dimension of the layer suggests a widening in the auditory tuning of L4 across the rostral-caudal axis on a microcircuit level.

Since we know that SPNs receive input from the thalamus and project to L4 in a thalamocortical manner (Zhao et al., 2009), we also know that there are corticothalamic projections from L4 back to the subplate in somatosensory cortex (Viswanathan et al., 2016). Our results suggest that the primary auditory cortex undergoes considerable changes in regulating excitatory and inhibitory inputs to layer 4 based on a laminar preference. While the basic columnar inputs from L2/3 to 4 are preserved, emphasis on L2/3 for lateral inhibition, and L4 for excitation, adjust throughout development. Therefore this highlights the functional microcircuit changes throughout the auditory critical period in the developing rat.

Chapter 5: Neonatal hypoxia-ischemia causes functional intracortical circuit changes in developing rat auditory cortex

Abstract:

Normal brain development is requires the proper maturation of neural circuits for normal cognitive functioning. White matter brain injury during development results in disruption of normal brain maturation and consequently increases risk of developing these disorders such as epilepsy and cerebral palsy. Neonatal hypoxia-ischemia (HI) causes brain damage selective to different brain structures over development, and in the preterm human HI results in damage to subcortical developing white matter, a condition referred to as periventricular leukomalacia (PVL). HI can damage neurons in the developing white matter, subplate neurons (SPNs). SPNs are among the first cortical neurons to be born and are necessary for normal functional development of the cerebral cortex. Thus, while it is clear that SPNs play a major role in the maturation of developing brain circuitry, it is unclear how HI alters SPN circuits. Moreover, it is unknown if Mild HI injuries that do not cause overt histological changes in the cortex can alter SPN circuits. Using a rat HI model we induced either Mild or Moderate HI at P1. While Moderate HI resulted in a slight loss of SPNs mild HI did not. We used laser-scanning photostimulation (LSPS) in acute thalamocortical slices of rat auditory cortex during P5-10 to study the functional connectivity of SPN and layer 4 neurons in both injury categories. Both severities of HI result in hyperconnectivity of excitatory and inhibitory circuits to SPNs. Mild HI did not alter connectivity within layer 4. In contrast, Moderate HI also

causes hypoconnectivity of excitatory and inhibitory connections to layer 4 while. Our results suggest that SPNs are uniquely susceptible to HI and that HI causes a rearrangement of SPN circuits. Given the unique role of SPNs in thalamocortical development, our results suggest that the altered SPN circuits lead to the abnormal cortical function observed after HI.

Introduction:

Early birth or disruptions of prenatal brain development result in increased risk of cognitive impairments. For example, hypoxic-ischemic brain injuries commonly affect attention, memory, executive function, and speed of processing depending on the severity of the injury (Anderson and Arciniegas, 2010). While in-utero, the embryo is very vulnerable to injuries and insults that have potential to cause long-term health problems and disorders such as cerebral palsy and epilepsy (Jantzie et al., 2014). Hypoxia-Ischemia (HI) is a disorder in which the preterm infant undergoes a lack of oxygen and blood flow to the brain. About 0.2-0.3 percent of the 4 million infants born per year develop moderate hypoxia-ischemia encelphalopathy (HIE), with mortality rates of about 6-30 percent (Raghuveer and Cox, 2011). Specifically, injury to the premature white matter of the brain results in disruption of the normal maturation of the brain and consequently increases risk of developing cerebral palsy and epilepsy in infants (Rumajogee et al., 2016). While cortical activity is impaired (Ranasinghe et al., 2015), it is unclear which specific circuits are affected by HI and how this change is translated in reduced overall network activity.

One key neuronal circuit present in early cortical development whose damage results in abnormal brain function is formed by subplate neurons (SPNs). SPNs are a largely transient neuronal structure that is highly overrepresented in humans (Kanold and Luhmann, 2010). SPN lesions have been shown to prevent the functional maturation of thalamocortical circuits, normal sensory responses, and alter plasticity during the critical period (Kanold et al., 2003; Kanold and Shatz, 2006; Tolner et al., 2012). Particularly, SPN ablations prevent the development of early oscillatory cortical activity patterns (Tolner et al., 2012). In addition, HI injuries lesion a fraction of SPNs (McQuillen et al., 2003) and lead to abnormal functional cortical responses reminiscent of the effects of SPN lesions (Kanold et al., 2003; Kanold and Shatz, 2006; Failor et al., 2010; Tolner et al., 2012; Ranasinghe et al., 2015). Normal functional responses in sensory cortices depend on mature thalamocortical and intracortical circuits. While the effects of SPN damage on thalamocortical circuits have been established, effects on intracortical circuits are unknown.

To determine if HI has effects beyond SP lesions and if SPN damage from HI causes a change in intracortical circuits, we analyzed the functional spatial connection patterns of SPNs and layer 4 (L4) neurons during postnatal day (P) 5-10 using laser-scanning photostimulation (LSPS) in a thalamocortical slice preparation of auditory cortex (ACX). Specifically, we compared connection patterns for excitatory and inhibitory connections in cells from animals that underwent two different severities of neonatal (P1-2) HI and control animals. We find that HI causes changes in both excitatory and inhibitory circuits associated with SPN and L4 neurons. In particular, we find that Severe/Moderate HI causes cortical shrinkage combined with local

hyperconnectivity of SPN circuits and local hypoconnectivity of L4 circuits. In contrast, Mild HI did not result in overt anatomical changes but nevertheless caused hyperconnectivity in SP. We also find that Mild HI results in a strengthening of subplate inhibitory activity and the more severe form of HI results in a weakening of the layer 4 connectivity. Thus, both severities of neonatal HI cause major changes in cortical circuits in both the subplate and in thalamorecipient layer 4.

Results:

Neonatal Hypoxia-ischemia can cause cortical shrinkage

We sought to investigate the influence of HI on SPN circuits. Since the effects on SPNs and other neurons might depend on the amount of injury, we investigated the effect of different amounts of injury by utilizing two different surgical techniques to induce the ischemia: cauterization, which causes a temporary ischemia (Mild HI), compared to suture ligation for permanent ischemia (Mod HI). We first assessed the severity HI resulting from our two different procedures. Prior studies distinguished three categories of brain injury due to HI: Mild, moderate, and severe based on cortical shrinkage and loss of birth labeled SPNs (McQuillen et al., 2003; Failor et al., 2010). We harvested brains at P5-P10 and used Nissl staining to differentiate laminar boundaries and to measure the extent of the cortical layers (Fig. 5.1A). We found that compared to Control, cauterization (Mild HI) did not result in cortical shrinkage [$p = 0.18$, ANOVA](Fig. 5.1B) while ligation (Mod HI) results in cortical shrinkage [$p = 0.003$, ANOVA](Fig. 5.1B). The amount of cortical shrinkage after suture ligation

was similar in degree to the moderate category defined previously (McQuillen et al., 2003; Failor et al., 2010).

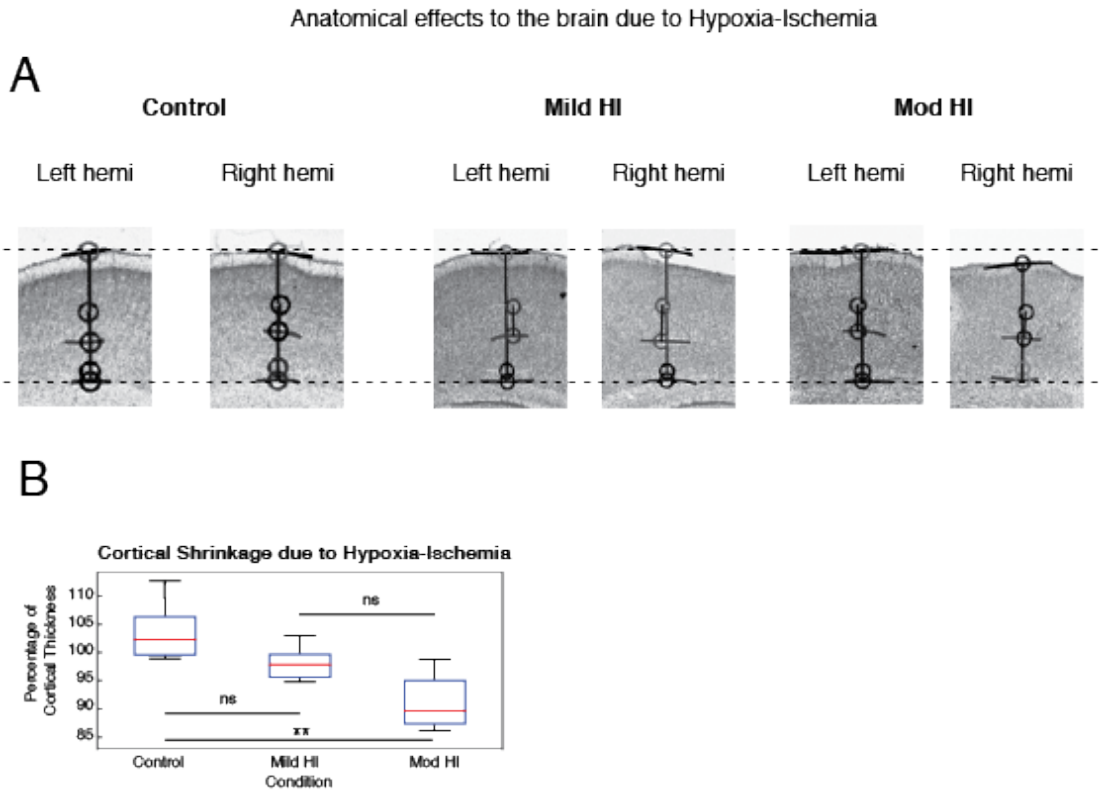

Figure 5.1: Neonatal HI injury can cause cortical shrinkage. A. Differential severities of HI injury. Examples of coronal 50 µm slices containing auditory cortex from different severities of hypoxia-ischemia. Slices were measured to obtain thicknesses of cortex. One example of each condition is pictured here. **B.** Percentage of cortical shrinkage due to hypoxia-ischemia. ANOVA reveals a significant difference in the percentage of cortical thickness between Control and Mod HI. Mod HI resulted in a significant percentage of cortical shrinkage. Mild HI did not result in a significant percentage of shrinkage compared to the control.

Behaviorally, we were able to observe seizure activity in pups with the more severe form of HI. Each morning, prior to preparing thalamocortical slices for LSPS recordings, we took three minute videos of the pups in their home cages from P5-10.

Videos were taken from a total of 34 pups (13 Control, 8 from Mild HI, and 13 from Mod HI). During those three minutes, we were able to observe seizures revealed in the shaking of the head of the pups. Sometimes the seizures were so severe that it was difficult for pups to walk properly, to the point where shaking of the body commenced and as they walked, they ended up falling over to the side. Over development, we noticed that seizures associated with HI were not observable at past P18. In the more mild form of HI, observable seizures were less prominent. In the most severe form of the HI (Mod HI), grand mal seizures were visible where the seizures began from the head and trembled down to the tip of their tails. From these criteria, we developed a seizure severity index to score the seizures observed. We used a stopwatch to record the length of time of the seizure (secs) and created a seizure time index. For example, if a seizure lasted 3-4 seconds, then the time index was 3. Thus we scored videos and found that there were significant differences between groups for the severity of the seizure and the time length of the seizures (Fig. 5.2). Specifically, the Mild HI had an increase in the severity of the seizure compared to Control, and Mod HI induced an even more severe seizure (either moderate severity or severe grand mal) (Fig. 5.2A). Additionally, Mod HI resulted in the longest seizure duration during P5-10 (Fig. 5.2B). Therefore our severities of HI similarly produce epileptic behavior as in preterm humans with HI (Lai and Yang, 2011).

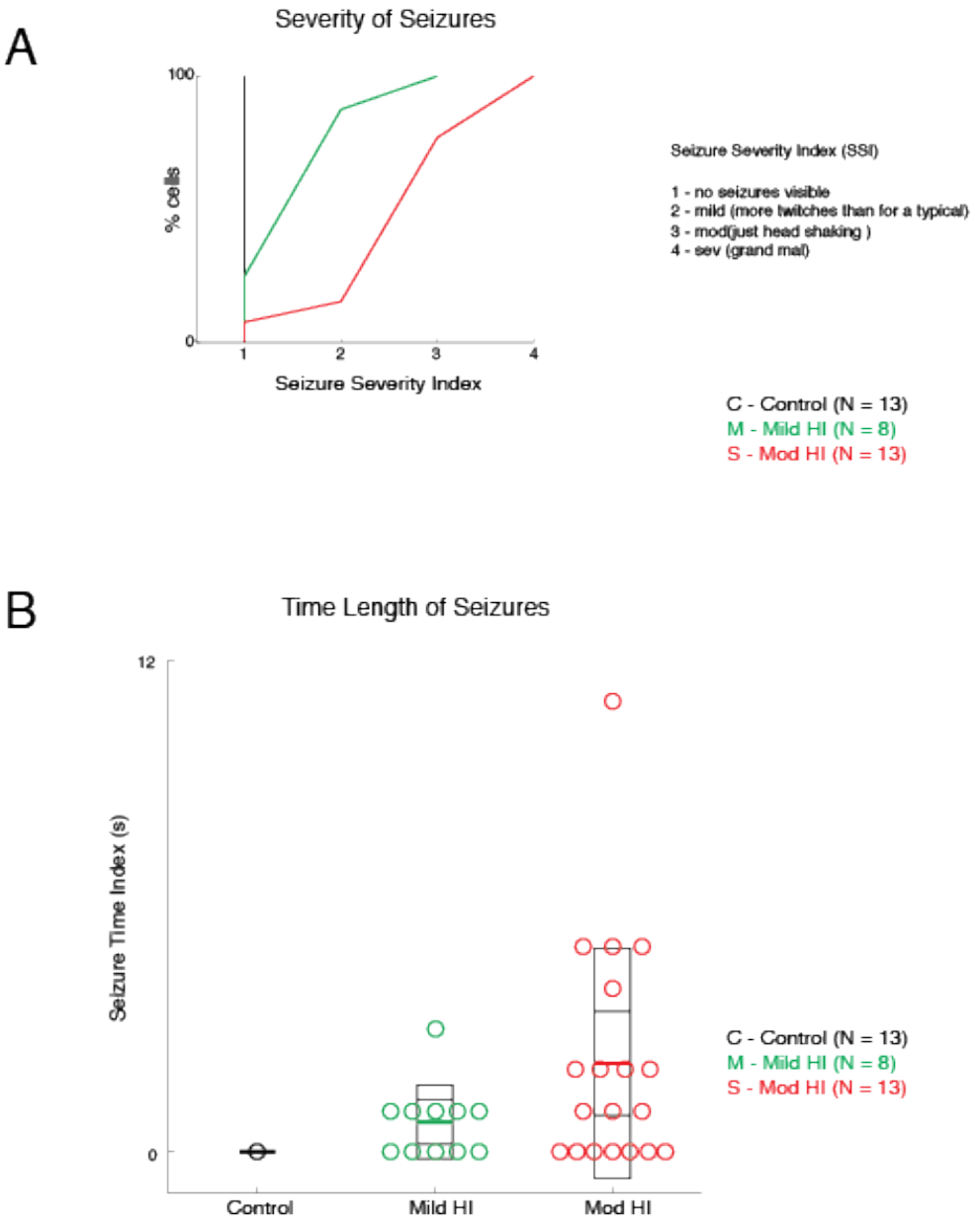

Figure 5.2: Mod HI results in greatest seizure severity and longest duration of seizure form P5-10. **A.** For the Seizure Severity Index (SSI), the index ranged from 1-4 (1: no seizures visible, 2: mild (more little twitches throughout the body than normal, 3: moderate (just the head shaking), 4: severe (grand mal seizure). Comparisons: (C-M) $p<0.01$, (C-S) $p<0.0001$, (M-S) $p<0.01$ with KS test. **B.** For the Seizure Time Index, the index represented the minimum second the seizure lasted. For example, if a seizure lasted 3-4 seconds, the seizure time index was 3. For comparisons, (C-S) $p<0.0001$ with one-way ANOVA.

Mild and Moderate Neonatal Hypoxia-Ischemia cause functional hyperconnectivity in excitatory subplate circuits from P5-10

In humans, HI can cause a variety of outcomes such as severe motor loss, fine and gross motor dysfunction, sensorineural hearing loss, speech and language development, cerebral palsy, epilepsy, and abnormalities in cognitive function(Robertson and Perlman, 2006); (Lai and Yang, 2011) likely caused by different severities of injury and related circuit changes. While we found that HI with ligation causes brain shrinkage the mild form of HI did not cause gross morphological changes. However Mild HI could have cause subtle changes in functional cortical circuits without lesioning cortical neurons. To investigate this possibility we used laser-scanning photostimulation (LSPS) of caged glutamate combined with whole-cell patch clamp recordings (Shepherd et al., 2003; Meng et al., 2014) to spatially map the connectivity of excitatory (AMPA) and inhibitory (GABA) inputs to A1 SPNs (N = 121 cells; 46 cells in Control, 38 cells in Mild HI, and 37 cells in Mod HI) at P5-P10.

We chose this age range because this is before the onset of hearing from P11-12 in the rat(Zhang et al., 2001). It is also during this timeframe that there is a high density of subplate neurons present in the developing brain (Hoerder-Suabedissen and Molnar, 2015).

In order to investigate the spatial pattern of excitatory connections to SPNs from the cortical plate of ACX, 900 stimulation sites with a spatial resolution of about 40 μm were mapped sequentially in a pseudorandom pattern (Viswanathan et al., 2012) in order to cover the entire radial extent of the cortical column from ventricle to

pia (Fig. 5.3E). By calculating the charge of the evoked excitatory postsynaptic current (EPSC), we were able to quantify the strength of the excitatory inputs to SPNs. These were plotted in two-dimensional maps of connectivity (Fig. 5.3F). In order to determine the spatial resolution of LSPS as a result of these injuries, we performed loose-patch or cell-attached recordings from SP, layer 5/6, layer 4, and layer 2/3 from P5-10 and measured the spatial distribution of stimulation sites that lead to action potentials in the recorded neuron (Fig. 5.3G).

We recorded SPNs in thalamocortical slices with the holding potential of -70 mV and 0 mV. If a connection was present between a stimulated neuron and the recorded neuron, a postsynaptic current (PSC) was revealed. During voltage-clamp recordings when the SPNs were held at -70 mV, photostimulation was able to evoke two types of responses: 1) a large inward current with short onset latency ($\leq$ 8ms); and 2) a smaller amplitude inward current with a longer latency (Fig. 5.3D). The shorter latency response is attributable to direct activation of the recorded cell while the longer latency response is dependent on synaptic release from presynaptic cells (Meng et al., 2014).

We first analyzed the excitatory circuits associated with SPNs by holding cells at -70mV. We then stimulated 900 sites for each cell and then for stimulation sites that showed evoked EPSCs measured the size of the EPSC (Fig. 5.3F) resulting in a map of excitatory connectivity for each cell. This map indicates the location of presynaptic cells to the recorded SPN.

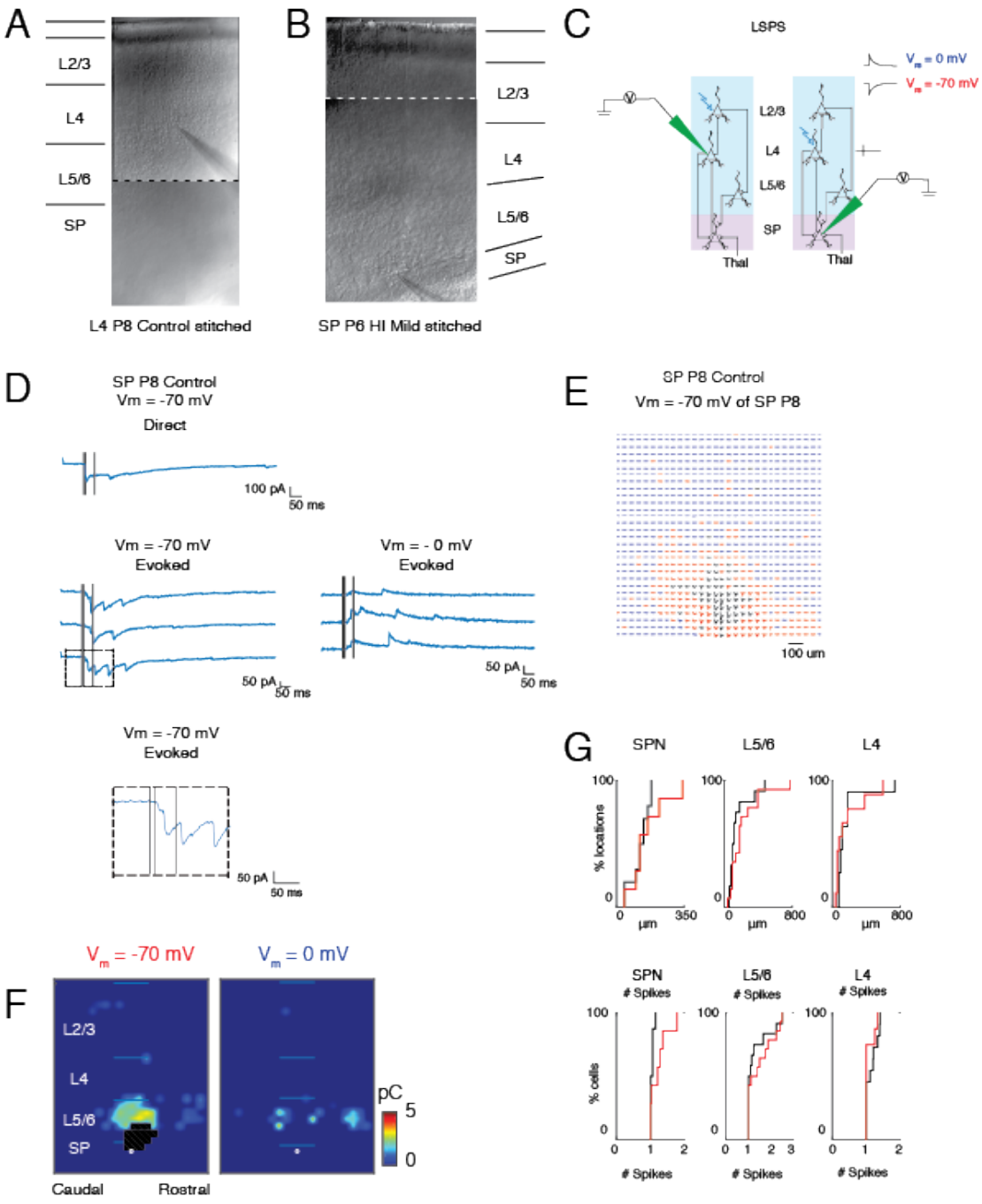
A
L2/3
L4
L5/6
SP
L4 P8 Control stitched
B
L2/3
L4
L5/6
SP
SP P6 HI Mild stitched
C
LSPS
Vm = 0 mV
Vm = -70 mV
L2/3
L4
L5/6
SP
Thal
Thal
D
SP P8 Control
Vm = -70 mV
Direct
100 pA
50 ms
Vm = -70 mV
Evoked
50 pA
50 ms
Vm = - 0 mV
Evoked
50 pA
50 ms
Vm = -70 mV
Evoked
50 pA
50 ms
E
SP P8 Control
Vm = -70 mV of SP P8
100 um
F
Vm = -70 mV
Vm = 0 mV
L2/3
L4
L5/6
SP
pC
5
0
Caudal
Rostral
G
SPN
L5/6
L4
% locations
100
0
0
µm
350
800
800
SPN
L5/6
L4
Spikes
% cells
100
0
0
1
2
3
Spikes

Figure 5.3: LSPS and mapping method of intracortical connections of L4 and SPNs. **A.** Infrared DIC image of a thalamocortical brain slice of a P8 rat with a patch pipette on a layer 4 neuron. Because the 10X magnification field of view was smaller than the entire brain slice, multiple images were taken along the entire cortical extent into the hippocampal region in order to show the location of the pipette along the rostral-caudal axis with respect to the hippocampus (stitched). **B.** Infrared stitched DIC image of a thalamocortical brain slice of a P6 rat with a patch pipette on a SPN. **C.** Reference view of electrode positioning in the layer recorded and example laser photostimulation location for both SPNs and L4 neurons (photostimulation from pia to L4- see methods for more details). **D.** Whole-cell voltage clamp recordings at holding potentials of -70 mV and 0 mV of a P8 SPN distinguish between photostimulation-evoked excitatory and inhibitory currents. Shown are example traces obtained with photostimulation at different locations. The solid black lines on the blue traces indicate the time of the photostimulation; far left marks time 0 ms, next to it marks 8-ms, and left of that marks 50-ms post stimulus. 8 ms is the minimum latency for synaptic responses, and 50 ms marks the end of the analysis window. **E.** These are traces obtained by LSPS when hold one P6 L4 neuron at -70 mV. Traces in black show large-amplitude direct responses. Postsynaptic responses from 8 to 50 ms are the red traces, and the rest of the traces are in blue. **F.** Pseudocolor maps of a P6 L4 neuron show postsynaptic current (PSC) charge at each stimulus location for 1 example layer 4 neuron. Direct responses in black were set to zero pC. The white filled circle indicates the location of the soma and the horizontal bars indicate the layer boundaries and serve as scale bars of 200 μm. **G.** Distribution of distance within which 80% of action potentials were evoked (top) and number of evoked action potentials (bottom: spike count). Top: SPN p=3.440298e-01, L5/6 p=4.361332e-01, L4 p=2.074770e-01. Spike count (bottom): SPN p=7.230557e-02, L5/6 p=7.502278e-01, L4 p=7.337290e-01. Cell-attached cells: Control N = 37 cells (SP (N = 16), L5/6 (N = 15), L4 (N = 18); Mod HI N = 41 cells (SP (N = 16), L5/6 (N = 15), L4 (N = 17)).

We then aligned the maps to the soma position and calculated for every spatial location the probability of being connected to a given SPN resulting in a spatial connection probability map (Fig. 5.3F). Compared to Control, Mild HI qualitative inspection showed that excitatory input to the recorded SPNs seemed expanded in HI possibly indicating hyperconnectivity. Quantification of the total cortical area that gave rise to excitatory inputs to SPNs confirmed that both HI conditions caused a hyperconnectivity of excitatory inputs to SPNs (Fig. 5.4D). We next calculated the mean size of EPSCs evoked from a particular location (Fig. 5.4C), which looked similar between conditions. We next sought to identify which specific cortical circuits were altered. We thus analyzed separately the input from the different cortical laminae to SPNs (Fig. 5.4E). Mild HI resulted in an increase in excitatory input from with the subplate, while Mod HI resulted in a larger total area of excitatory input from L5/6 to SPNs (Fig. 5.4D). In contrast, the total charge for excitatory postsynaptic current (EPSC) to SPNs was similar regardless of condition (Fig. 5.4E).

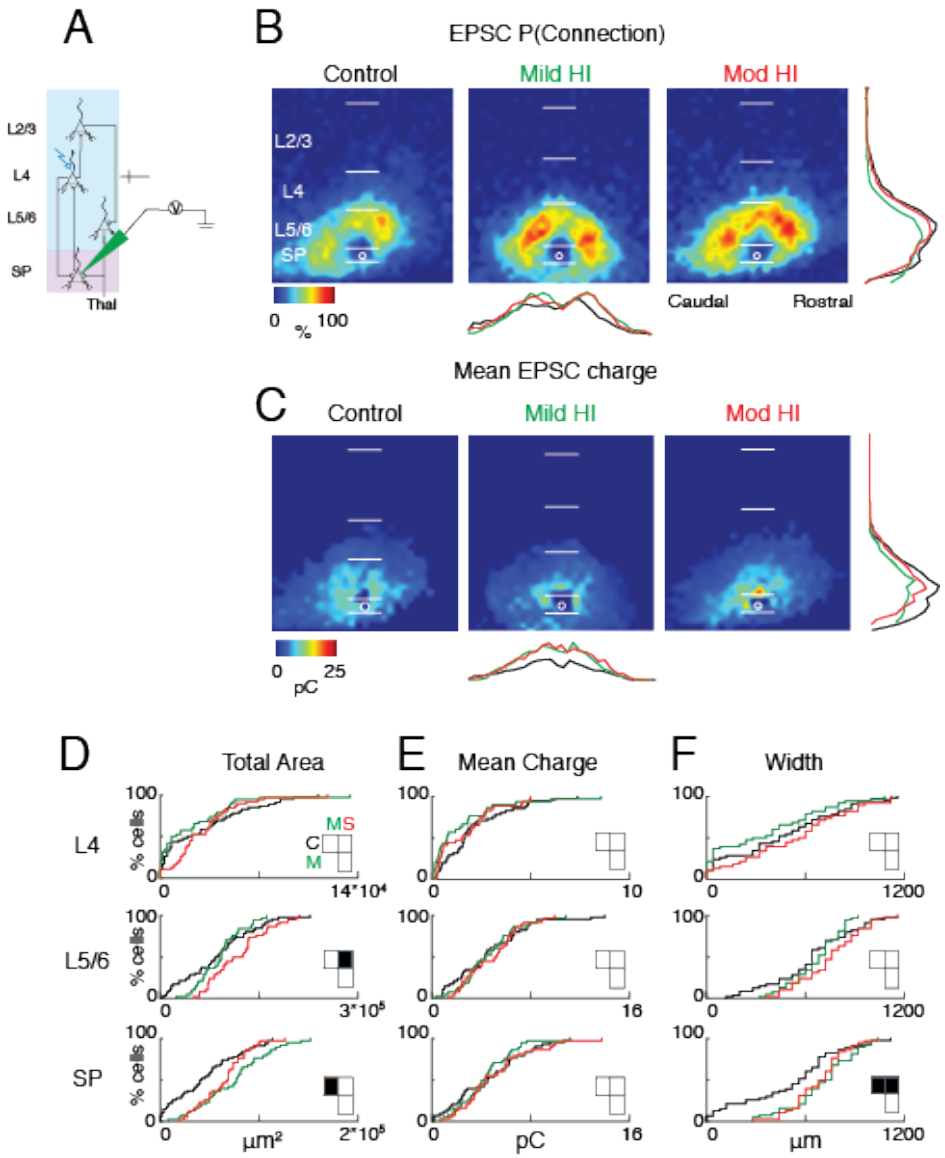

Figure 5.4: Mild HI results in hyperconnectivity of excitation in SP, while Mod HI results in hyperconnectivity of L5/6 A. Reference view of electrode positioning in the layer recorded and example laser photostimulation location (photostimulation from pia to SP- see methods for more details). **B.** Spatial distribution of sites of excitatory input to SPNs that alter due to the different HI injuries. Probability of connection occurrence P(Connection) for excitatory (-70 mV) activity. **C.** Spatial distribution of transferred charge (Mean EPSC Charge) for excitatory (-70 mV) activity. **D.-F** Cumulative distribution function (CDF) of excitatory input to SPNs. Layer totals for area (left), mean transferred charge (middle), and marginal width along rostral-caudal axis (right) for L4, L5/6, and SPN input to the recorded SPN. Horizontal bars indicate layer boundaries and serve as scale bar of 200 um. Black, green, and red overlaying traces on the side of the maps indicate summed EPSC marginal distributions for each group. Black squares in the matrix denote significance, white squares are not significant. Comparisons D) L5/6 (C-S) $P \leq 0.05$, SP (C-M) $P \leq 0.001$. E) No significant differences. F) SP (C-M) $P \leq 0.01$, (C-S) $P \leq 0.01$. C is control, M is mild, S is moderate HI.

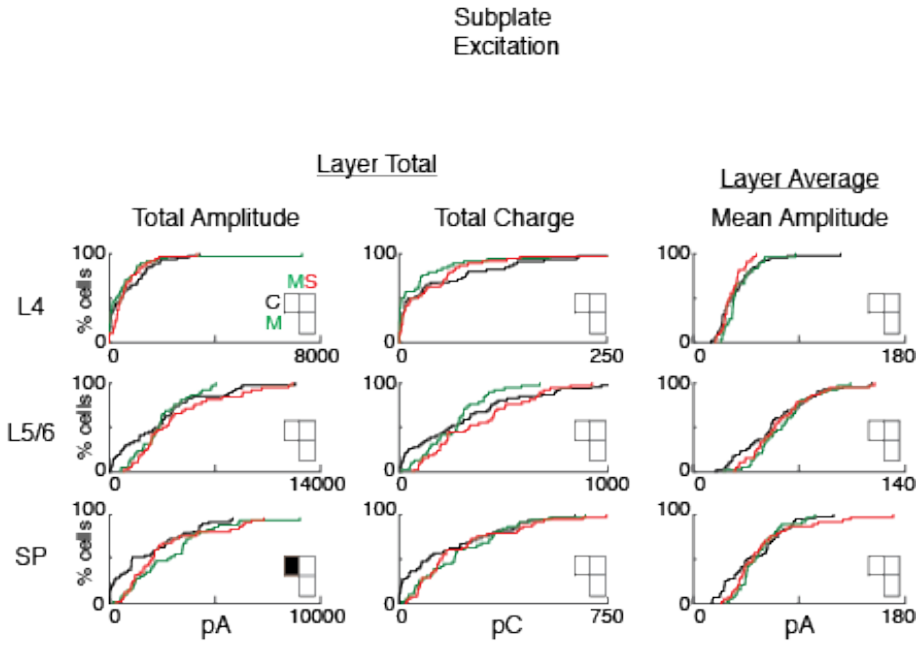

Figure 5.5) Related to figure 5.4. Layer totals for EPSC amplitude (left) and charge (right) for L4, L5/6, and SP. Layer average for EPSC amplitude (right) for L4, L5/6, and SP. SP) Total Amplitude (C-M) $P \leq 0.05$.

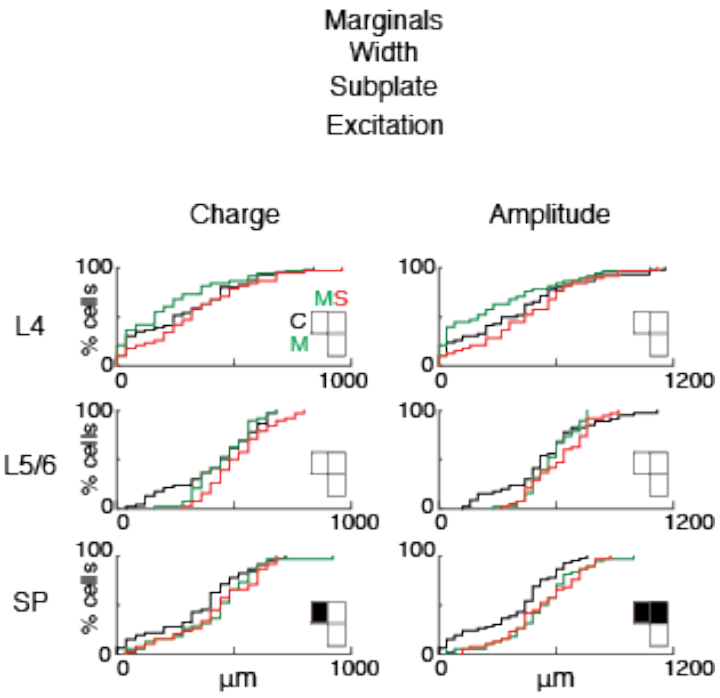

Figure 5.6) Related to figure 5.4. Marginal rostral-caudal width for EPSC for charge (left) and amplitude (right) for L4, L5/6, and SP. SP charge (C-M) $P \leq 0.01$; SP amplitude (C-M) $P \leq 0.05$, (C-S) $P \leq 0.05$.

Our results show that SPNs receive increased excitatory inputs from within SPN or L5/6 consequent to HI. Since our thalamocortical slices preserve the tonotopic axis of A1 along the lateral (columnar) dimension of the slice, the extent of inputs to a particular cells is related to the amount of integration across the different frequency areas of A1. We thus analyzed the columnar pattern of the inputs to SPNs by averaging the inputs within each rostral-caudal location and then measuring the extent of input in the rostral-caudal direction. Compared to Control, both Mild and Mod HI results in a wider marginal area of excitatory input within the subplate indicating a larger range of integration across the tonotopic axis (Fig. 5.4F).

The hyperconnectivity from within SP suggests that there are more excitatory synapses on subplate neurons, which could be due to larger dendritic area. The area that results in short-latency direct responses is a measure of the extent of the proximal dendrite and soma. Measuring the area that resulted in direct responses revealed no difference in total direct area of input to subplate between conditions suggesting that there were no large-scale changes in dendritic structure and that hyperconnectivity seen reflects an increase number of synaptic connections (Fig. 5.7C).

Therefore, both Mild and Mod HI result in hyperconnectivity of excitatory inputs to SPNs. The increase in integration across the tonotopic axis suggests that SPNs receive inputs from a wider range of frequency channels.

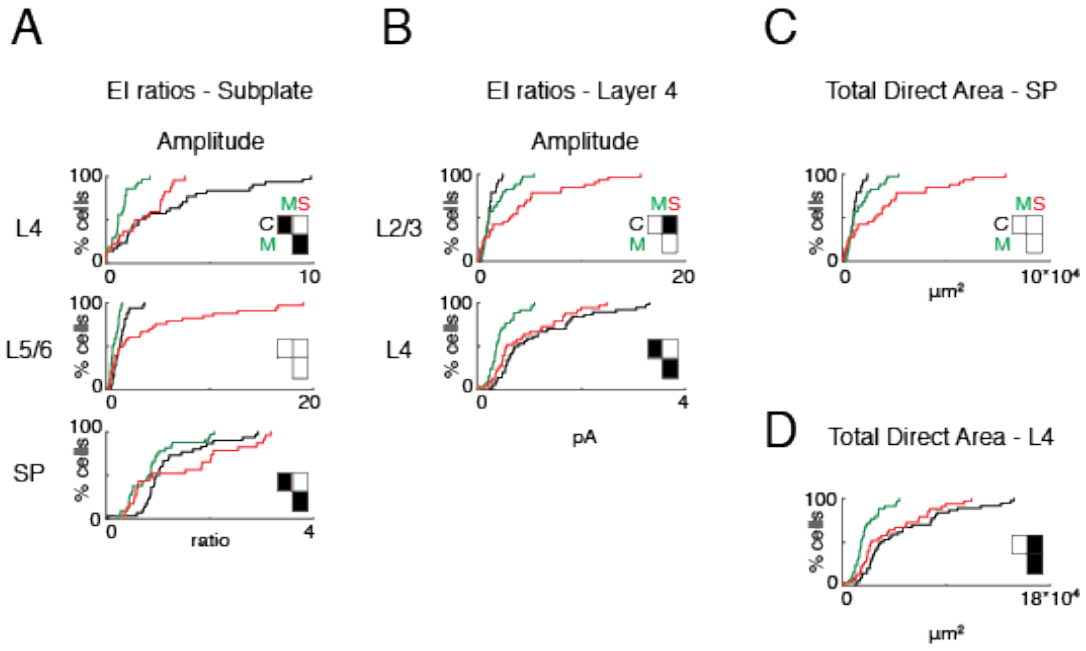

Figure 5.7 CDFs for EI ratios amplitudes and direct response areas. A. CDF of EI ratios for amplitude for SPNs. L4: (C-M) $p \leq 0.001$, (M-S) $p \leq 0.05$. SPNs: (C-M) $p \leq 0.01$, (M-S) $p \leq 0.001$. **B.** CDF of EI ratio for amplitude for L4 neurons. L2/3: (C-S) $p \leq 0.05$. L4: (C-M) $p \leq 0.0001$, (M-S) $p \leq 0.01$. **C.** Total direct response area of SPNs. **D.** Total direct response area of L4 neurons. (C-S) $p \leq 0.001$, (M-S) $p \leq 0.05$.

Mild Hypoxia-Ischemia causes functional changes in inhibitory subplate circuits from P5-10

Hypoxia-ischemia encephalopathy (HIE) results in variable severity of neuropsychological sequelae. About 25% of affected infants develop epilepsy and cerebral palsy (Lai and Yang, 2011). In our animal model, we observed seizures in our neonatal rat pups during as a result of HI and these seizures persisted until about P10 (Fig. 5.2). Since seizures are thought to be due to altered inhibition (Bromfield et al., 2006) and since HI results in decrease in parvalbumin expression levels (Failor et al., 2010) we hypothesized that GABAergic circuits were altered consequent to HI.

To test if the spatial pattern of inhibitory inputs to SPNs was altered we held cells at 0 mV and performed LSPS. Mild HI results in a larger total area of inhibitory input within the subplate to the recorded SPNs indicating that inhibitory neurons from a wider extent of cortex contact SPNs (Fig. 5.8B, D, F). In contrast, Mod HI did not result in changes to inhibitory connection probability. Therefore, Mild HI results in hyperconnectivity of inhibitory input within the subplate.

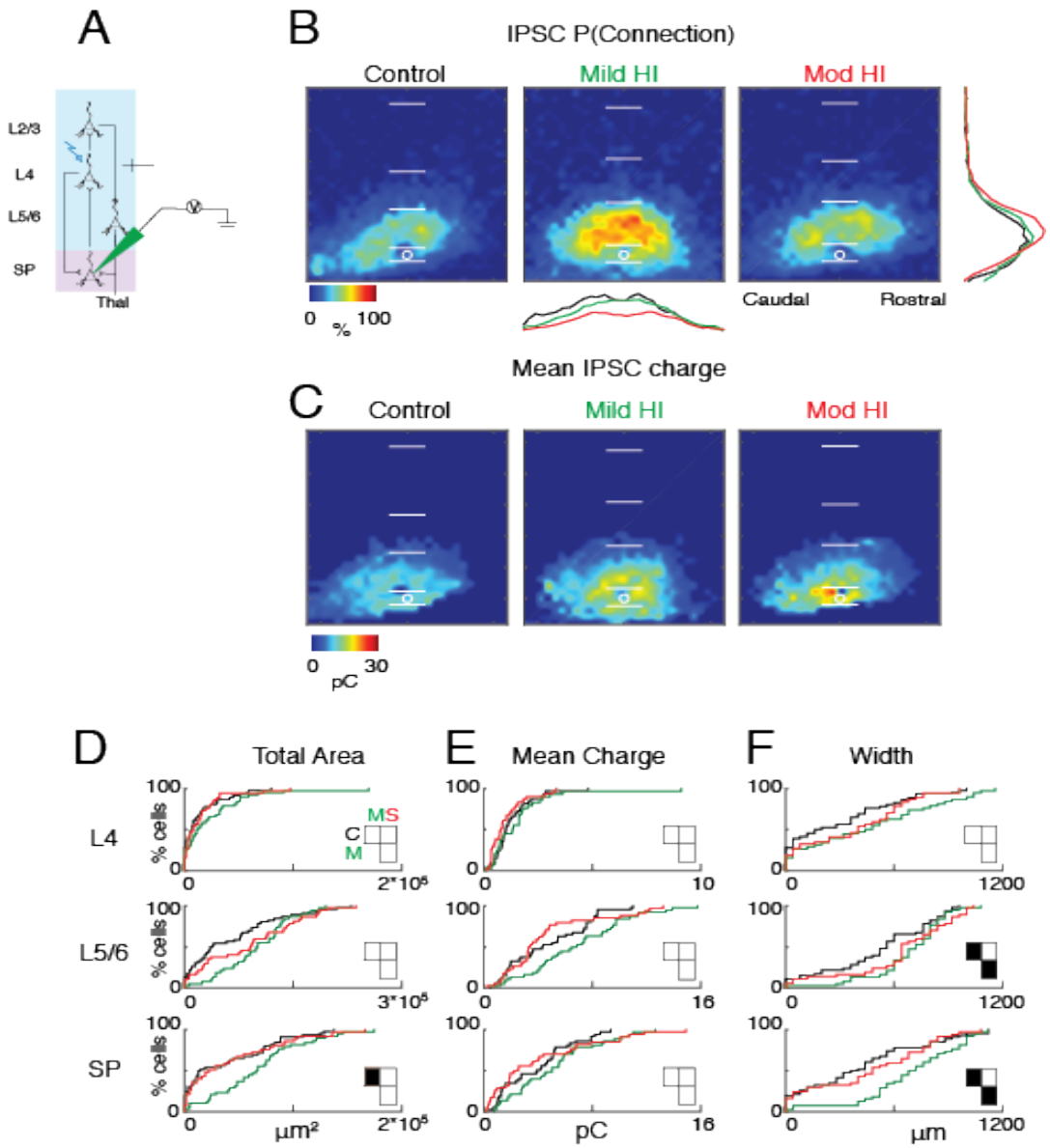

Figure 5.8: Mild HI results in hyperconnectivity of inhibition in SP A. Reference view of electrode positioning in the layer recorded and example laser photostimulation location (photostimulation from pia to SP- see methods for more details). **B.** Spatial distribution of sites of inhibitory input to SPNs that alter due to the different HI injuries. Probability of connection occurrence P(Connection) for inhibitory (0 mV) activity. **C.** Spatial distribution of transferred charge (Mean IPSC Charge) for inhibitory (0 mV) activity. **D-F.** Cumulative distribution function (CDF) of inhibitory input to SPNs. Layer totals for area (left), mean transferred charge (middle), and marginal width along rostral-caudal axis (right) for L4, L5/6, and SPN input to the recorded SPN. Horizontal bars indicate layer boundaries and serve as scale bar of 200 um. Black, green, and red overlaying traces on the side of the maps indicate summed IPSC marginal distributions for each group. Comparisons: D) SP (C-M) $p \leq 0.05$; F) L5/6 (C-M) $p \leq 0.05$; (M-S) $p \leq 0.01$; SP (M-S) $p \leq 0.001$, (M-S) $p \leq 0.0001$.

Mild HI results also results in an increase in IPSC charge compared to Control for inputs from both from L5/6 and within SP (Fig. 5.9). Compared to Control, Mild HI results in a wider marginal area of inhibitory input from L5/6 to subplate (Fig. 5.8F). In contrast, Mod HI did not result in changes to IPSC size (Fig. 5.9). Together, our results show that HI results in hyperconnectivity of excitatory as well as inhibitory circuits. Importantly Mild HI, which did not cause morphological defects on a gross histological level, results in significant changes on the level of functional connectivity.

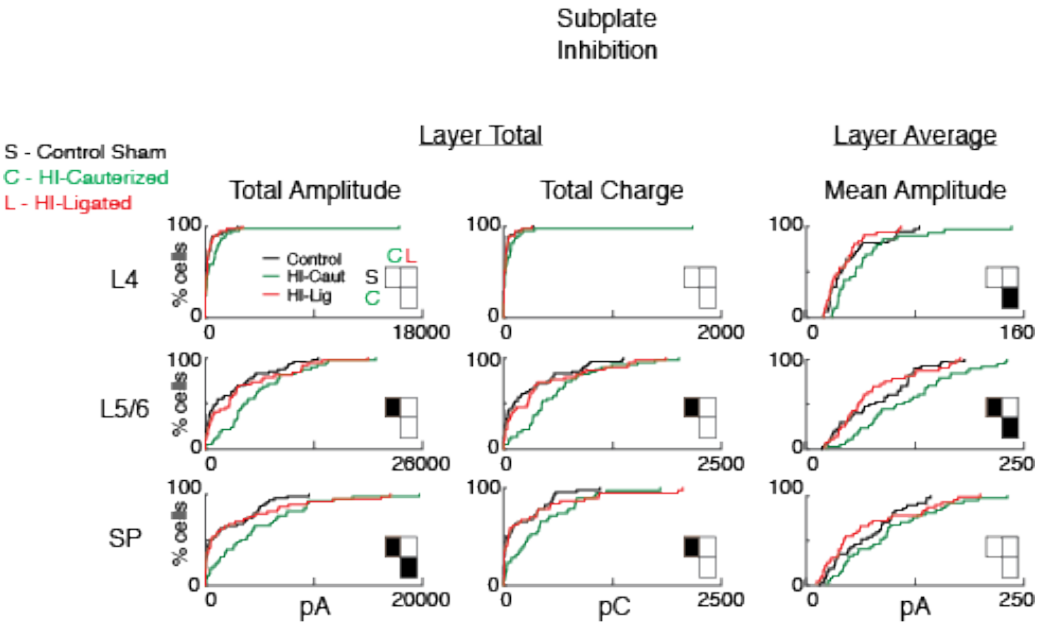

Figure 5.9) Related to figure 5.8: CDFs for layer totals of IPSC amplitude and charge for L4, L5/6, and SP. Layer average for amplitude (right) for L4, L5/6, and SP. L4 mean amplitude (M-S) $P \leq 0.05$; L5/6 total amplitude (C-M) $P \leq 0.01$; L5/6 total charge (C-M) $P \leq 0.01$; L5/6 mean amplitude (C-M) $P \leq 0.05$, (M-S) $P \leq 0.05$; SP total amplitude (C-M) $P \leq 0.01$, (M-S) $P \leq 0.05$; SP total charge (C-M) $P \leq 0.01$

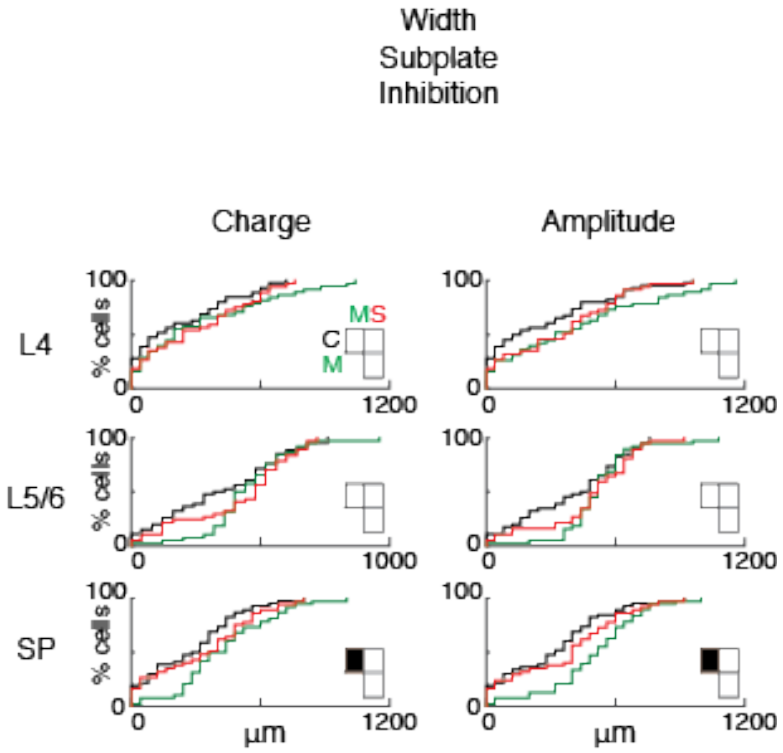

Figure 5.10) Related to figure 5.8: CDFs for marginal rostral-caudal width for IPSC for charge (left) and amplitude (right) for L4, L5/6, and SP. SP charge (C-M) $P \leq 0.01$; SP amplitude (C-M) $P \leq 0.01$.

Moderate but not Mild Hypoxia-Ischemia causes functional connectivity changes in Layer 4 from P5-10

Because the SPNs project to and excite layer 4 (L4) (Zhao et al., 2009; Viswanathan et al., 2016) and because SPNs are crucial for the maturation of L4 circuits (Kanold et al., 2003; Kanold, 2009; Tolner et al., 2012), we investigated if functional circuits within L4 also changed subsequent to HI. Similar to the SP recordings, we recorded from L4 neurons (N = 117 cells; 40 cells in Control, 39 cells in Mild HI, and 38 cells in Mod HI) and performed LSPS (Fig. 5.11, 5.14). Since A1 L4 cells receive most input from subplate, L4 and L2/3, we focused on mapping granular and supragranular layers.

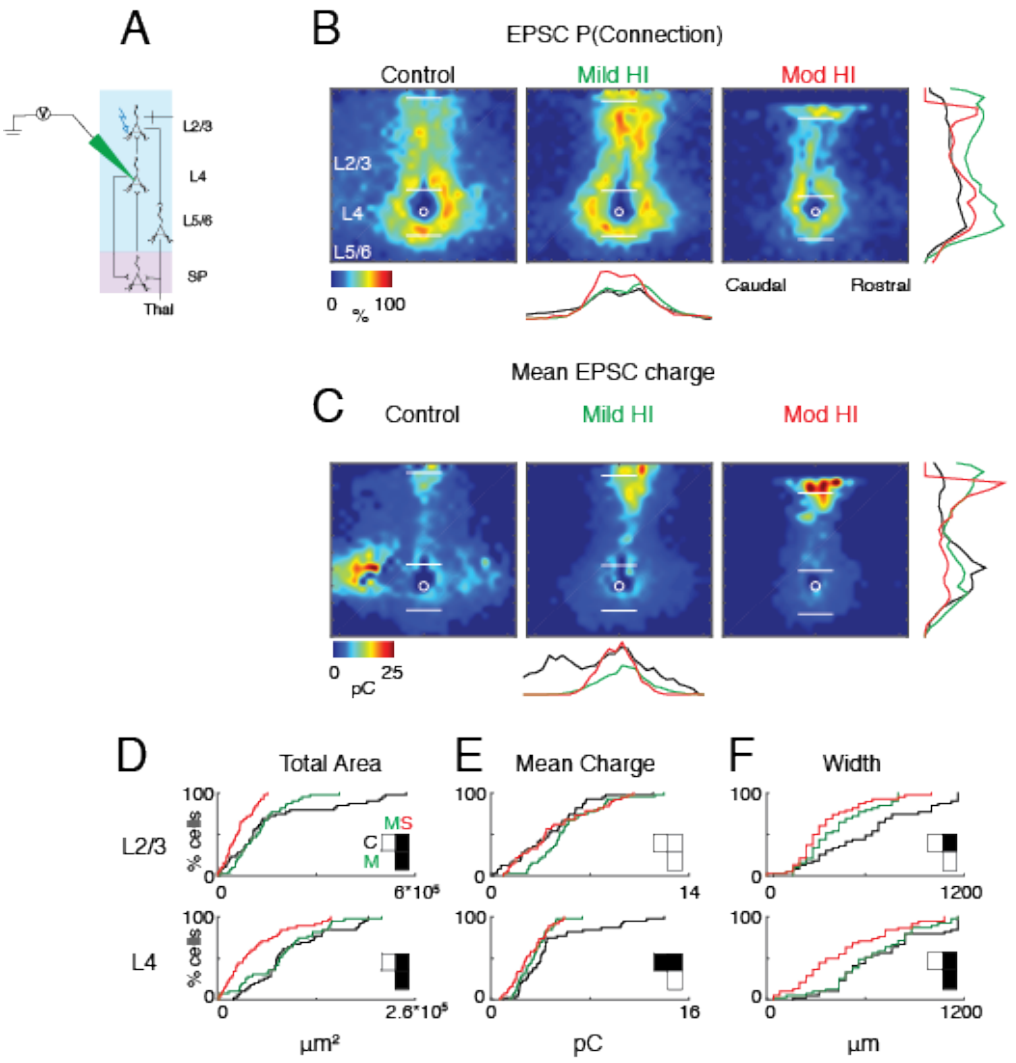

Figure 5.11: Mod HI alters L4 excitatory connectivity of L2/3 and L4, and weakens average EPSC charge of L4 A. Reference view of electrode positioning in the layer recorded and example laser photostimulation location (photostimulation from pia to L4- see methods for more details). **B.** Spatial distribution of sites of excitatory input to L4 neurons that alter due to the different HI injuries. Probability of connection occurrence P(Connection) for excitatory (-70 mV) activity. **C.** Spatial distribution of transferred charge (Mean EPSC Charge) for excitatory (-70 mV) activity. **D-F.** Cumulative distribution function (CDF) of excitatory input to L4 neurons. Layer totals for area (left), mean transferred charge (middle), and marginal width along rostral-caudal axis (right) for L2/3 and L4 input to the recorded L4. Horizontal bars indicate layer boundaries and serve as scale bar of 200 um. Black, green, and red overlaying traces on the side of the maps indicate summed EPSC marginal distributions for each group. Comparisons: L2/3 D) (C-S) $P \leq 0.0001$, (M-S) $P \leq 0.05$; L4 - (C-S) $P \leq 0.001$, (M-S) $P \leq 0.01$. E) L4 - (C-M) $P \leq 0.01$, (C-S) $P \leq 0.001$. F) L2/3 - (C-S) $P \leq 0.001$; L4 - (C-S) $P \leq 0.001$, (M-S) $P \leq 0.05$.

Layer 4 neurons in control animals showed extensive inputs from L4 and a columnar input from L2/3 (Fig. 5.11B). The connection probability map after Mild HI was similar to control. Quantification of the laminar inputs showed that the amount or columnar extent of input from within L4 and from L2/3 did not change after Mild HI (Fig. 5.11B, D). However, the laminar extent showed a trend to reduction indicating that the 2- spatial profile of inputs has subtly changed. These changes could be due to changes in the laminar position of cells projecting to the given L4 neuron, e.g. fewer inputs from distant locations, but more inputs from proximal locations. This interpretation is consistent with the changes in appearance in the average maps (Fig. 5.11B). The average maps of connection strength differed qualitatively, but our cell based analysis showed that the mean EPSC charge did not change for input from L2/3, despite the trend to lower amplitude of connections from within L4 (Fig. 5.11E, 5.12A). The difference of the apparent changes in the mean connection map and the lack of change in the cell based measures indicate that as a population, L4 cells showed a more heterogeneous connection patterns after Mild HI.

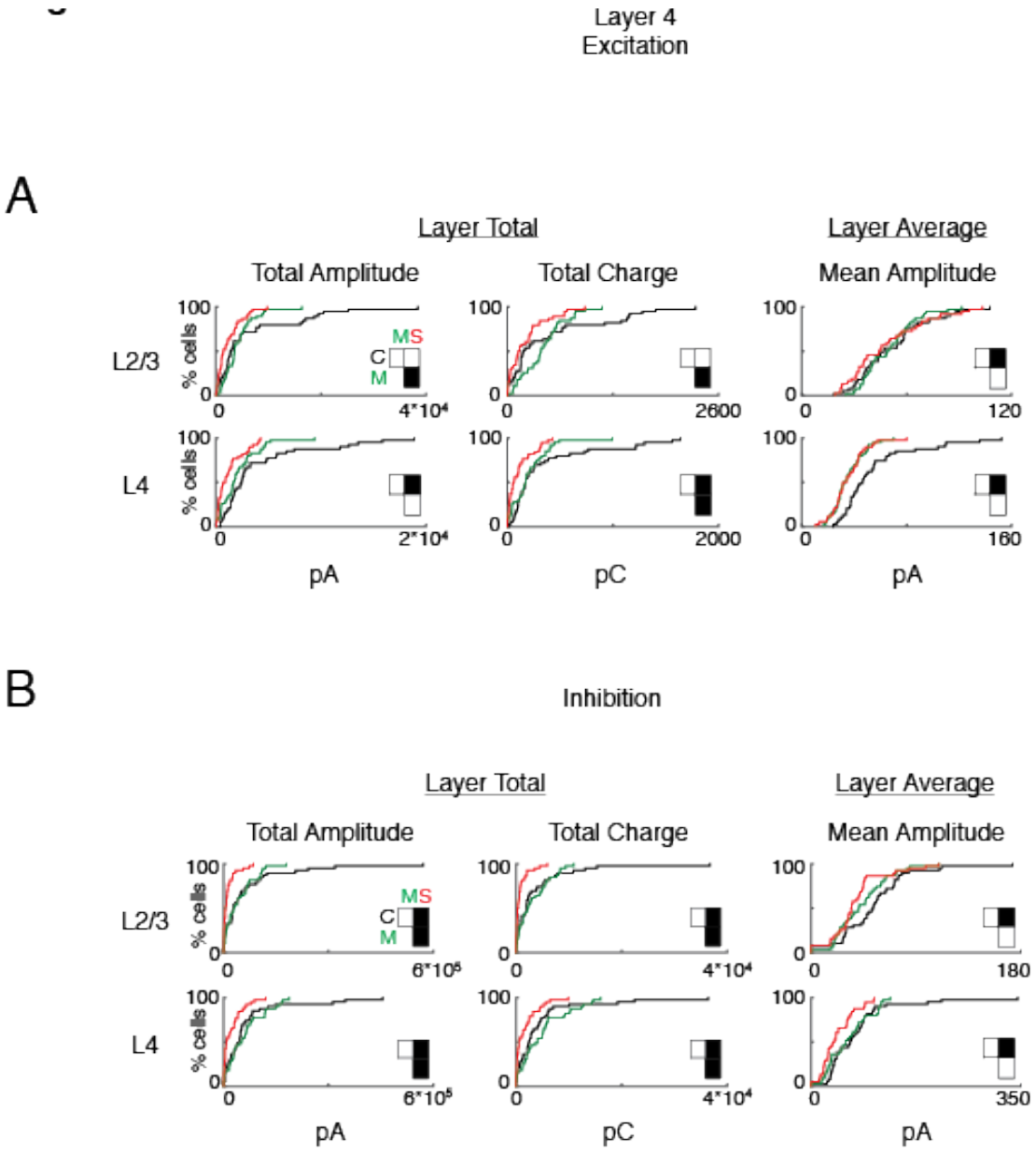

Figure 5.12) Related to figures 5.11 5.14: CDFs layer totals for EPSC (A) amplitude and charge, and IPSC (B) amplitude and charge for L2/3 and L4. Layer averaged amplitudes on the right for EPSCs (A) and IPSCs (B). **A.** L2/3 total amplitude (M-S) $P \leq 0.05$; L2/3 total charge (M-S) $P \leq 0.01$, L2/3 mean amplitude (C-S) $P \leq 0.05$. L4 total amplitude (C-S) $P \leq 0.01$; L4 total charge (C-S) $P \leq 0.001$, (M-S) $P \leq 0.05$; L4 mean amplitude (C-S) $P \leq 0.01$. **B.** L2/3 total amplitude (C-S) $P \leq 0.01$, (M-S) $P \leq 0.001$; L2/3 total charge (C-S) $P \leq 0.01$, (M-S) $P \leq 0.0001$; L2/3 mean amplitude (C-S) $P \leq 0.05$. L4 total amplitude (C-S) $P \leq 0.01$, (M-S) $P \leq 0.05$; L4 total charge (C-S) $P \leq 0.05$, (M-S) $P \leq 0.0001$; L4 mean amplitude (C-S) $P \leq 0.01$.

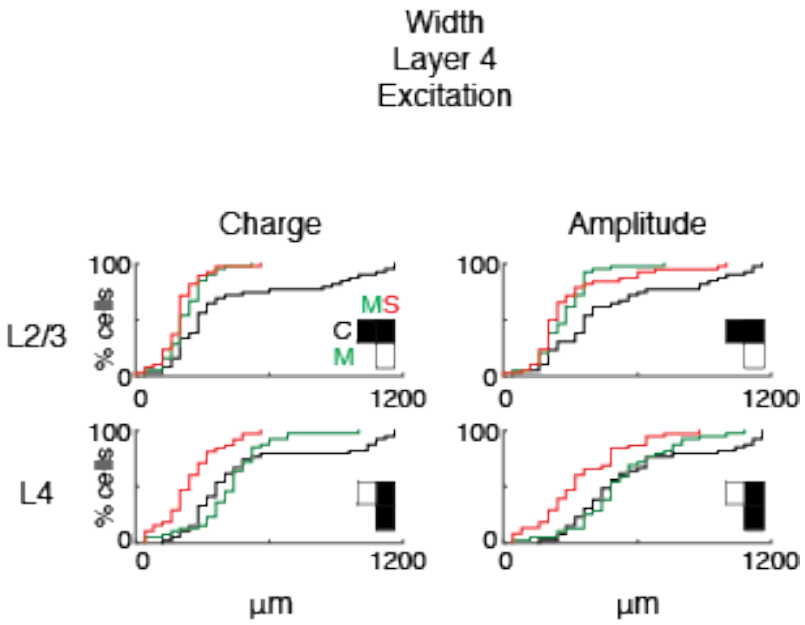

Figure 5.13: CDFs for marginal rostral-caudal width for EPSC for charge (left) and amplitude (right) for L2/3 and L4. L2/3 charge (C-M) $P \leq 0.05$, (C-S) $P \leq 0.001$; amplitude (C-M) $P \leq 0.05$, (C-S) $P \leq 0.01$. L4 charge (C-S) $P \leq 0.0001$, (M-S) $P \leq 0.001$; amplitude (C-S) $P \leq 0.001$, (M-S) $P \leq 0.001$.

In contrast, after Mod HI, excitatory inputs to L4 neurons arose from a smaller area from within L4 and from L2/3 compared to Control (Fig. 5.11B, D, F). Therefore, Mod HI results in hypoconnectivity of L4 neurons. Besides the hypoconnectivity, after Mod HI the average strength (amplitude and charge) of excitatory inputs to L4 weakened (Fig. 5.12B). The hypoconnectivity from within L4 suggests that there are fewer excitatory synapses on L4 neurons consistent with prior studies showed that HI resulted in reduced dendritic complexity in cortical pyramidal cells (Ranasinghe et al., 2015). Consistent with reduced dendritic complexity, we find that compared to Control, Mod HI results in a decrease in total direct input area to L4 (Fig. 5.7D).

Mild HI did not result in any changes in the total area of inhibitory input (Fig. 5.14B, D, F) nor in strength of inhibitory inputs to L4 (Fig. 5.14C, E). In contrast compared to Control, Mod HI results in a decrease in the total area of inhibitory input from L2/3 to L4, and from within L4 (Fig. 5.9B, D, F). Therefore, Mod HI results in both excitatory and inhibitory hypoconnectivity from L2/3 and within L4. Moreover, Mod HI results in a reduced strength of inhibitory input from L2/3 to L4, as well as from within L4 (Fig. 5.9C, E,; 5.8B). Thus while Mod HI has an effect on both excitatory and inhibitory L4 circuits, Mild HI did not affect L4 circuits.

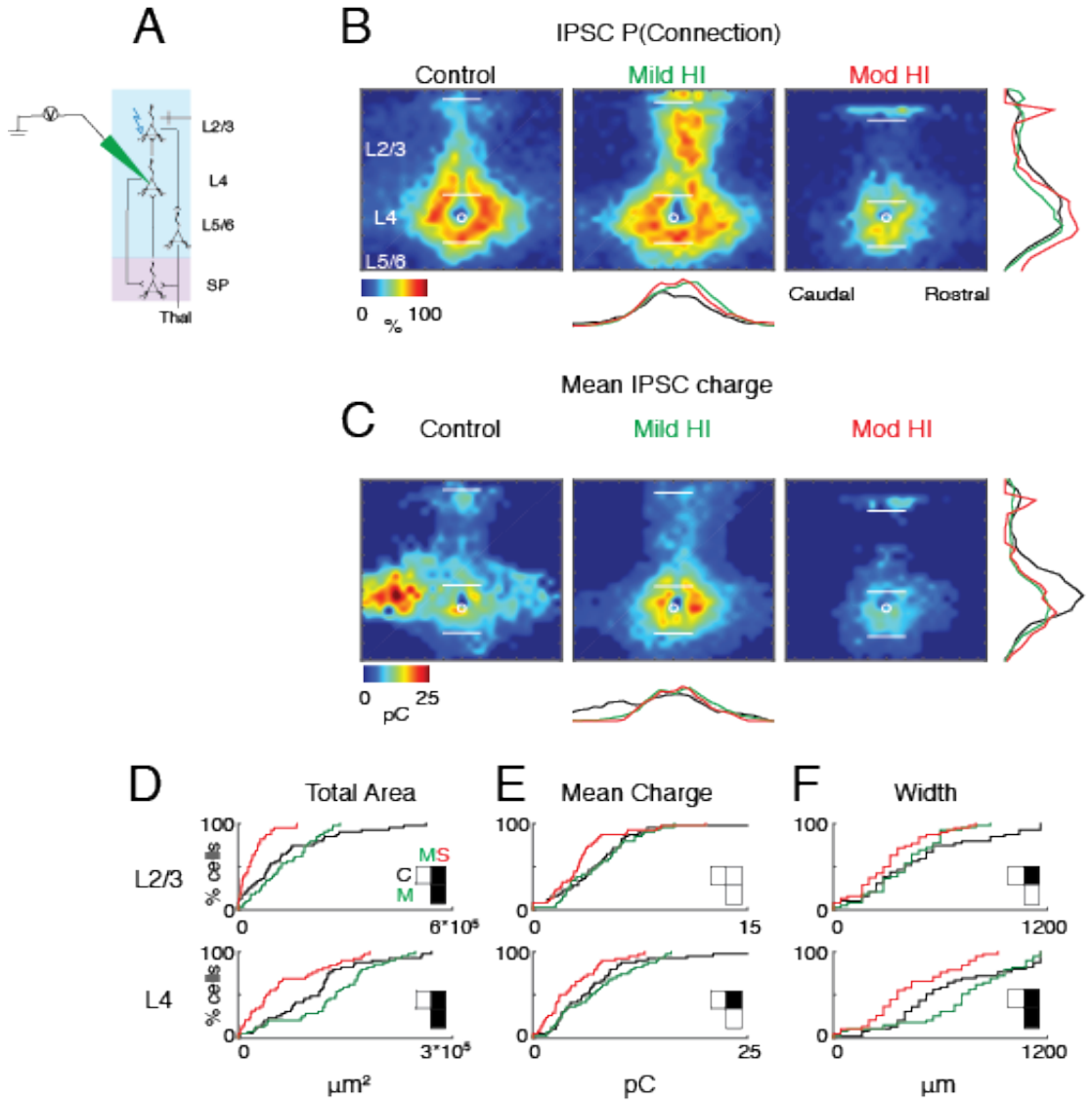

Figure 5.14: Mod HI results in hyperconnectivity of inhibition in L2/3 and L4, in addition to weakening of L4 IPSCs. A. Reference view of electrode positioning in the layer recorded and example laser photostimulation location (photostimulation from pia to L4- see methods for more details). **B.** Spatial distribution of sites of inhibitory input to L4 neurons that alter due to the different HI injuries for P5-10 rats. Probability of connection occurrence P(Connection) for inhibitory (0 mV) activity. **C.** Spatial distribution of transferred charge (Mean IPSC Charge) for excitatory (-70 mV) activity. **D-F.** Cumulative distribution function (CDF) of inhibitory input to L4 neurons. Layer totals for area (left), mean transferred charge (middle), and marginal width along rostral-caudal axis (right) for L2/3 and L4 input to the recorded L4. Horizontal bars indicate layer boundaries and serve as scale bar of 200 um. Black, green, and red overlaying traces on the side of the maps indicate summed IPSC marginal distributions for each group. Comparisons: L2/3 E) (C-S) $P \leq 0.001$, (M-S) $P \leq 0.0001$; L4 - (C-S) $P \leq 0.01$, (M-S) $P \leq 0.0001$. F) L4 - (C-S) $P \leq 0.05$, G) L2/3 - (C-S) $P \leq 0.0001$; L4 - (C-S) $P \leq 0.001$, (M-S) $P \leq 0.0001$.

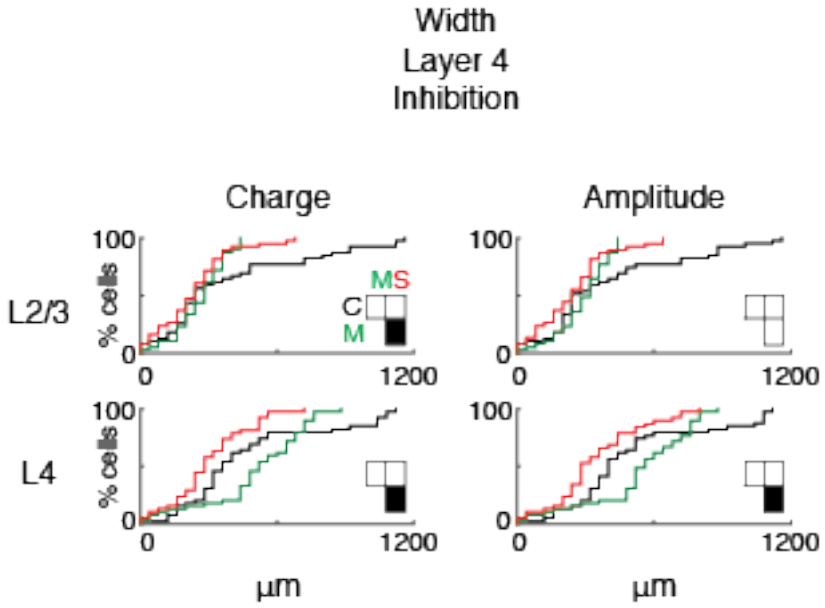

Figure 5.15: CDFs for marginal rostral-caudal width for IPSC for charge (left) and amplitude (right) for L2/3 and L4. L2/3 charge (M-S) $P \leq 0.01$; L4 charge (M-S) $P \leq 0.0001$; L4 amplitude (M-S) $P \leq 0.001$.

Hypoxia-Ischemia causes an excitation/inhibition imbalance in subplate and layer 4

We observed differential changes in excitatory and inhibitory circuits in both SPNs and L4 neurons. For normal brain function, a balance of excitation to inhibition is required. For example, an imbalance towards hyperexcitation could lead to increased seizure activity, which we had observed with Mod HI. Thus, we tested if the combined changes led to an imbalance of excitatory and inhibitory input. To investigate the combined changes we calculated for each cell, the ratio of the area and charge of the excitatory (AMPA) to inhibitory (GABAergic) input (EI ratio) for every stimulation site, which is a measure of the relative connection changes. Compared to Control, Mild HI results in a reduced ratio of EI for total input area from L4. Thus, there is an increase in the contribution of inhibitory activity from L4 to SPNs (Fig. 5.16A, B). In contrast, there is no significant difference in the EI ratio for Mod HI for total input area from L4 to SPNs. Similar changes in the EI ratio were present in inputs arising from L5/6. The reductions in EI ratio for Mild HI were also present in the ratio calculated based on total charge or amplitude indicating that the changes in synaptic strength did not compensate for the connection changes. Importantly, after Mod HI there is an increase in the EI ratio based on charge. Together, this analysis shows that after Mild HI, inhibitory inputs to SPNs are relatively more dominant thus reducing the net excitatory drive to SPNs. This suggests that after Mild HI there is reduced activity of SPNs. In contrast, after Mod HI there is a relative increase in excitation consistent with the occurrence of seizures. Thus both Mild and Mod HI differentially alter inputs to SPNs.

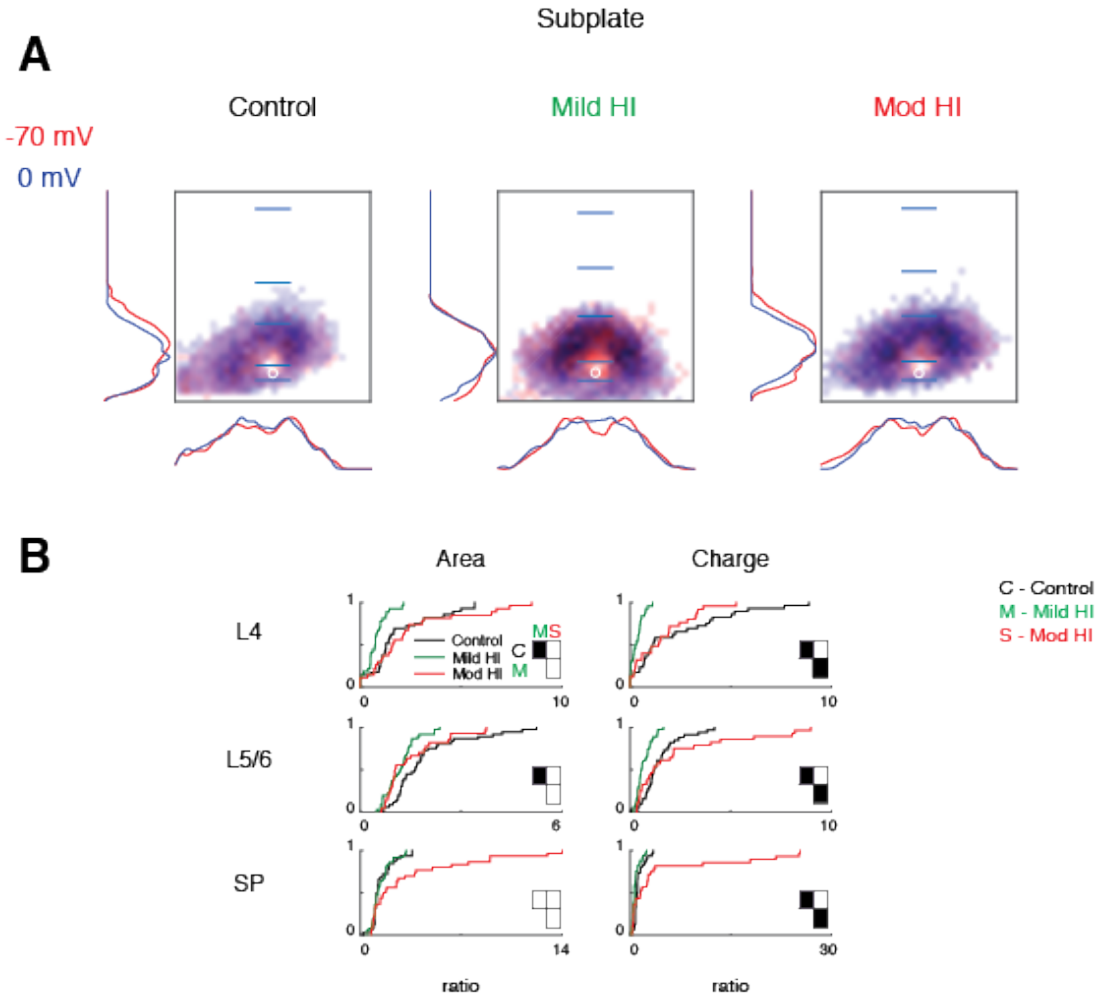

Figure 5.16: Overlay of excitation to inhibition of input to SP for the different conditions. A. Summary schematic of excitatory and inhibitory input to SPNs superimposed (Control, left; Mild HI, center; Mod HI, right). Red color represents excitatory input, and blue color represents inhibitory input to SP. Red and blue overlaying traces on the sides of the maps indicate summed EPSC and IPSC marginal distributions. Blue scale bar denotes 200 μm. **B.** Cumulative distribution function (CDF) of the ratio of excitatory to inhibitory input as it changes as a result of the different injuries for both area (left) and charge (right) for L4, L5/6, and SP. L4 area (C-M) $P \leq 0.01$; L4 charge (C-M) $P \leq 0.001$, (M-S) $P \leq 0.01$. L5/6 area (C-M) $P \leq 0.01$; L5/6 charge (C-M) $P \leq 0.001$, (C-S) $P \leq 0.01$. SP charge (C-M) $P \leq 0.05$, (M-S) $P \leq 0.01$.

Despite the fact that L4 neurons did not show significant changes in excitation or inhibition after HI, calculating the EI ratio revealed changes in inputs to L4 neurons indicating that there are subtle and coordinated changes in both excitatory

and inhibitory inputs to L4 neurons after HI (Fig. 5.17A,B). After Mild HI, L4 neurons receive increased inhibitory input from within L4 for Mild HI while Mod HI resulted in a relative increase and strengthening of input from L2/3. Thus, the relative changes in L4 mirror those in SPNs.

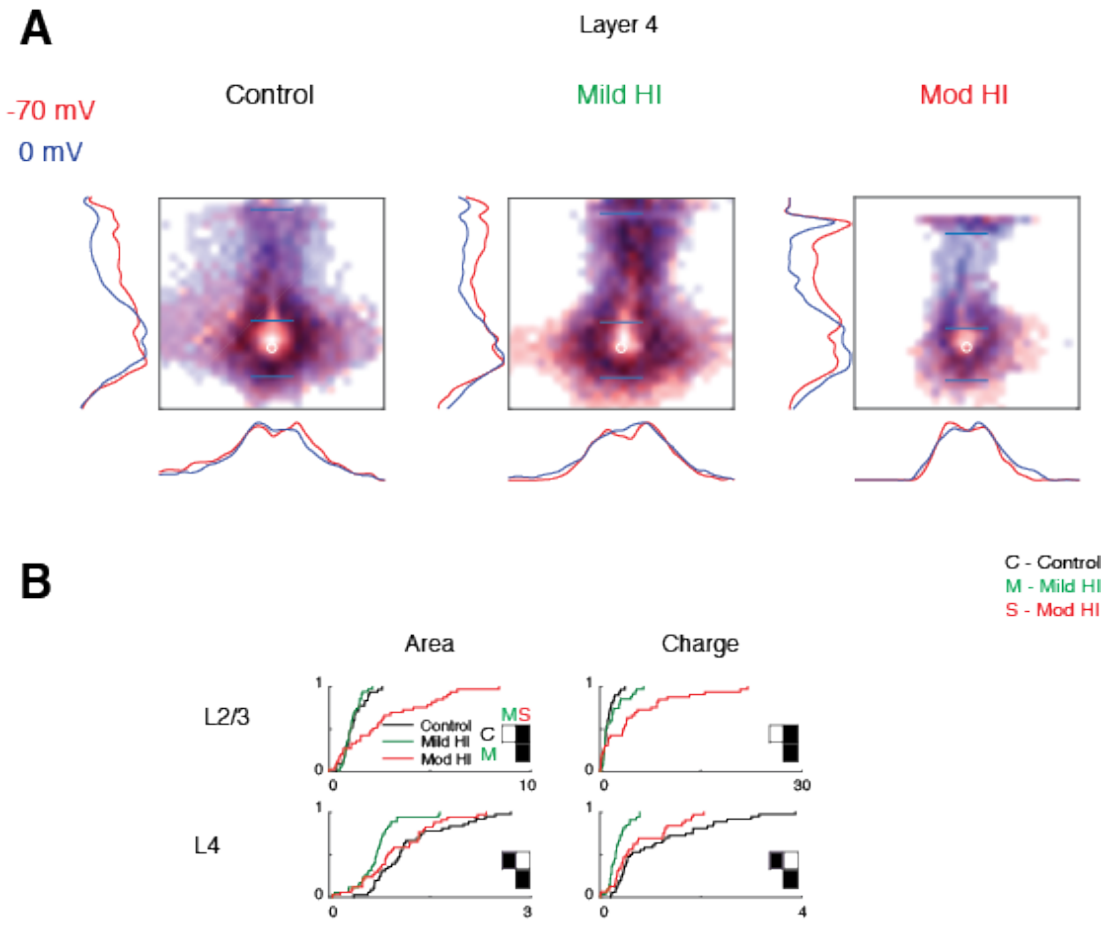

Figure 5.17: Overlay of excitation to inhibition of input to L4 for the different conditions. A. Summary schematic of excitatory and inhibitory input to L4 neurons superimposed (Control, left; Mild HI, center; Mod HI, right). Red color represents excitatory input, and blue color represents inhibitory input to L4. Red and blue overlaying traces on the sides of the maps indicate summed EPSC and IPSC marginal distributions. Blue scale bar denotes 200 μm. **B.** Cumulative distribution function (CDF) of the ratio of excitatory to inhibitory input as it changes as a result of the different injuries for both area (left) and charge (right) for L2/3 area (C-S) $P \leq 0.0001$, (M-S) $P \leq 0.0001$; L2/3 charge (C-S) $P \leq 0.0001$, (M-S) $P \leq 0.001$. L4 area (C-M) $P \leq 0.0001$, (M-S) $P \leq 0.05$; L4 charge (C-M) $P \leq 0.0001$, (M-S) $P \leq 0.01$.

Discussion:

Here we show that an animal model of HI causes distinct changes to functional cortical microcircuits in the neonatal rodent. The functional circuit changes were most pronounced in cortical SPNs and thus suggest that early HI insults to the developing cortex exert most of their influence on SPNs.

Specifically, we show that transient Mild HI causes functional changes in the absence of gross histological changes. In contrast, moderate HI caused cortical shrinkage in the auditory cortex that was already detectable by P5-10 similar to what has been reported in the visual cortex at P32 (McQuillen et al., 2003; Failor et al., 2010). Nevertheless we find that in both conditions, SPN circuits are showing excitatory hyperconnectivity. Thus SPNs change as a result of both conditions. In contrast, L4 circuits are only altered for the more severe form of HI. Thus our results suggest potentially worse tuning in primary auditory cortex. Therefore, SPN circuits seem to be uniquely vulnerable to HI and show circuit changes within a few days after the HI insult. Thus functional microcircuit mapping (LSPS) is a sensitive measure to identify functional connectivity changes on a laminar-specific microcircuit level as a result of HI. Moreover, we are able to delineate distinct circuit changes with two severities of HI injury (Fig. 18). Since moderate HI causes cell loss, our results suggest that while reduced SPN activity due to relative increased inhibition leads to changes in the spatial pattern of excitatory inputs to L4, cell loss within the subplate leads to the loss of connections to L4.

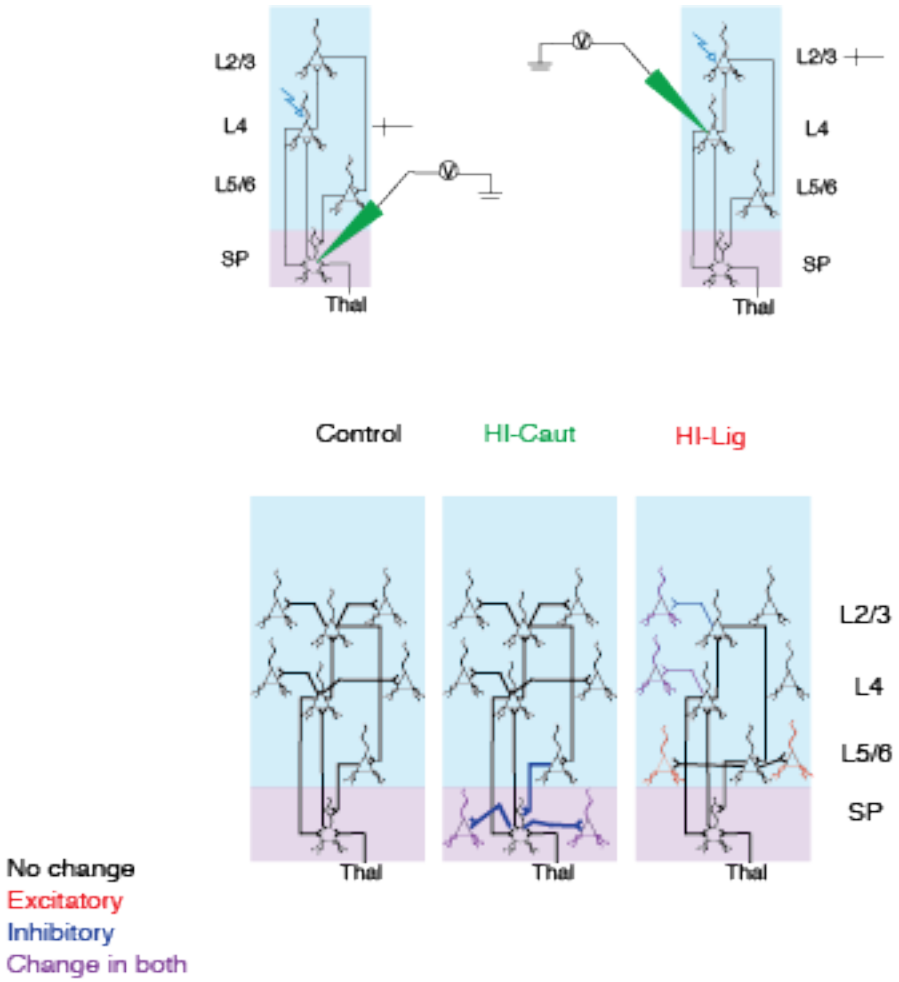

Figure 5.18: Summary schematic of microcircuit changes in density and strength of connections as a result of the differing injuries and with respect to the different layers. Top: representation of location of recorded neuron and the stimulation areas. Bottom: changes in strength of connections are represented with either thickening or narrowing of axons. Changes in density of connections are represented as the addition of neurons or the removal of neurons in the particular layer. Red represents excitatory input, blue for inhibitory input, and purple for both excitatory and inhibitory input.

SPNs are amongst the earliest born neurons in the cerebral cortex and are among the first to receive input from the thalamus as well as from intercortical sources and project to L4 (Zhao et al., 2009; Kanold and Luhmann, 2010; Meng et al., 2014; Viswanathan et al., 2016). Here we show that HI causes an imbalance of excitatory and inhibitory intracortical inputs to SPNs. Thus the integrative role of

SPNs is altered after HI. Additionally, SPNs are required for the maturation of excitatory and inhibitory circuits to L4 (Kanold et al., 2003; Kanold and Shatz, 2006; Tolner et al., 2012). Given the excitatory input from SPNs to L4, the altered SPN connections we observe here would predict similarly altered connections to L4 neurons. Indeed, we observe a hypoconnectivity of excitatory connections in L4 after moderate HI consistent with the cell loss and connection changes in SP. Moreover, moderate HI results in decreased GluR1 expression in cortical layer 4 and 6 (Ranasinghe et al., 2015), consistent with our results. Since SPNs innervate L4 neurons (Zhao et al., 2009; Viswanathan et al., 2016), we speculate that because Mod HI is also associated with loss of SPNs, the total SPN mediated activity to L4 neurons is reduced leading to hypoconnectivity.

SPNs take part in the generation of spontaneous cortical oscillations (Dupont et al., 2006), and SPN lesions abolish spindle burst activity in primary somatosensory cortex (Tolner et al., 2012). Moderate HI in rodents resulted in transiently diminished EEG background activity (Ranasinghe et al., 2015). Thus our results here suggest that altered SPN and L4 circuits underlie these changed EEG signals.

Overall, our results show on a microcircuit cortical level of the dynamic and laminar-specific effects of differing severities of HI as a possible substrate for how HI can lead to an imbalance of excitation and inhibition as early as P5-10 days in the rodent, which is about 25-30 gestational weeks (GW) in the human.

Here, we find abnormalities in the functional connectivity of the auditory cortex consequent to HI, consistent with language impairments associated with neonatal HIE in humans (Martinez et al., 2014). The widening of input within

subplate along the tonotopic rostro-caudal axis as a result of either severities of HI suggests a worsening of auditory selectivity within subplate. Regardless of the severity of the HI, we find that the basic interlaminar circuitry of the primary auditory cortex remains intact, indicating that potentially the observed circuit changes especially after Mild HI, which did not result in cell loss, are reversible. Thus targeted interventions, which selectively strengthen SPN circuits, might be able to reverse the effects of early HI. Current treatment for HI is hypothermia (Lai and Yang, 2011) which presumably reduces activity in all neurons thus will also prevent the strengthening of proper connections to SPNs. More efficient treatments might involve targeting different, SPN specific, receptors instead of trying to use a global treatment. For example, SPNs express a variety of neuromodulatory receptors such as ACh and serotonin (Hanganu and Luhmann, 2004; Kilb et al., 2008; Liao and Lee, 2011, 2014) thus transient activation of these systems might mediate the effects of HI. Given the fact that SPNs are a unique cell population selectively expressing multiple genes, (Hoerder-Suabedissen et al., 2009; Kanold and Luhmann, 2010; Hoerder-Suabedissen and Molnar, 2015; Viswanathan et al., 2016), the development of SPN specific pharmacological treatments might be a promising avenue. Finally, our results show that SPN circuits are vulnerable to hypoxic-ischemic brain injury and it is likely that other insults to the developing brain at the earliest stages also alter SPN circuitry.

Chapter 6: Neonatal hypoxia-ischemia causes functional intracortical circuit changes in P18-23 rat auditory cortex

Normal brain development requires the proper maturation of neural circuits for normal cognitive functioning. White matter brain injury during development results in disruption of normal brain maturation and consequently increases risk of developing these disorders such as epilepsy and cerebral palsy. Neonatal hypoxia-ischemia (HI) causes brain damage selective to different brain structures over development, and in the preterm human HI results in damage to subcortical developing white matter, a condition referred to as periventricular leukomalacia (PVL). HI can damage neurons in the developing white matter, subplate neurons (SPNs). SPNs are among the first cortical neurons to be born and are necessary for normal functional development of the cerebral cortex. Thus, while it is clear that SPNs play a major role in the maturation of developing brain circuitry, it is unclear how HI alters the thalamorecipient layer 4 circuits later in development. Moreover, it is unknown if Mild HI injuries that do not cause overt histological changes in the cortex can alter L4 circuits. Using a rat HI model, we induced either Mild or Moderate HI at P1. Previous work in this dissertation showed that while SPNs are selectively vulnerable to mild HI injury, and it is the more moderate form of HI that impacts L4 circuitry from P5-10. Thus, we used laser-scanning photostimulation (LSPS) in acute thalamocortical slices of rat auditory cortex during P18-23 to study the functional connectivity of layer 4 neurons in both injury categories. We find that moderate hypoxia-ischemia (Mod HI) causes strengthening of excitatory L4 circuits

from P18-23. Additionally, we find that Mod HI causes strengthening of inhibitory L4 circuits and hyperconnectivity along the rostral-caudal extent. Also by P18-23, excitation and inhibition of L4 circuits are rebalanced after HI injuries. Thus by P18-23, there are less pronounced changes in the functional microcircuitry than at P5-10 for L4 input, and this may account for the absence of observed seizures after neonatal HI in the rat.

Introduction:

Early birth or disruptions of prenatal brain development result in increased risk of cognitive impairments. For example, hypoxic-ischemic brain injuries commonly affect attention, memory, executive function, and speed of processing depending on the severity of the injury (Anderson and Arciniegas, 2010). While in-utero, the embryo is very vulnerable to injuries and insults that have potential to cause long-term health problems and disorders such as cerebral palsy and epilepsy (Jantzie et al., 2014). Hypoxia-Ischemia (HI) is a disorder in which the preterm infant undergoes a lack of oxygen and blood flow to the brain. About 0.2-0.3 percent of the 4 million infants born per year develop moderate hypoxia-ischemia encelphalopathy (HIE), with mortality rates of about 6-30 percent (Raghuveer and Cox, 2011). Specifically, injury to the premature white matter of the brain results in disruption of the normal maturation of the brain and consequently increases risk of developing cerebral palsy and epilepsy in infants (Rumajogee et al., 2016). While cortical activity is impaired after HI (Ranasinghe et al., 2015), it is unclear which specific circuits are affected by HI and how this change is translated in reduced overall network activity.

One key neuronal circuit present in early cortical development whose damage results in abnormal brain function is formed by subplate neurons (SPNs). SPNs are a largely transient neuronal structure that is highly overrepresented in humans (Kanold and Luhmann, 2010). SPN lesions have been shown to prevent the functional maturation of thalamocortical circuits, normal sensory responses, and alter plasticity during the critical period (Kanold et al., 2003; Kanold and Shatz, 2006; Tolner et al., 2012). Particularly, SPN ablations prevent the development of early oscillatory cortical activity patterns (Tolner et al., 2012). In addition, HI injuries lesion a fraction of SPNs (McQuillen et al., 2003), and lead to abnormal functional cortical responses reminiscent of the effects of SPN lesions (Kanold et al., 2003; Kanold and Shatz, 2006; Failor et al., 2010; Tolner et al., 2012; Ranasinghe et al., 2015). Normal functional responses in sensory cortices depend on mature thalamocortical and intracortical circuits. While the effects of SPN damage on thalamocortical circuits have been established, effects on intracortical circuits are unknown.

To determine if HI has effects beyond SP lesions and if SPN damage from HI causes a change in intracortical circuits later in development, we analyzed the functional spatial connection patterns of layer 4 (L4) neurons during postnatal day (P) 18-23 using laser-scanning photostimulation (LSPS) in a thalamocortical slice preparation of auditory cortex (ACX). Specifically, we compared connection patterns for excitatory and inhibitory connections in cells from animals that underwent two different severities of neonatal (P1-2) HI and control animals. We find that moderate hypoxia-ischemia (Mod HI) causes strengthening of excitatory L4 circuits from P18-23. Additionally, we find that Mod HI causes strengthening of inhibitory L4 circuits

and hyperconnectivity along the rostral-caudal extent. Also by P18-23, excitation and inhibition of L4 circuits are rebalanced after HI injuries. Thus by P18-23, there are less pronounced changes in the functional microcircuitry than at P5-10 for L4 input, and this may account for the absence of observed seizures after neonatal HI in the rat.

Results:

Moderate hypoxia-ischemia causes strengthening of excitatory L4 circuits from P18-23

We sought to investigate the influence of HI on L4 circuits later in development of the auditory cortex. Since we saw effects on SPN circuits and L4 circuits from P18-23, we wondered if these same deficits to the circuits would persist later in development. To investigate this possibility we used laser-scanning photostimulation (LSPS) of caged glutamate combined with whole-cell patch clamp recordings (Shepherd et al., 2003; Meng et al., 2014) to spatially map the connectivity of excitatory (AMPA) and inhibitory (GABA) inputs to A1 L4 neurons (N = 115 cells; 40 cells in Control, 40 cells in Mild HI, and 35 cells in Mod HI) at P18-23. During this age, many SPNs have disappeared however a small amount still persist (Kanold and Luhmann, 2010) and this age range is towards the end of the auditory critical period(Zhang et al., 2001).

In order to investigate the spatial pattern of excitatory connections to L4 neurons from the cortical plate of ACX, 900 stimulation sites with a spatial resolution of about 40 μm were mapped sequentially in a pseudorandom pattern (Viswanathan et al., 2012) in order to cover the entire radial extent of the cortical column from

ventricle to pia (Fig. 5.3E). By calculating the charge of the evoked excitatory postsynaptic current (EPSC), we were able to quantify the strength of the excitatory inputs to L4 neurons. These were plotted in two-dimensional maps of connectivity (Fig. 5.3F).

We recorded L4 neurons in thalamocortical slices with the holding potential of -70 mV and 0 mV. Again, if a connection was present between a stimulated neuron and the recorded neuron, a postsynaptic current (PSC) was revealed. During voltage-clamp recordings when the SPNs were held at -70 mV, photostimulation was able to evoke two types of responses: 1) a large inward current with short onset latency ($\leq$ 8ms); and 2) a smaller amplitude inward current with a longer latency (Fig. 5.3D). The shorter latency response is attributable to direct activation of the recorded cell while the longer latency response is dependent on synaptic release from presynaptic cells (Meng et al., 2014).

We first analyzed the excitatory circuits associated with L4 neurons by holding cells at -70mV. We then stimulated 900 sites for each cell and then for stimulation sites that showed evoked EPSCs measured the size of the EPSC (Fig. 5.3F) resulting in a map of excitatory connectivity for each cell. This map indicates the location of presynaptic cells to the recorded L4 neuron. We then aligned the maps to the soma position and calculated for every spatial location the probability of being connected to a given L4 neuron resulting in a spatial connection probability map (Fig. 6.1B).

Compared to Control, Mod HI qualitative inspection showed that excitatory input to the recorded L4 neurons resulted in slight hyperconnectivity however

quantitative single-cell measured revealed no change in the density of connections to L4 (Fig. 6.1B). Mod HI resulted in a strengthening of EPSC mean charge from within L4 only (Fig. 6.1E). Similarly, Mod HI resulted in an increase in the total EPSC charge within L4 (Fig. 6.2A). Additionally, there was no change in the injuries for the width of EPSC input from either L2/3 or L4 (Fig. 6.1F). Qualitatively the average maps showed that the more distinct differences we saw previously in L4 from P5-10 evened out by P18-23 for the milder form of HI.

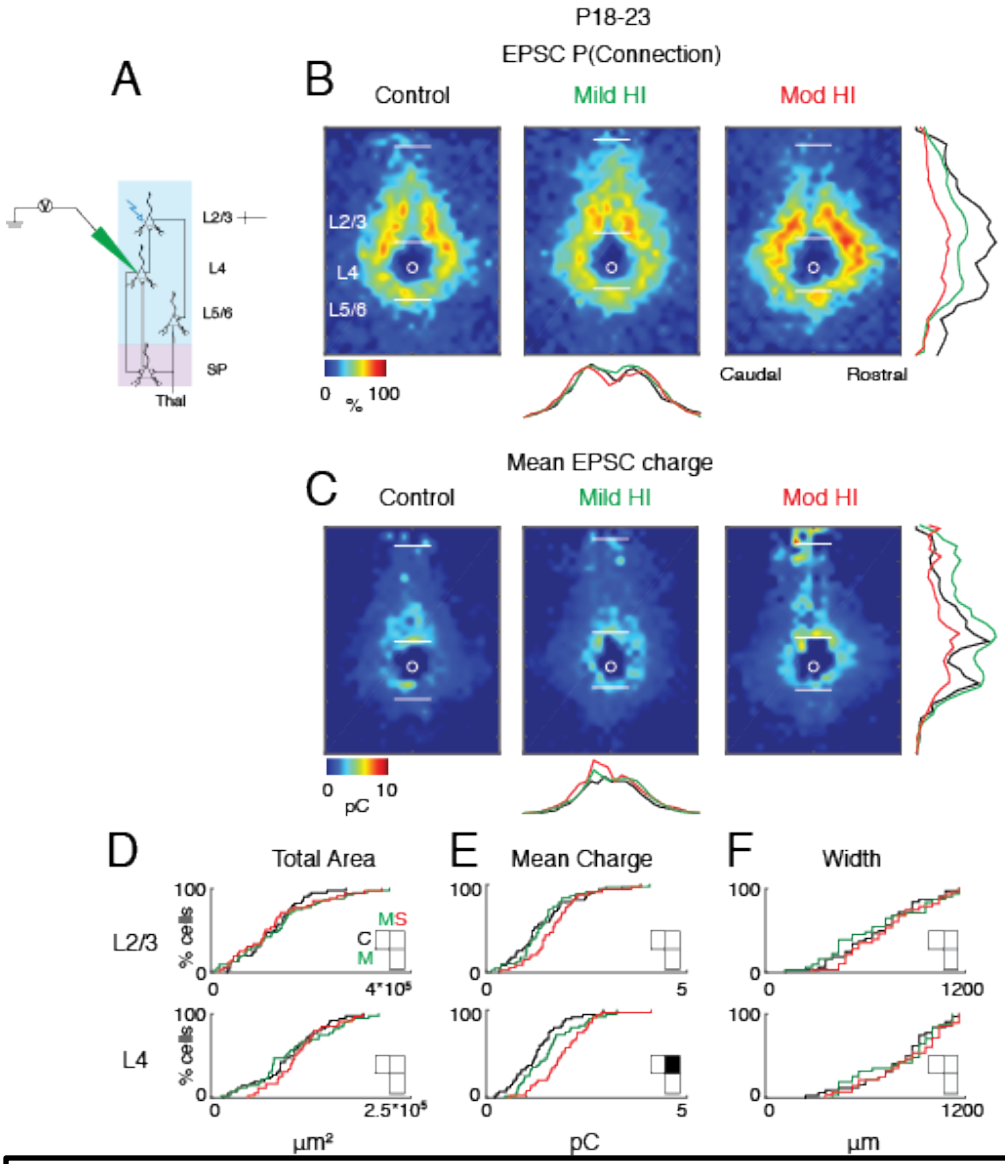

Figure 6.1: By P18-23, Mod HI results in a strengthening of EPSCs within L4. A. Reference view of electrode positioning in the layer recorded and example laser photostimulation location (photostimulation from pia to L4 in P18-23 rats- see methods for more details). **B.** Spatial distribution of sites of excitatory input to L4 neurons that alter due to the different HI injuries. Probability of connection occurrence P(Connection) for excitatory (-70 mV) activity. **C.** Spatial distribution of transferred charge (Mean EPSC Charge) for excitatory (-70 mV) activity. **D-F.** Cumulative distribution function (CDF) of excitatory input to L4 neurons. Layer totals for area (left), mean transferred charge (middle), and marginal width along rostral-caudal axis (right) for L2/3 and L4 input to the recorded L4. Horizontal bars indicate layer boundaries and serve as scale bar of 200 um. Black, green, and red overlaying traces on the side of the maps indicate summed EPSC marginal distributions for each group. Comparisons: L4 - (C-S) $p \leq 0.001$.

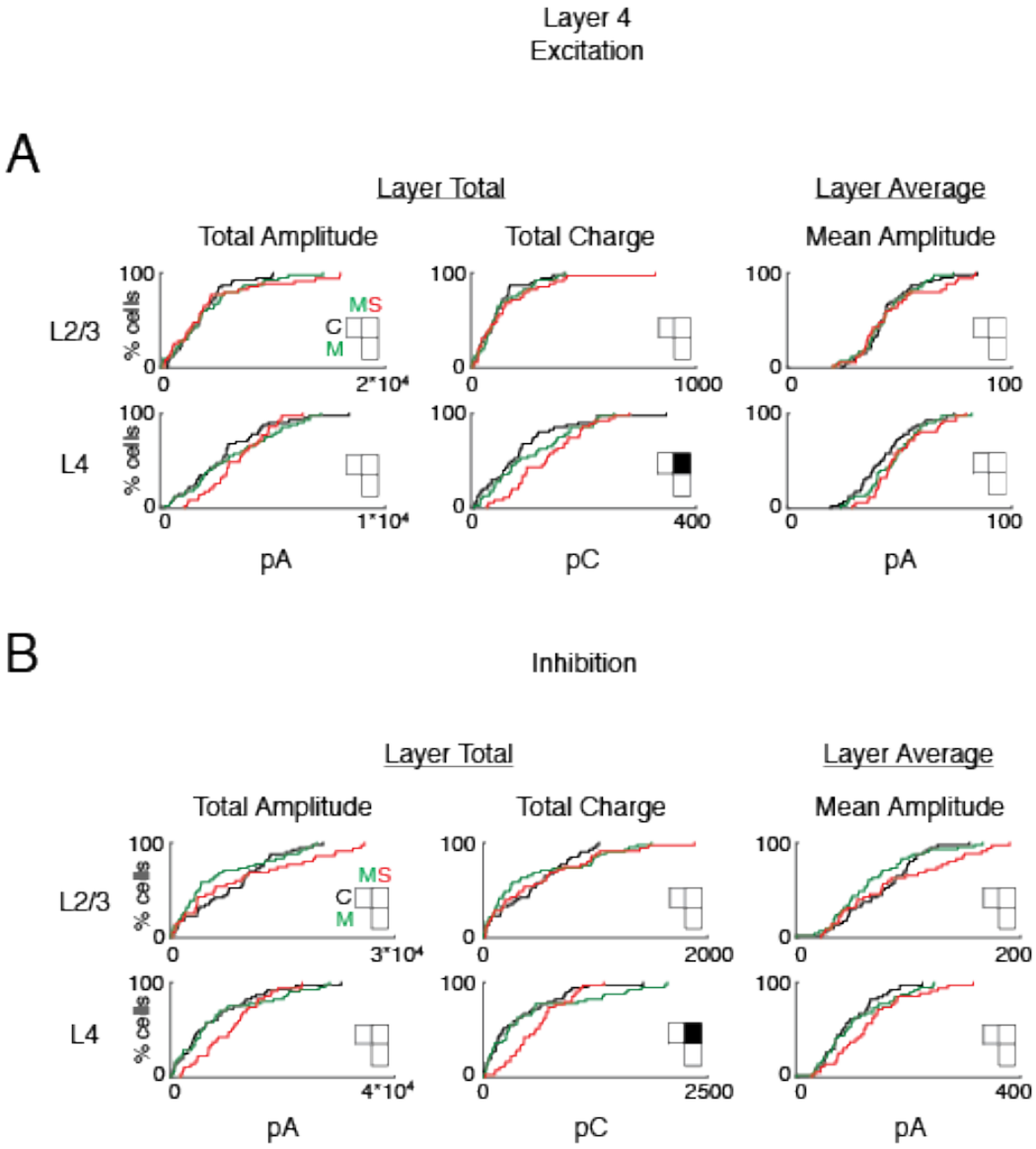

Figure 6.2) Related to figure 6.1: A. Supplemental CDFs for layer totals for EPSC amplitude (left) and charge (right) for L2/3 and L4 for P18-23 rats. Layer average for EPSC amplitude (right) for L2/3 and L4. L4 total charge (C-S) $p \leq 0.01$. **B.** Layer totals for IPSC amplitude (left) and charge (right) for L2/3 and L4. Layer average for IPSC amplitude (right) for L2/3 and L4. L4 total charge (C-S) $p < 0.05$.

Moderate hypoxia-ischemia causes strengthening of inhibitory L4 circuits and hyperconnectivity along the rostral-caudal extent from P18-23

In our previous work, we observed seizures in our neonatal rat pups during as a result of HI and these seizures persisted until about P10 (Fig. 5.2). Therefore this led us to investigate if the seizures persisted past P10. Seizure occurrence was not observable from P18-23 from our three-minute videos taken the morning of the in vitro recordings. From this we hypothesized that GABAergic circuits were different compared to the inhibitory results at P5-10 from our previous work. By P18-23, we find that Mod HI results in a strengthening of IPSCs within L4 and an expansion in L2/3 and L4 of IPSCs along the rostral-caudal extent (Fig. 6.3E, F). Additionally, Mod HI results in an increase in the total charge of the ISPCs within L4 (Fig. 6.2B). Qualitatively, this is reflected in the dense hot spots of inhibitory connections in the Mod HI average maps (Fig. 6.3B).

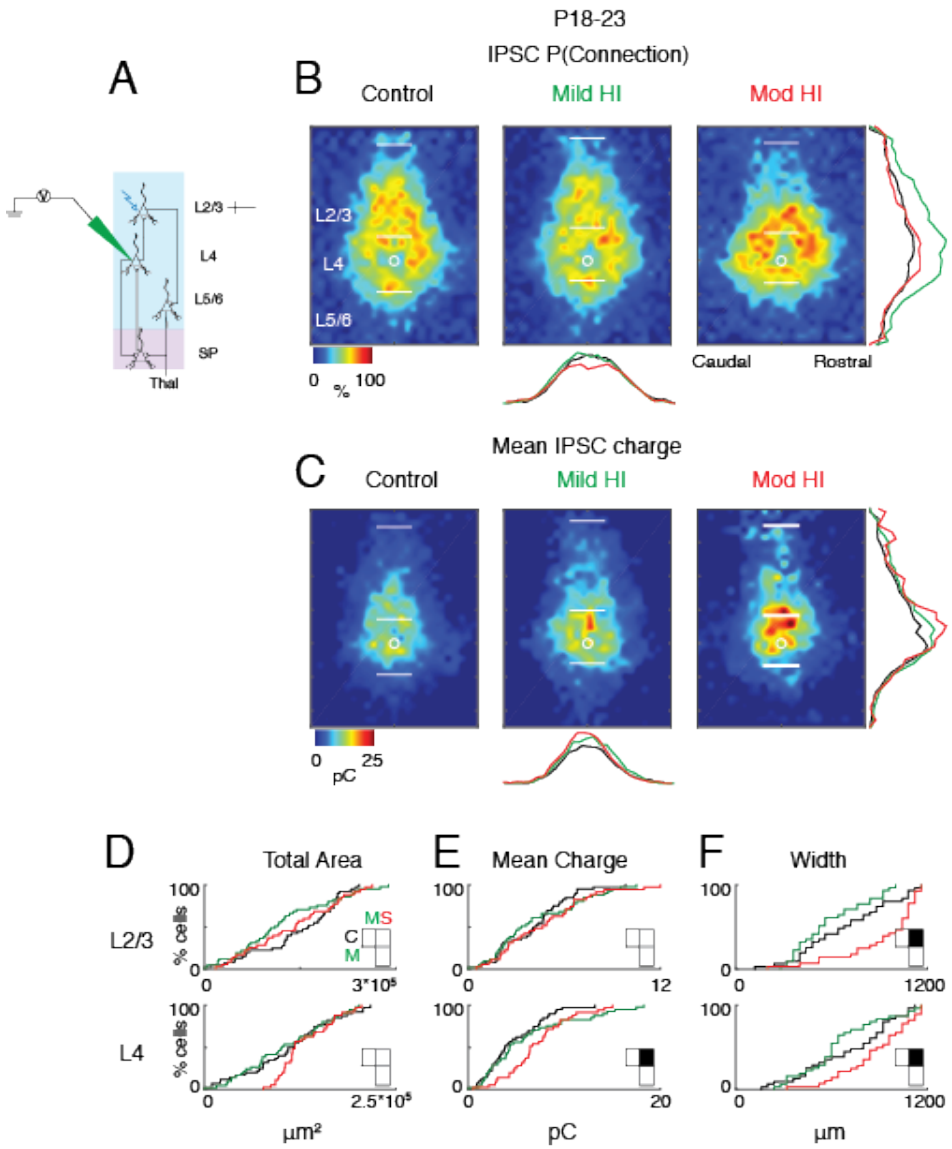

Figure 6.3: By P18-23, Mod HI results in a strengthening of IPSCs within L4 and an expansion in L2/3 and L4 of IPSCs along the rostral-caudal extent A. Reference view of electrode positioning in the layer recorded and example laser photostimulation location (photostimulation from pia to L4- see methods for more details). **B.** Spatial distribution of sites of inhibitory input to L4 neurons that alter due to the different HI injuries in P18-23 rats. Probability of connection occurrence P(Connection) for inhibitory (0 mV) activity. **C.** Spatial distribution of transferred charge (Mean IPSC Charge) for inhibitory (0 mV) activity. **D-F.** Cumulative distribution function (CDF) of inhibitory input to L4 neurons. Layer totals for area (left), mean transferred charge (middle), and marginal width along rostral-caudal axis (right) for L2/3 and L4 input to the recorded L4. Horizontal bars indicate layer boundaries and serve as scale bar of 200 um. Black, green, and red overlaying traces on the side of the maps indicate summed IPSC marginal distributions for each group. Comparisons: L4 mean charge (C-S) $p \leq 0.05$; L2/3 width (C-S) $p \leq 0.01$; L4 width (C-S) $p \leq 0.01$.

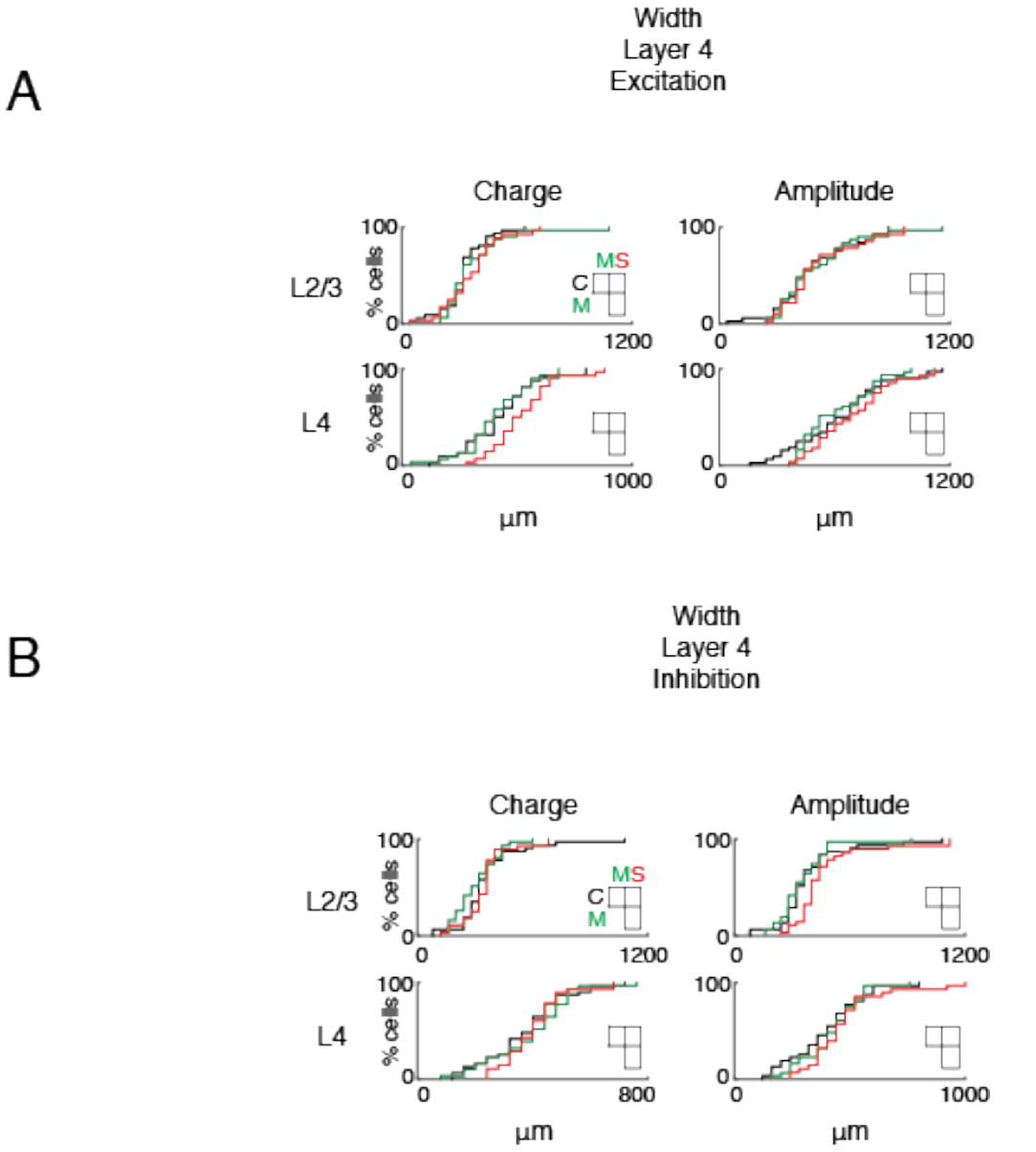

Figure 6.4: A. CDFs for marginal rostral-caudal width for EPSC for charge (left) and amplitude (right) for L2/3 and L4 for P18-23 rats. **B.** CDFs for marginal rostral-caudal width for IPSC for charge (left) and amplitude (right) for L2/3 and L4 for P18-23 rats. White squares denote no significant differences.

By P18-23, excitation and inhibition rebalance L4 circuits despite mild and moderate hypoxia-ischemia at P1-2

Because we did not see seizures from P18-23, we hypothesized that the excitation and inhibition (EI ratio) that was imbalanced during P5-10 in our previous work, rebalances. We find that despite the injuries we induced at P1-2, by P18-23 the EI ratios were balanced (Fig. 6.5) for area and charge of L2/3 and L4.

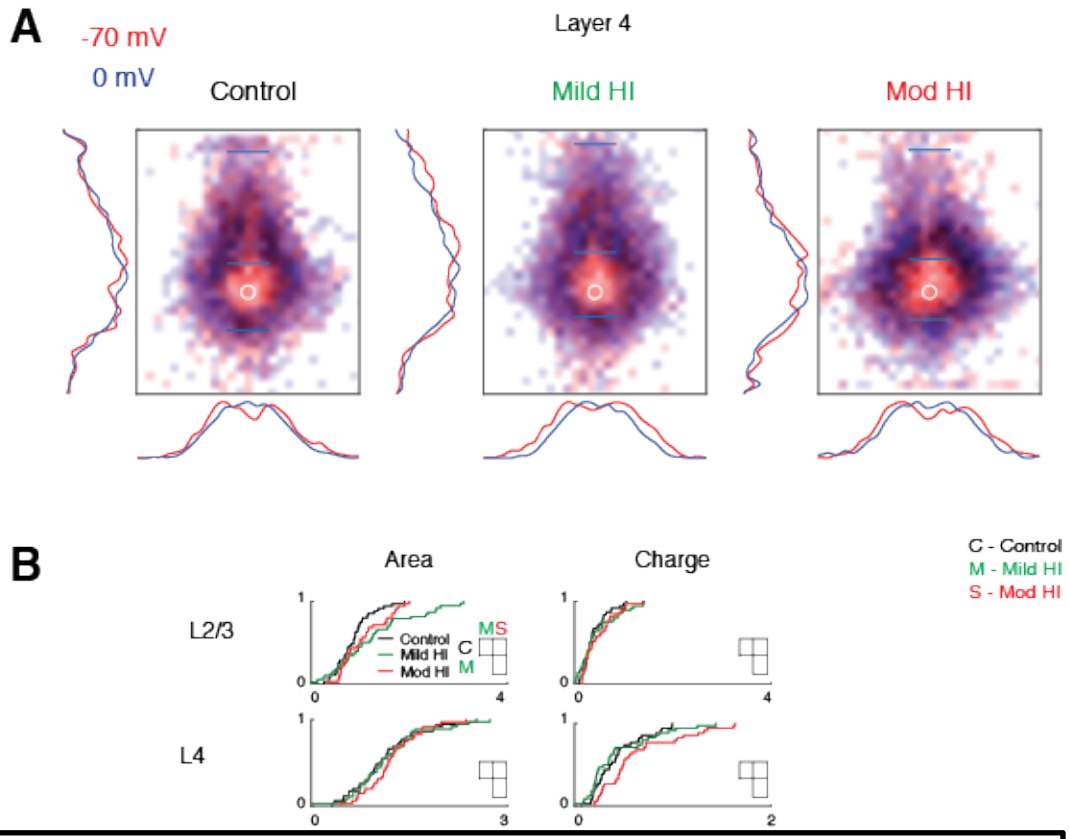

Figure 6.5: Overlay of excitation to inhibition of input to L4 for the different conditions in P18-23 rats. A. Summary schematic of excitatory and inhibitory input to L4 neurons superimposed (Control, left; Mild HI, center; Mod HI, right). Red color represents excitatory input, and blue color represents inhibitory input to L4. Red and blue overlaying traces on the sides of the maps indicate summed EPSC and IPSC marginal distributions. Blue scale bar denotes 200 μm. **B.** Cumulative distribution function (CDF) of the ratio of excitatory to inhibitory input as it changes as a result of the different injuries for both area (left) and charge (right) for L2/3 and L4. There are no significant differences in area or charge for the EI ratios.

Discussion:

During P18-23, many defects seen earlier in development are less numerous and less pronounced. Not surprisingly, the occurrences of seizures seen at P5-10 were absent by P18-23. This may be due to the rebalancing of excitation and inhibition. However, the rebalancing of inputs may be due to pruning of synapses that were weakened earlier in development due to injury. Therefore the strongest connections are the ones that are preserved by P18-23. Despite the rebalancing of excitation to inhibition, Mod HI was severe enough to show deficits persisting through P18-23. However Mild HI did not reveal any differences in any manner from P18-23. Therefore this suggests differential time windows of treatment intervention. For example, since the deficits due to Mild HI are only detectable from P5-10, but Mod HI continues to show reduced in number but persistent defects from P18-23, then Mild HI has a smaller time window for treatment. However, since most of the differences seen earlier in development are during P5-10 and less from P18-23, our results suggest that optimal treatment regardless of the severity of injury should happen earlier in development rather than later. Regardless, we are able to show that on an in vitro level, we are still able to detect changes in the functional synaptic microcircuitry from P18-23 in the HI rat model in auditory cortex later in development.

As seen earlier in P5-10, by P18-23 we show that the basic interlaminar circuitry of primary auditory cortex remains intact indicating that potentially, the observed circuit changes seen from P18-23 as a result of Mod HI despite their detrimental effects to the brain, are still treatable. The current treatment for HI is

hypothermia, and while the effects of hypothermia on subplate circuits are not known, L4 is still impacted by Mod HI injury from P18-23. Since we know that SPNs feed input into L4 (Zhao et al., 2009) and L4 feeds back to the subplate and subplate back to the thalamus (Viswanathan et al., 2016), it is worth testing if hypothermia is able to alter L4 circuits of auditory cortex later in development to see if the changes in the effectiveness of hypothermia later in development or around the time of birth of the human (GW 40). Translating the ages from rodent to human, P18-23 in the rat is about the end of the third trimester in the human thus this suggests that treatment for Mod HI can also happen right after birth if there are surgical complications. However right after birth, treatment for Mild HI may not have as significant as an effect seeing as there were no changes to AMPA and GABAergic activity and the EI ratio was rebalanced from P18-23 in the rat. Nevertheless, the rebalancing of excitation and inhibition possibly due to pruning of dendritic connections as seen by other studies (Ranasinghe et al., 2015), the brain may be losing crucial connections in the auditory cortex that would otherwise be optimal for proper language and communication development. Unfortunately, current treatment of hypothermia presumably reduces activity in all neurons(Lai and Yang, 2011) thus one wonders if this treatment would further reduce the remaining, potentially pruned, L4 connections by P18-23 in the rat and this would potentially impair the computational processing of the developing cortex.

Chapter 7: Neonatal hypoxia causes functional intracortical circuit changes in developing rat auditory cortex from P5-10 and P18-23

Abstract:

Normal brain development requires the proper maturation of neural circuits for normal cognitive functioning. SPNs are among the first cortical neurons to be born and are necessary for normal functional development of the cerebral cortex. Thus, while it is clear that SPNs play a major role in the maturation of developing brain circuitry, it is unclear how hypoxia without ischemia alters SPN circuits. Moreover, it is unknown if Mild HI injuries that do not cause overt histological changes in the cortex can alter SPN circuits. Using a rat HI model, we induced hypoxia at 5% oxygen at P1-2 and exposed the common carotid artery (CCA) but did not impair blood flow in any way (thus no ischemia) so we could compare our study to our earlier investigation of hypoxia-ischemia on the functional microcircuits of auditory cortex over development. We used laser-scanning photostimulation (LSPS) in acute thalamocortical slices of rat auditory cortex during P5-10 to study the functional connectivity of SPN and layer 4 neurons in both injury categories. We find that during P5-10, hypoxia results in hyperconnectivity of SPNs and strengthening of excitatory connections, and hyperconnectivity and strengthening of inhibitory connections from L4 and L5/6 to SPNs**.** In addition, we find that from P5-10, hypoxia results in excitatory hypoconnectivity to L4 neurons and weakened connections within L4. Yet as the brain matures through P18-23, hypoxia results in strengthening

of average excitatory inputs to L4 neurons. However inhibition is not impacted for L4 inputs from either P5-10 or P18-23 as a result of hypoxia alone.

Introduction:

Early birth or disruptions of prenatal brain development result in increased risk of cognitive impairments. Specifically, injury to the premature white matter of the brain results in disruption of the normal maturation of the brain and consequently increases risk of developing cerebral palsy and epilepsy in infants (Rumajogee et al., 2016). Hypoxia during early development often leads to epileptic seizures and these seizures may cause permanent cognitive and neurological deficits (Mordel et al., 2016). While consequent to neonatal hypoxia-ischemia, cortical activity is impaired (Ranasinghe et al., 2015), it is unclear if specific circuits are affected by hypoxia alone (without ischemia).

One key neuronal circuit present in early cortical development whose damage results in abnormal brain function is formed by subplate neurons (SPNs). SPNs are a largely transient neuronal structure that is highly overrepresented in humans (Kanold and Luhmann, 2010). SPN lesions have been shown to prevent the functional maturation of thalamocortical circuits, normal sensory responses, and alter plasticity during the critical period (Kanold et al., 2003; Kanold and Shatz, 2006; Tolner et al., 2012). Particularly, SPN ablations prevent the development of early oscillatory cortical activity patterns (Tolner et al., 2012). Normal functional responses in sensory cortices depend on mature thalamocortical and intracortical circuits. While the effects of SPN damage on thalamocortical circuits have been established, effects of hypoxia

(which does not result in anatomical brain damage) on intracortical circuits are unknown. However our previous studies in the mouse somatosensory cortex with hypoxia only, at 8% oxygen, reveal that while during early development, moderate hypoxia induced increased hyperexcitability and thus increased epileptiform activity which reduced by P28-30, thus highlighting the transient circuit effects from hypoxia(Mordel et al., 2016).

To determine if hypoxia without ischemia has effects on SPN circuitry, or results in changes to intracortical circuits, we analyzed the functional spatial connection patterns of SPNs and layer 4 (L4) neurons during postnatal day (P) 5-10, and L4 neurons at P18-23 using laser-scanning photostimulation (LSPS) in a thalamocortical slice preparation of auditory cortex (ACX). Specifically, we compared connection patterns for excitatory and inhibitory connections in cells from animals that underwent two different severities of neonatal (P1-2) hypoxia sham and control sham animals. In particular, we find that during P5-10, hypoxia results in hyperconnectivity of SPNs and strengthening of excitatory connections, and hyperconnectivity and strengthening of inhibitory connections from L4 and L5/6 to SPNs**.** In addition, we find that from P5-10, hypoxia results in excitatory hypoconnectivity to L4 neurons and weakened connections within L4. Yet as the brain matures through P18-23, hypoxia results in strengthening of average excitatory inputs to L4 neurons. However inhibition is not impacted for L4 inputs from either P5-10 or P18-23 as a result of hypoxia alone.

Results:

During P5-10, hypoxia results in hyperconnectivity of SP and strengthening of excitatory connections

Similar to how neonatal hypoxia-ischemia deficits in the cortex are poorly understood, hypoxia without ischemia also needs investigation on the level of the cortex. Thus we sought to investigate the influence of hypoxia alone on SPN circuits. Since the brain is anatomically normal on a gross histological level after hypoxia (Fig. 5.1), the effects on SPNs and other neurons from hypoxia alone, we investigated the effects of 5% hypoxia compared to a control sham-operated rat over development from P5-10 by using laser-scanning photostimulation (LSPS) of caged glutamate combined with whole-cell patch clamp recordings(Shepherd et al., 2003) to spatially map the connectivity of excitatory (AMPA) and inhibitory (GABA) inputs to A1 SPNs (N = 86 cells; 46 cells for control, and 40 cells for hypoxia). We used the same hypoxia procedure as in the HI projects so we can focus on the effects of hypoxia without surgically induced ischemia.

In order to investigate the spatial pattern of excitatory connections to SPNs and L4 neurons from the cortical plate of ACX, 900 stimulation sites with a spatial resolution of about 40 μm were mapped sequentially in a pseudorandom pattern (Viswanathan et al., 2012) in order to cover the entire radial extent of the cortical column from ventricle to pia (Fig. 5.3E). By calculating the charge of the evoked excitatory postsynaptic current (EPSC), we were able to quantify the strength of the excitatory inputs to SPNs and L4 neurons. These were plotted in two-dimensional maps of connectivity (Fig. 5.1F).

We recorded SPNs and L4 neurons in thalamocortical slices with the holding potential of -70 mV and 0 mV. Again, if a connection was present between a stimulated neuron and the recorded neuron, a postsynaptic current (PSC) was revealed. During voltage-clamp recordings when the SPNs were held at -70 mV, photostimulation was able to evoke two types of responses: 1) a large inward current with short onset latency ($\leq$ 8ms); and 2) a smaller amplitude inward current with a longer latency (Fig. 5.1D). The shorter latency response is attributable to direct activation of the recorded cell while the longer latency response is dependent on synaptic release from the presynaptic cells (Meng et al., 2014).

We first analyzed the excitatory circuits associated with SPNs by holding cells at -70mV. We then stimulated 900 sites for each cell and then for stimulation sites that showed evoked EPSCs measured the size of the EPSC (Fig. 5.1F) resulting in a map of excitatory connectivity for each cell. This map indicates the location of presynaptic cells to the recorded SPN or L4 neuron. We then aligned the maps to the soma position and calculated for every spatial location the probability of being connected to a given SPN neuron resulting in a spatial connection probability map (Fig. 5.1F).

We find that during P5-10, hypoxia results in hyperconnectivity of SP with respect to the total area and strengthening of excitatory connections represented as the mean EPSC charge (Fig. 7.1B, D). We also find that hypoxia results in an expansion along the rostral-caudal extent across SP, L5/6, and L4. While the total area of EPSCs within L5/6 and L4 do not alter, it is because their input spreads laterally and not as much in the columnar extent (Fig. 7.1D, F). For P5-10, EPSC amplitudes and charge

increase in L5/6, and within SP as a result of hypoxia (Fig. 7.2A). However for IPSC total amplitudes and total charge within L4 do not alter as a result of hypoxia (Fig. 7.2B). Additionally, total IPSC amplitudes within SP and L5/6 increase, and total charge of IPSCs increase in L5/6 and L4 as a result of hypoxia (Fig. 7.2B). Layer averages for mean amplitude of EPSCs increase in L5/6 and SP as a result of hypoxia. In addition, mean amplitudes of IPSCs increase within L5/6 and L5 due to hypoxia (Fig. 7.2B).

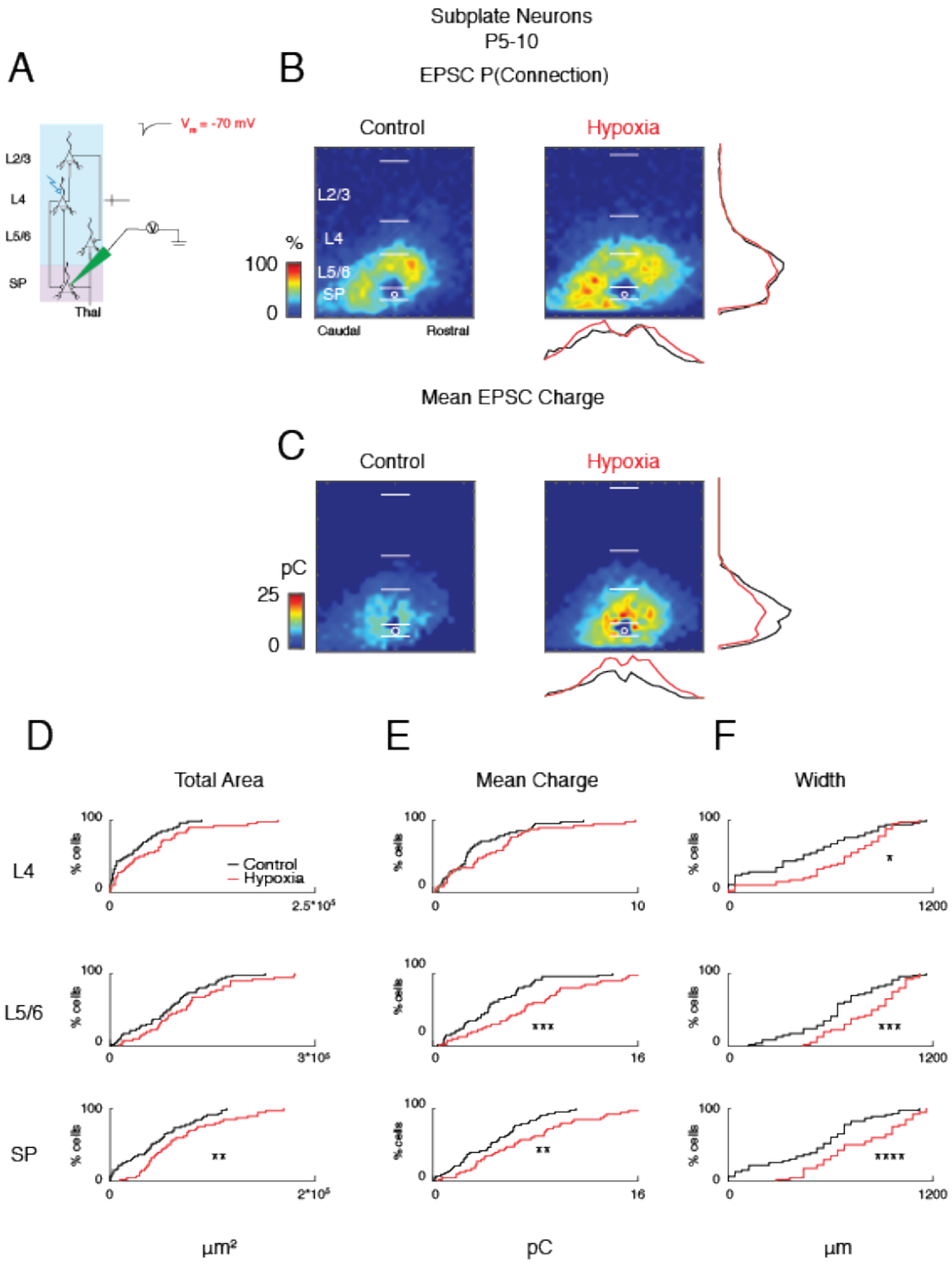
Subplate Neurons
P5-10
A
B
EPSC P(Connection)
L2/3
L4
L5/6
SP
Thal
Control
Hypoxia
%
100
0
Caudal
Rostral
Mean EPSC Charge
C
pC
25
0
D
E
F
Total Area
Mean Charge
Width
Control
Hypoxia
% cells
2.5*10⁵
3*10⁵
2*10⁵
10
16
1200
µm²
pC
µm

Figure 7.1: During P5-10, hypoxia results in hyperconnectivity of SP and strengthening of excitatory connections. A. Reference view of electrode positioning in the layer recorded and example laser photostimulation location (photostimulation from pia to SP- see methods for more details). **B.** Spatial distribution of sites of excitatory input to SPNs that alter due to hypoxia at P5-10. Probability of connection occurrence P(Connection) for excitatory (-70 mV) activity. **C.** Spatial distribution of transferred charge (Mean EPSC Charge) for excitatory (-70 mV) activity. **D-F.** Cumulative distribution function (CDF) of excitatory input to SPNs. Layer totals for area (left), mean transferred charge (middle), and marginal width along rostral-caudal axis (right) for L4, L5/6, and SPN input to the recorded SPN. Horizontal bars indicate layer boundaries and serve as scale bar of 200 um. Black and red overlaying traces on the side of the maps indicate summed EPSC marginal distributions for each group. Black squares in the matrix denote significance, white squares are not significant. Comparisons: SP total area ($p \leq 0.01$); mean charge L5/6 ($p \leq 0.001$), mean charge SP ($p \leq 0.01$); marginal rostral-caudal width L4 ($p \leq 0.05$), width L5/6 ($p \leq 0.001$), width ($p \leq 0.0001$).

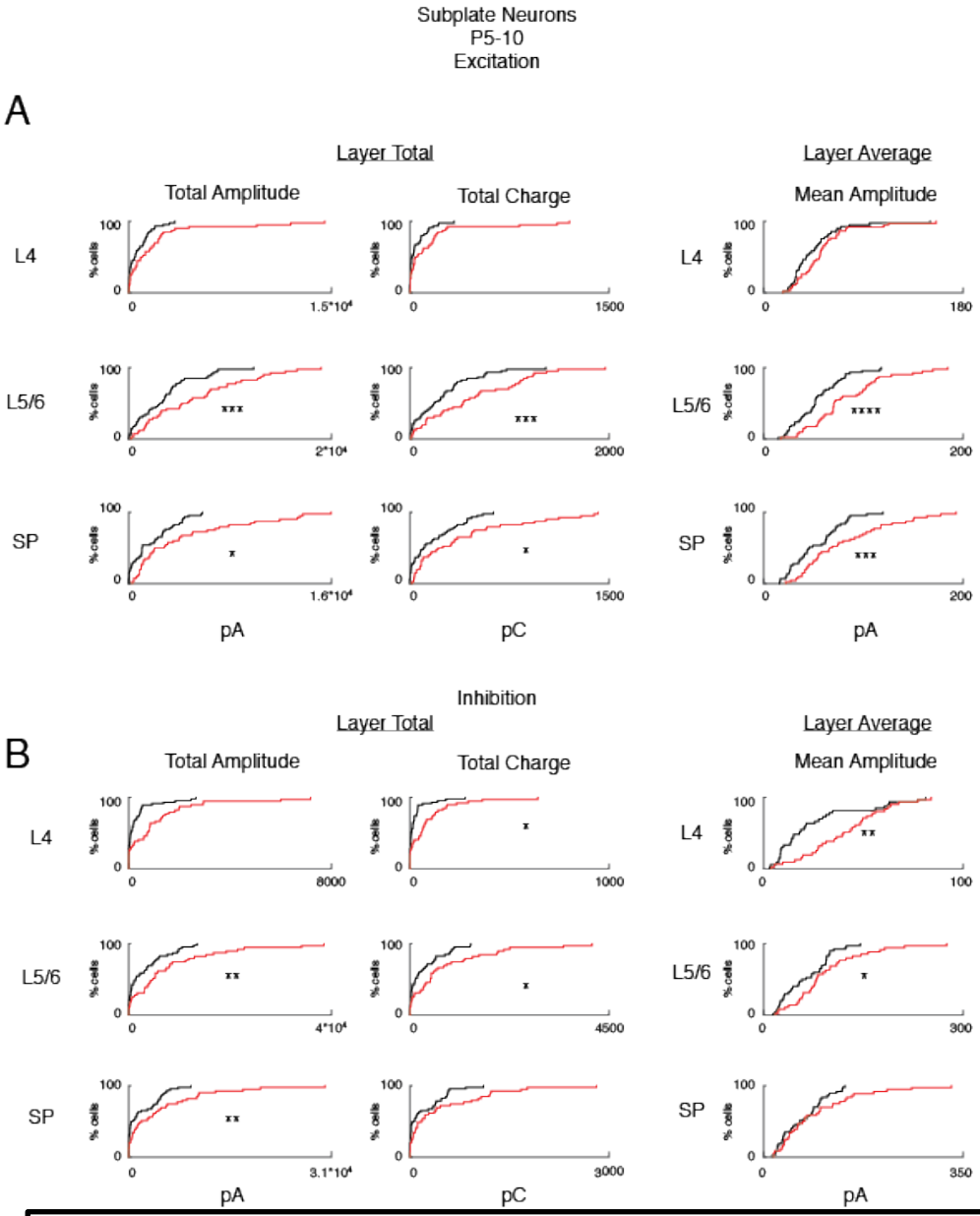

Figure 7.2) Related to figures 7.1, 7.3: Cumulative distribution functions of layer totals and layer averages for excitatory input and inhibitory input to SPNs. Layer totals for amplitude of PSCs (left), total charge (middle), and mean amplitude (right) for L4, L5/6 and SPN input to the recorded SPN. **A.** For excitatory input (EPSC): SP total amplitude ($p \leq 0.05$), L5/6 total amplitude ($p \leq 0.001$), SP charge ($p \leq 0.05$), L5/6 charge ($p \leq 0.001$), SP mean amplitude ($p \leq 0.001$), L5/6 mean amplitude ($p \leq 0.0001$) **B.** For inhibitory input (IPSC): SP total amplitude ($p \leq 0.01$), L5/6 total amplitude ($p \leq 0.01$), L5/6 total charge ($p \leq 0.05$), L4 total charge ($p \leq 0.05$), L5/6 mean amplitude ($p \leq 0.05$), L4 mean amplitude ($p < 0.01$).

During P5-10, hypoxia results in hyperconnectivity and strengthening of inhibitory connections from L4 and L5/6 to SP

We find that from P5-10, hypoxia alone results in an increase in the total area of inhibitory input from L5/6 and L4 to SP (Fig. 7.3B,D). Additionally, the mean IPSC charge strengthens for L5/6 and L4 input to SP as a result of hypoxia (Fig. 7.3C, E). However while the total area of inhibitory input from within SP does not change, the width along the rostral-caudal axis does expand laterally within SP and arising from L5/6 (Fig. 7.3F). For the layer totals we find that after hypoxia, IPSC total amplitude increases within SP and L5/6 (Fig. 7.2B). Additionally, we find that the total charge of IPSCs strengthens within L5/6 and L4 due to hypoxia (Fig. 7.2B). While the total IPSC amplitude increases within SP after hypoxia, the mean amplitude of IPSC input within SP does not change. This reveals that when you average the IPSC input over the area of the SP, the amplitude of the IPSCs does not change within SP (Fig. 7.2B).

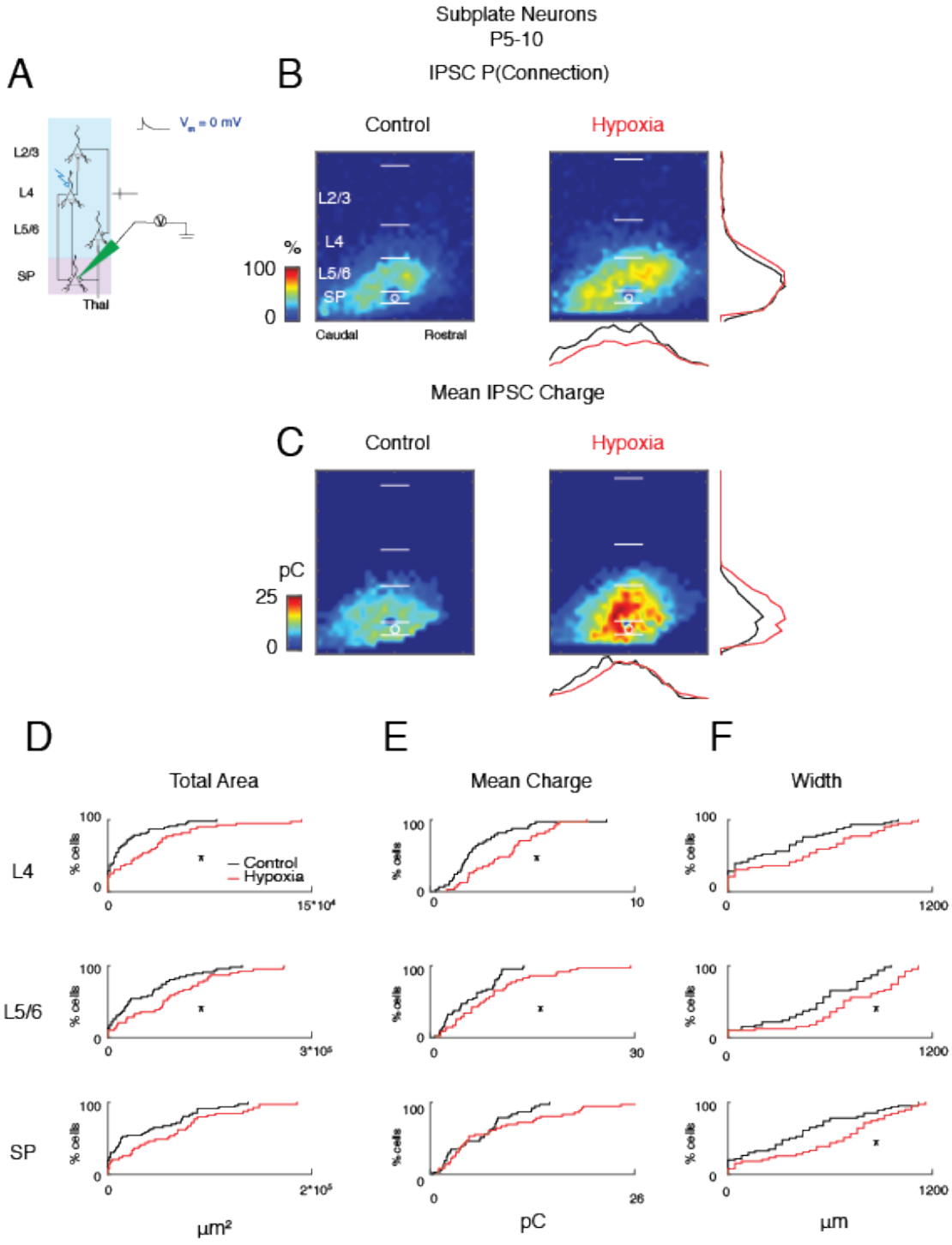
Subplate Neurons
P5-10
A
B
IPSC P(Connection)
L2/3
L4
L5/6
SP
Thal
Control
Hypoxia
%
100
0
Caudal
Rostral
Mean IPSC Charge
C
pC
25
0
D
E
F
Total Area
Mean Charge
Width
L4
L5/6
SP
% cells
Control
Hypoxia
15*10⁴
3*10⁵
2*10⁵
µm²
10
30
26
pC
1200
µm

Figure 7.3: During P5-10, hypoxia results in hyperconnectivity of inhibitory connections and strengthening of connections from L4 and L5/6 to SP. A. Reference view of electrode positioning in the layer recorded and example laser photostimulation location (photostimulation from pia to SP- see methods for more details). **B.** Spatial distribution of sites of inhibitory input to SPNs that alter due to hypoxia at P5-10. Probability of connection occurrence P(Connection) for inhibitory (0 mV) activity. **C.** Spatial distribution of transferred charge (Mean IPSC Charge) for inhibitory (0 mV) activity. **D-F.** Cumulative distribution function (CDF) of inhibitory input to SPNs. Layer totals for area (left), mean transferred charge (middle), and marginal width along rostral-caudal axis (right) for L4, L5/6, and SPN input to the recorded SPN. Horizontal bars indicate layer boundaries and serve as scale bar of 200 um. Black and red overlaying traces on the side of the maps indicate summed IPSC marginal distributions for each group. Black squares in the matrix denote significance, white squares are not significant. Comparisons: L4 total area ($p \leq 0.05$), L5/6 total area ($p \leq 0.05$); L4 mean charge ($p \leq 0.05$), L5/6 mean charge ($p \leq 0.05$), width L5/6 ($p \leq 0.05$), width SP ($p \leq 0.05$).

From P5-10, hypoxia results in excitatory hypoconnectivity to L4 neurons and weakened connections within L4

Next, we investigated the effects of 5% hypoxia compared to a control sham-operated rat over development from P5-10 by using laser-scanning photostimulation (LSPS) of caged glutamate combined with whole-cell patch clamp recordings(Shepherd et al., 2003) to spatially map the connectivity of excitatory (AMPA) and inhibitory (GABA) inputs to A1 L4 neurons (N = 80 cells; 40 cells for control, and 40 cells for hypoxia). From P5-10 we find that after hypoxia, L4 input from L2/3 decreases with respect to the total area from L2/3 (Fig. 7.4B, D). We also find that the width along the rostral-caudal extent from both L2/3 and L4 also become more narrow after hypoxia (Fig. 7.4C, F). Thus there is reduction in the columnar extent and a narrowing of connectivity in the laminar extent from L2/3 to L4 for excitation. With regards to the strength of EPSCs, we find that there is a weakening

of excitatory connections within L4 (Fig. 7.4C, E). Similarly, we find that hypoxia reduces total EPSC amplitude, total EPSC charge, and the mean EPSC amplitude from within the SP (Fig. 7.2A).

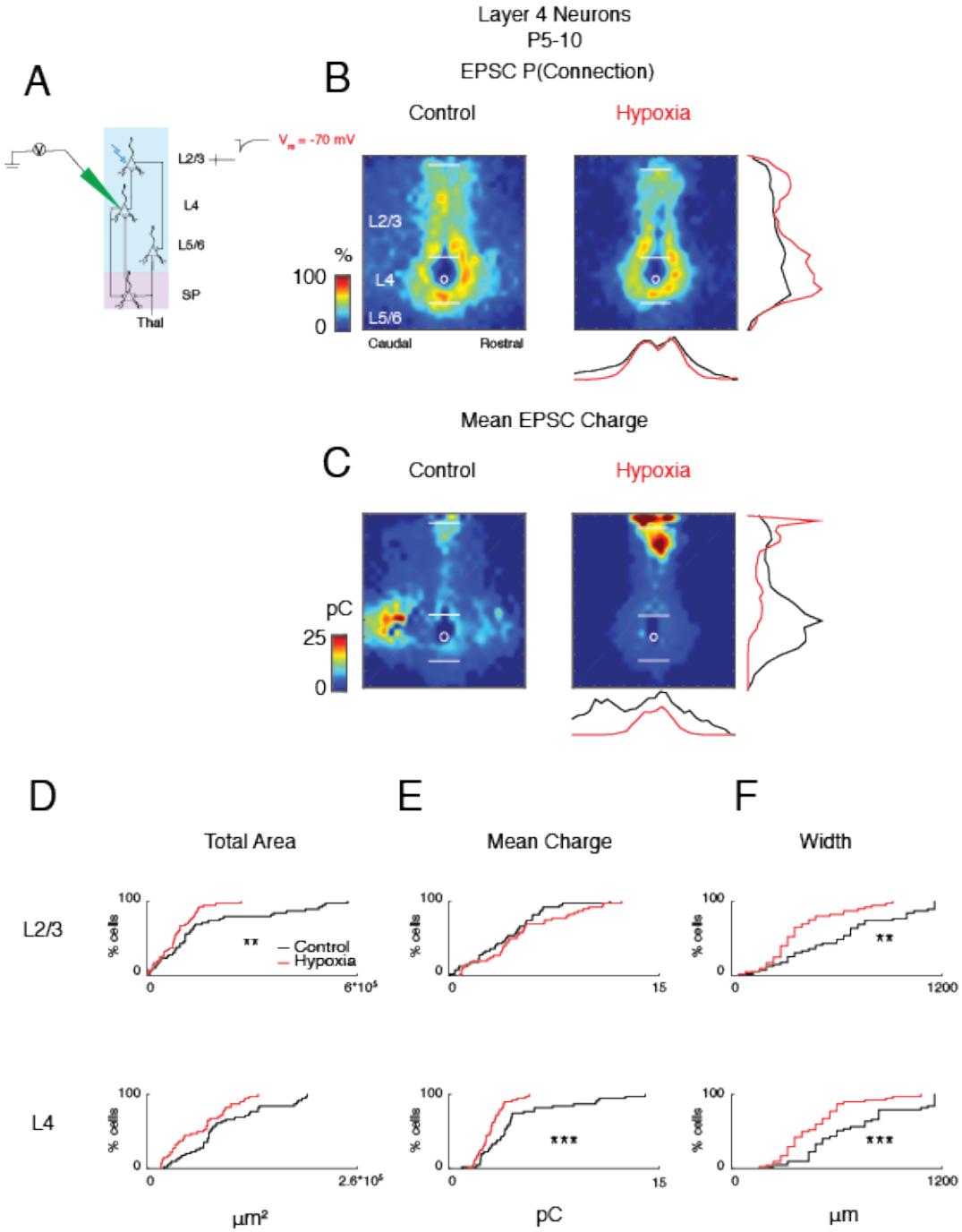

Figure 7.4: From P5-10, hypoxia results in excitatory hypoconnectivity to L4 neurons and weakened connections within L4. A. Reference view of electrode positioning in the layer recorded and example laser photostimulation location (photostimulation from pia to L4- see methods for more details). **B.** Spatial distribution of sites of excitatory input to L4 that alter due to hypoxia at P5-10. Probability of connection occurrence P(Connection) for excitatory (-70 mV) activity. **C.** Spatial distribution of transferred charge (Mean EPSC Charge) for excitatory (-70 mV) activity. **D-F.** Cumulative distribution function (CDF) of excitatory input to L4. Layer totals for area (left), mean transferred charge (middle), and marginal width along rostral-caudal axis (right) for L2/3 and L4 input to the recorded L4 neuron. Horizontal bars indicate layer boundaries and serve as scale bar of 200 um. Black and red overlaying traces on the side of the maps indicate summed EPSC marginal distributions for each group. Black squares in the matrix denote significance, white squares are not significant. Comparisons: total area L2/3 ($p \leq 0.01$), mean charge L4 ($p \leq 0.001$), width L2/3 ($p \leq 0.01$), width L4 ($p \leq 0.001$).

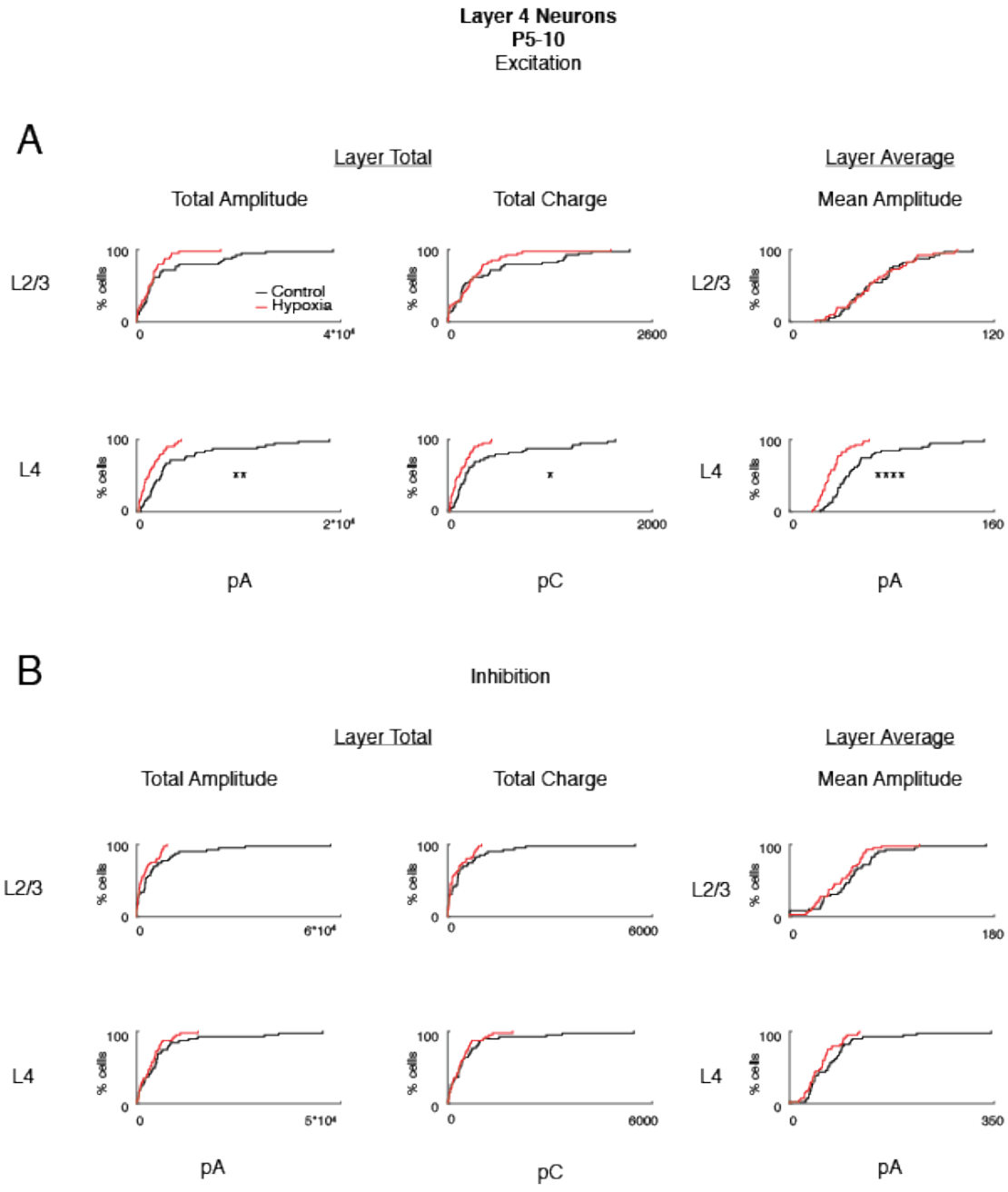

Figure 7.5) Related to figures 7.4, 7.6: Cumulative distribution functions of layer totals and layer averages for excitatory input and inhibitory input to L4 neurons. Layer totals for amplitude of PSCs (left), total charge (middle), and mean amplitude (right) for L2/3 and L4 input to the recorded L4 neuron. **A.** For excitatory input (EPSC): L4 total amplitude ($p \leq 0.01$), L4 total charge ($p \leq 0.05$), L4 mean amplitude ($p \leq 0.0001$) **B.** For inhibitory input (IPSC): no significant differences.

During P5-10, hypoxia results in no changes to inhibitory connectivity to L4 neurons

For inhibition of input to L4, we find that after hypoxia there are no changes in total area, mean charge, or width of IPSCs (Fig. 7.6D, E, F). However qualitatively in the appearance of the average maps, there seems to be a narrowing within L4 and a weakening of IPSC charge within L4 and L2/3 (Fig. 7.6B, C). Nevertheless, single-cell quantitative analysis reveals that there are no differences in any of these measures in either L2/3 or L4 (Fig. 7.6D, E, F, 7.5B).

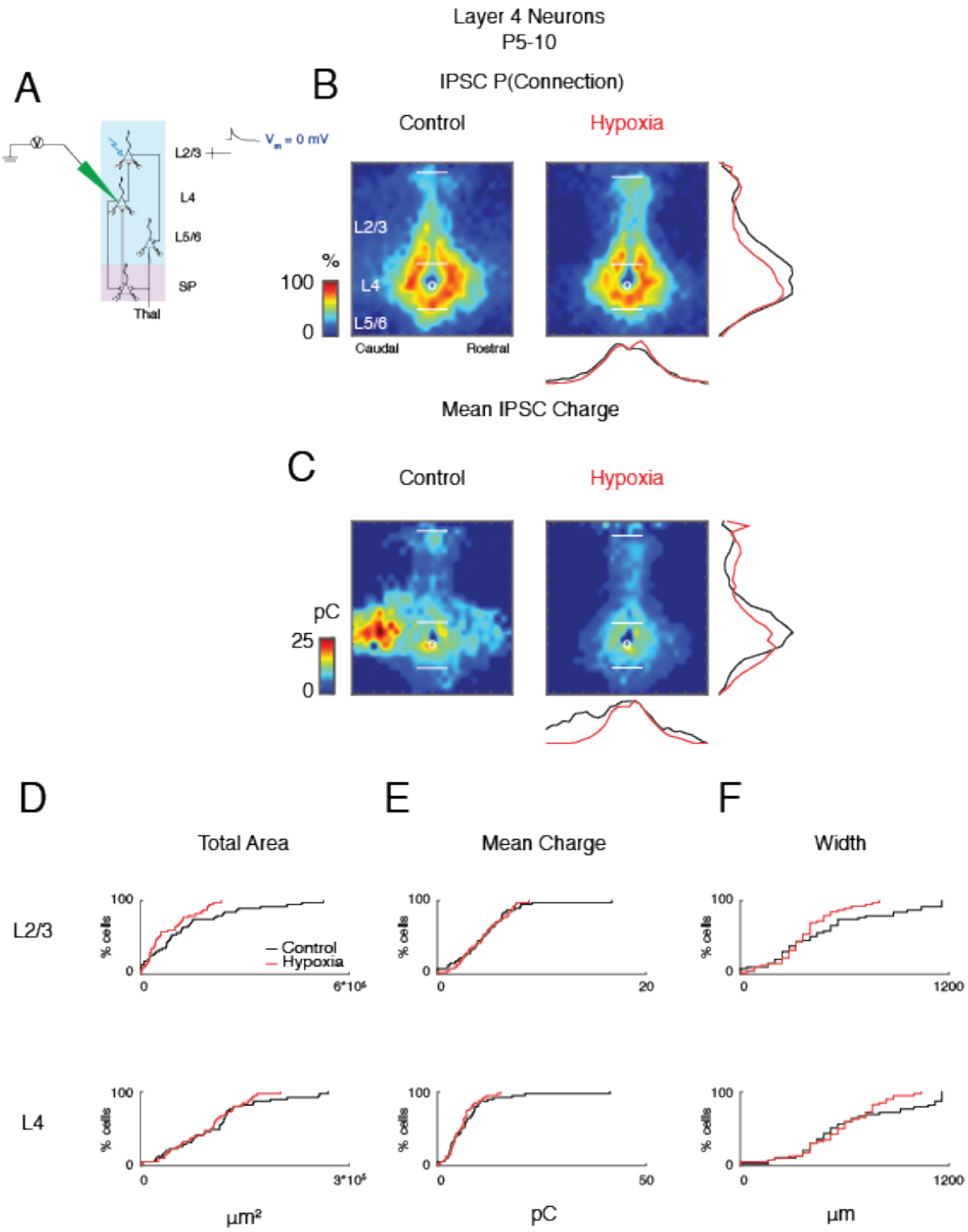
Layer 4 Neurons
P5-10
A
B
IPSC P(Connection)
Control
Hypoxia
L2/3
L4
L5/6
SP
Thal
V_m = 0 mV
%
100
0
Caudal
Rostral
Mean IPSC Charge
C
pC
25
0
D
E
F
Total Area
Mean Charge
Width
L2/3
L4
% cells
Control
Hypoxia
6*10⁵
3*10⁵
20
50
1200
µm²
pC
µm

Figure 7.6: During P5-10, hypoxia results in no changes to inhibitory connectivity to L4 neurons. A. Reference view of electrode positioning in the layer recorded and example laser photostimulation location (photostimulation from pia to L4- see methods for more details). **B.** Spatial distribution of sites of inhibitory input to L4 that alter due to hypoxia at P5-10. Probability of connection occurrence P(Connection) for inhibitory (0 mV) activity. **C.** Spatial distribution of transferred charge (Mean IPSC Charge) for inhibitory (0 mV) activity. **D-F.** Cumulative distribution function (CDF) of inhibitory input to L4. Layer totals for area (left), mean transferred charge (middle), and marginal width along rostral-caudal axis (right) for L2/3 and L4 input to the recorded L4 neuron. Horizontal bars indicate layer boundaries and serve as scale bar of 200 um. Black and red overlaying traces on the side of the maps indicate summed IPSC marginal distributions for each group. Black squares in the matrix denote significance, and white squares are not significant. Comparisons: no significant differences.

As the brain matures through P18-23, hypoxia results in strengthening of average excitatory inputs to L4 neurons

Next, we investigated the effects of 5% hypoxia compared to a control sham-operated rat over from P18-23 by using laser-scanning photostimulation (LSPS) of caged glutamate combined with whole-cell patch clamp recordings(Shepherd et al., 2003) to spatially map the connectivity of excitatory (AMPA) and inhibitory (GABA) inputs to A1 L4 neurons (N = 80 cells; 40 cells for control, and 40 cells for hypoxia). After hypoxia from P1-2, we find that from P18-23 the mean EPSC charge for input arising from L2/3 and within L4 strengthens as the brain matures (Fig. 7.7C, E). We also find no differences in the density of connectivity of EPSCs from either L2/3 or L4 from P18-23 after hypoxia (Fig. 7.7D, F). Similarly, we find that there is an increase in the total EPSC charge from within L4 after hypoxia (Fig. 7.8A). However the total amplitude and mean amplitudes of EPSCs from L2/3 and within L4 were unaltered after hypoxia (Fig. 7.8A). The charge is the transferred charge of the PSC,

thus while the peak amplitude is unchanging, the trace of the EPSC is widening and thus a longer decay time of the EPSC to compensate for no changes in the peaks of the EPSCs after hypoxia.

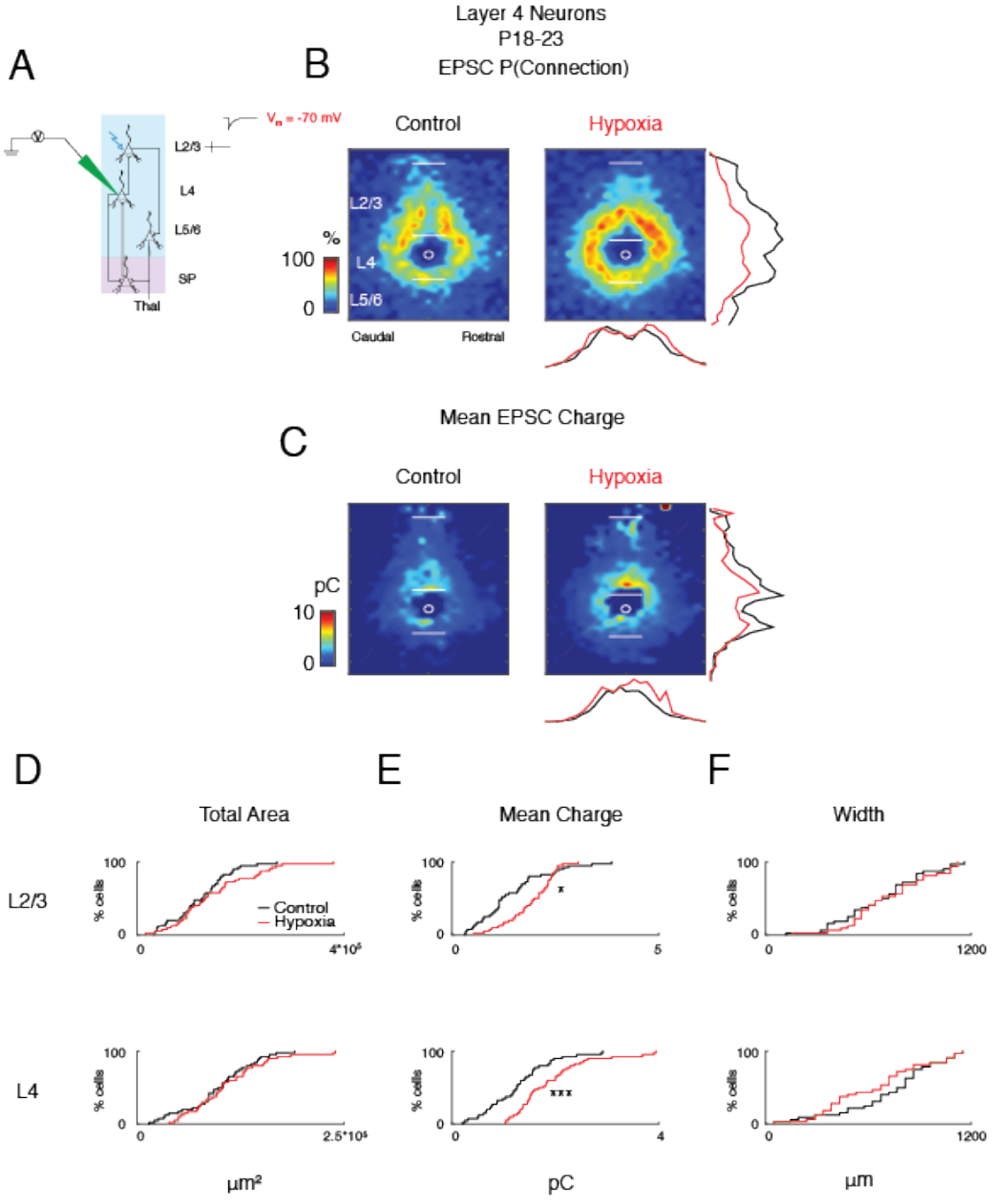

Figure 7.7: From P18-23, hypoxia results in strengthening of excitatory inputs to L4 A. Reference view of electrode positioning in the layer recorded and example laser photostimulation location (photostimulation from pia to L4- see methods for more details). **B.** Spatial distribution of sites of excitatory input to L4 that alter due to hypoxia at P18-23. Probability of connection occurrence P(Connection) for excitatory (-70 mV) activity. **C.** Spatial distribution of transferred charge (Mean EPSC Charge) for excitatory (-70 mV) activity. **D-F.** Cumulative distribution function (CDF) of excitatory input to L4. Layer totals for area (left), mean transferred charge (middle), and marginal width along rostral-caudal axis (right) for L2/3 and L4 input to the recorded L4 neuron. Horizontal bars indicate layer boundaries and serve as scale bar of 200 um. Black and red overlaying traces on the side of the maps indicate summed EPSC marginal distributions for each group. Black squares in the matrix denote significance, white squares are not significant. Comparisons: mean charge L2/3 ($p \leq 0.05$); mean charge L4 ($p \leq 0.001$).

During P18-23, hypoxia does not alter L4 inhibitory circuitry

Qualitatively, we find that the average map of inhibitory connectivity to L4 appears to be lessened in the columnar extent and was denser closer to the soma (Fig. 7.9B). However quantitatively, we find that after hypoxia the inhibitory input to L4 is unaltered from P18-23 (Fig. 7.9D, E, F). Similarly, we find that hypoxia does not alter total amplitude, total charge, or mean amplitude of the IPSC input to L4 on a single-cell analysis level (Fig. 7.8B).

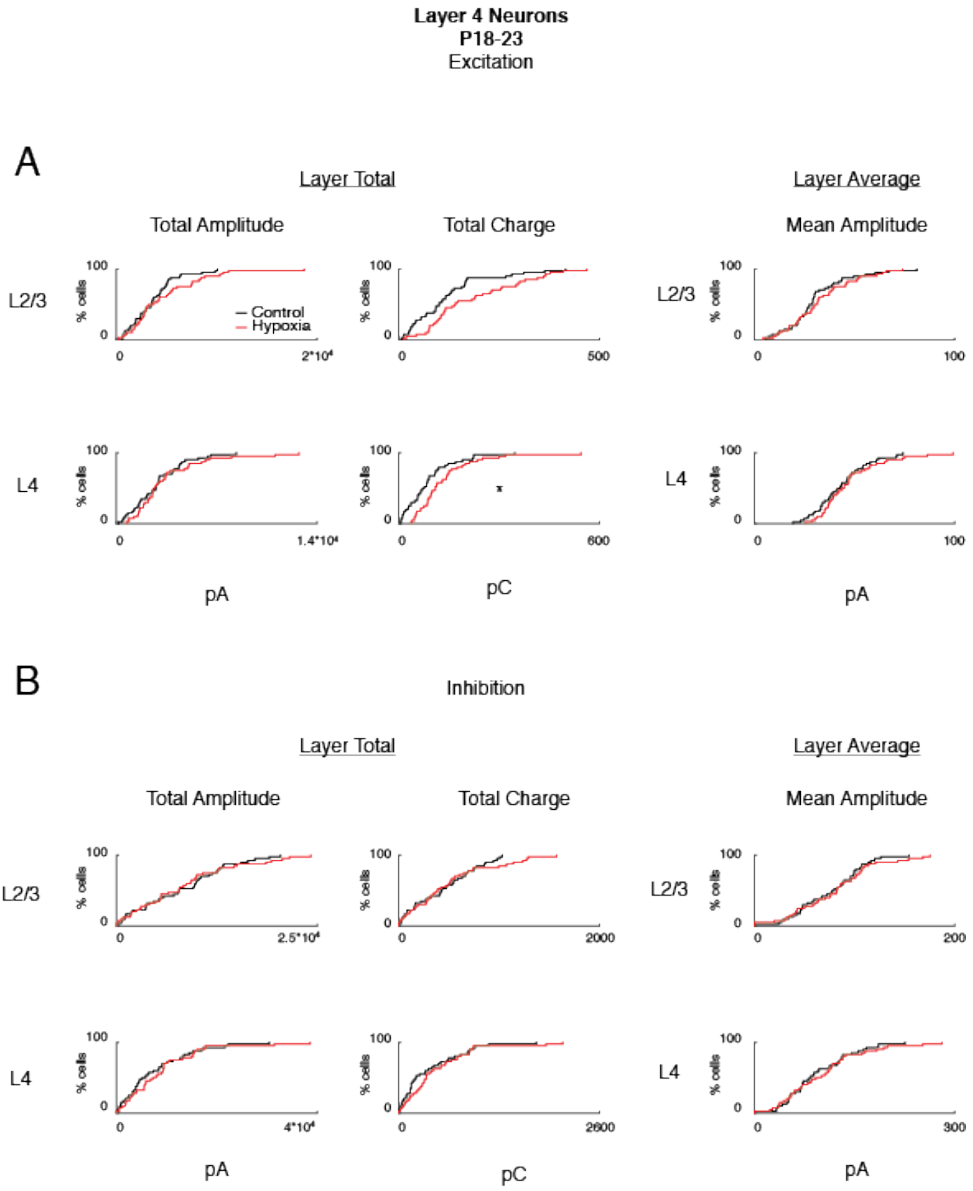

Figure 7.8) Related to figures 7.7, 7.9: Cumulative distribution functions of layer totals and layer averages for excitatory input and inhibitory input to L4 neurons. Layer totals for amplitude of PSCs (left), total charge (middle), and mean amplitude (right) for L2/3 and L4 input to the recorded L4 neuron. **A.** For excitatory input (EPSC): L4 total charge ($p \leq 0.05$). **B.** For inhibitory input (IPSC): no significant differences.

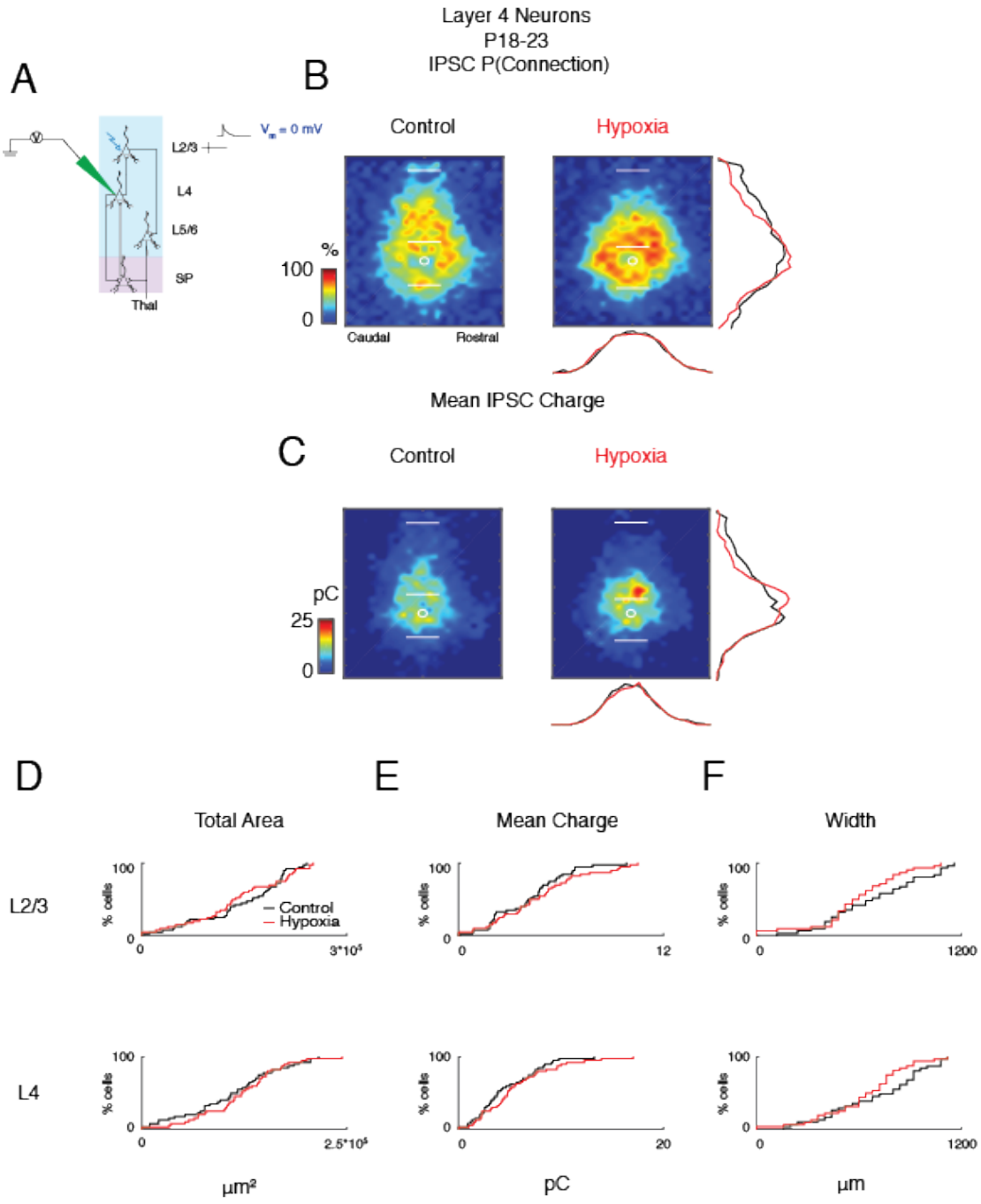
Layer 4 Neurons
P18-23
IPSC P(Connection)
A
B
C
D
E
F
L2/3
L4
L5/6
SP
Thal
Control
Hypoxia
%
100
0
Caudal
Rostral
Mean IPSC Charge
pC
25
0
Total Area
Mean Charge
Width
% cells
Control
Hypoxia
3*10⁵
12
1200
2.5*10⁵
20
µm²
pC
µm

Figure 7.9: During P18-23, hypoxia does not alter L4 inhibitory circuitry. A. Reference view of electrode positioning in the layer recorded and example laser photostimulation location (photostimulation from pia to L4- see methods for more details). **B.** Spatial distribution of sites of inhibitory input to L4 that alter due to hypoxia at P18-23. Probability of connection occurrence P(Connection) for inhibitory (0 mV) activity. **C.** Spatial distribution of transferred charge (Mean IPSC Charge) for inhibitory (0 mV) activity. **D-F.** Cumulative distribution function (CDF) of inhibitory input to L4. Layer totals for area (left), mean transferred charge (middle), and marginal width along rostral-caudal axis (right) for L2/3 and L4 input to the recorded L4 neuron. Horizontal bars indicate layer boundaries and serve as scale bar of 200 um. Black and red overlaying traces on the side of the maps indicate summed EPSC marginal distributions for each group. Black squares in the matrix denote significance, white squares are not significant. Comparisons: no significant differences.

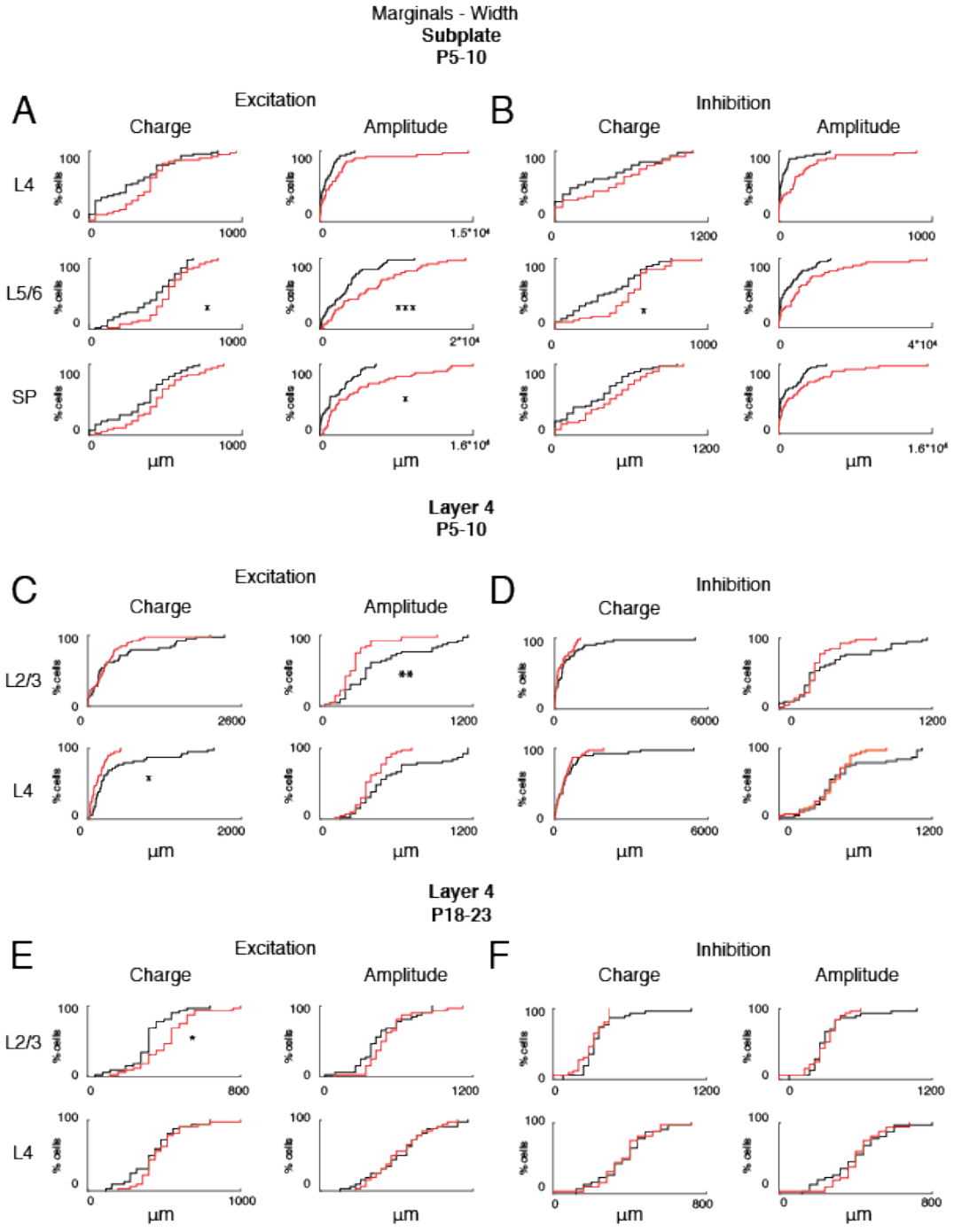
Marginals - Width
Subplate
P5-10
A
Excitation
Charge
Amplitude
B
Inhibition
Charge
Amplitude
L4
L5/6
SP
% cells
µm
Layer 4
P5-10
C
Excitation
Charge
Amplitude
D
Inhibition
Charge
L2/3
L4
Layer 4
P18-23
E
Excitation
Charge
Amplitude
F
Inhibition
Charge
Amplitude

Figure 7.10) Related to figures 7.1, 7.3, 7.4, 7.6, 7.7, 7.9: A. CDFs for marginal rostral-caudal width for EPSC for charge (left) and amplitude (right) for L4, L5/6 and SP for P5-10. Comparison: L5/6 charge ($p \leq 0.05$), SP amplitude ($p \leq 0.05$), L5/6 amplitude ($p \leq 0.001$). **B.** CDFs for marginal rostral-caudal width for IPSC for charge (left) and amplitude (right) for L4, L5/6 and SP for P5-10. Comparison: L5/6 charge ($p \leq 0.05$). **C.** CDFs for marginal rostral-caudal width for EPSC for charge (left) and amplitude (right) for L2/3 and L4 for P5-10. Comparison: L4 charge ($p \leq 0.05$), L2/3 amplitude ($p \leq 0.01$). **D.** CDFs for marginal rostral-caudal width for IPSC for charge (left) and amplitude (right) for L2/3 and L4 for P5-10. No significant differences. **E.** CDFs for marginal rostral-caudal width for EPSC for charge (left) and amplitude (right) for L2/3 and L4 for P18-23. Comparison: L2/3 charge ($p \leq 0.05$). **F.** CDFs for marginal rostral-caudal width for IPSC for charge (left) and amplitude (right) for L2/3 and L4 for P18-23. No significant differences.

From P5-10, excitatory and inhibitory input to SPNs are balanced after hypoxia

For normal brain function, a balance of excitation to inhibition is required. Because seizures are often due to an imbalance of excitatory and inhibitory activity, we sought to investigate if the balance of excitation to inhibition (EI ratio) was altered after hypoxia. Externally, we did not observe seizure activity in these pups therefore these results suggest that the EI ratio reflects that balanced excitation to inhibition we reveal through investigation of microcircuitry on a single-cell level in vitro. Despite the changes to input to SPNs, we find that overall the excitation and inhibition balances from P5-10 after hypoxia. Specifically, there is no difference in the EI ratios for the layer areas, and charges for SP, L5/6, and L4 (Fig. 7.11).

Subplate
P5-10
Overlay of Excitation to Inhibition
Connection Probability

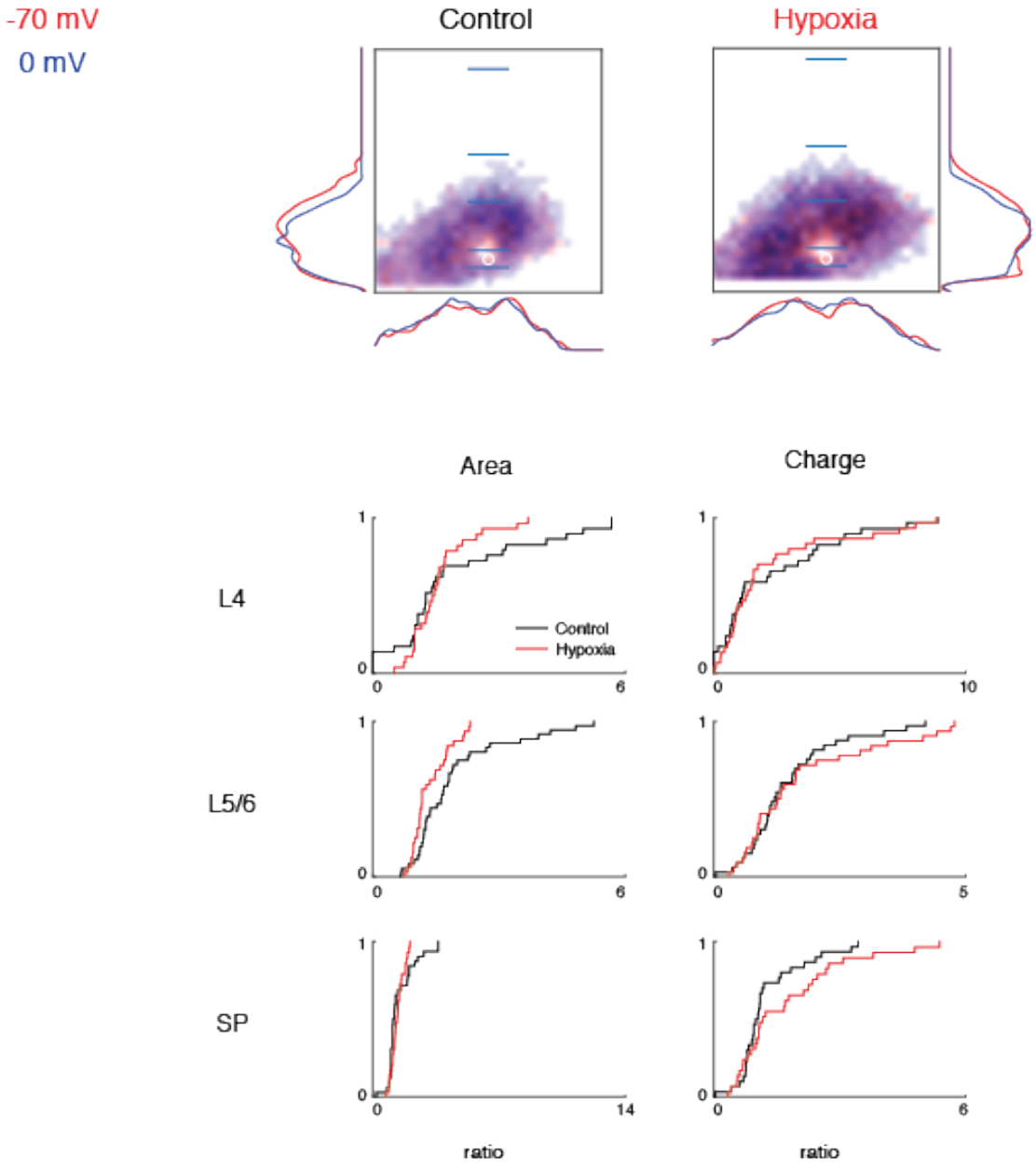

Figure 7.11: Overlay of balanced ratio of excitation to inhibition of input to SP as a result of hypoxia in P5-10 rats. A. Summary schematic of excitatory and inhibitory input to SPNs superimposed (Control, left; Hypoxia, right). Red color represents excitatory input, and blue color represents inhibitory input to SP. Red and blue overlaying traces on the sides of the maps indicate summed EPSC and IPSC marginal distributions. Blue scale bar denotes 200 μm. **B.** Cumulative distribution function (CDF) of the ratio of excitatory to inhibitory input as it changes as a result hypoxia for both area (left) and charge (right) for L4, L5/6, and SP. There are no significant differences in area or charge for the EI ratios.

Hypoxia causes an imbalance of excitatory and inhibitory input to L4 from P5-10 through P18-23

We know through other studies that SPNs project into L4 (Zhao et al., 2009) and there are reciprocal corticothalamic projections from L4 to SP (Viswanathan et al., 2016). Thus we investigated if L4 inputs were balanced as a result of hypoxia. We find that as early as P5-10, and through P18-23, there is an imbalance in the excitatory to inhibitory input to L4 (Fig. 7.12). However, the source of this imbalance shifts as the brain matures after hypoxia. Specifically during P5-10, the imbalance of inputs arises from within L4, where there is a decrease in the EI ratio (Fig. 7.12B). This represents an increase in inhibitory inputs from P5-10. However, as the brain matures from P18-23, the source of the EI ratio imbalance shifts superficially to L2/3 (Fig. 7.12C, D). We find an increase in the EI ratio from P18-23 within L2/3 and this represents an increase in the excitation component of the ratio.

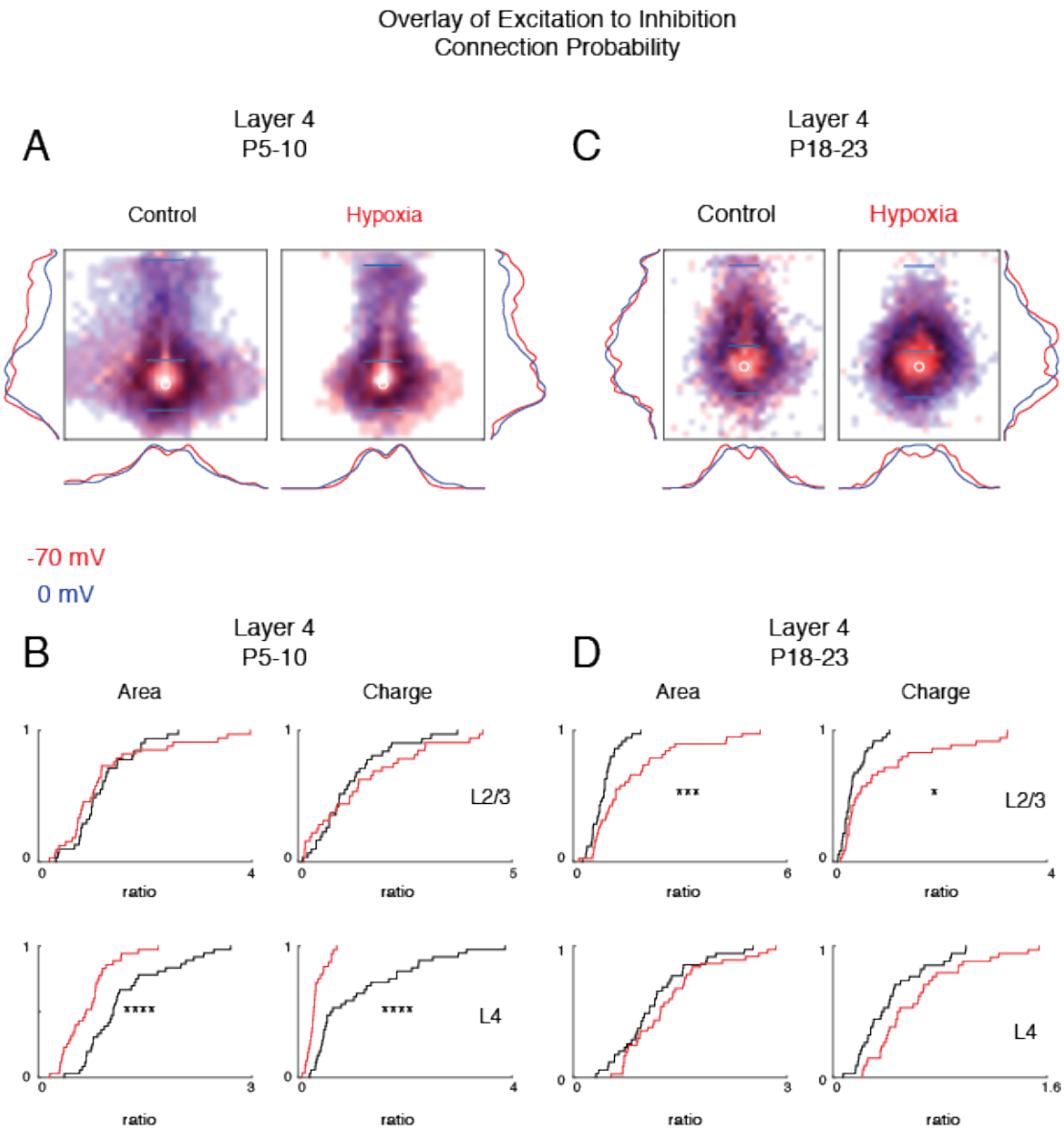

Figure 7.12: Overlay of excitation to inhibition of input to L4 for the as a result of hypoxia in P5-10 rats. A. Summary schematic of excitatory and inhibitory input to L4 neurons superimposed (Control, A ; Hypoxia, C). Red color represents excitatory input, and blue color represents inhibitory input to L4. Red and blue overlaying traces on the sides of the maps indicate summed EPSC and IPSC marginal distributions. Blue scale bar denotes 200 μm. **B.** Cumulative distribution function (CDF) of the ratio of excitatory to inhibitory input (EI ratio) as it changes as a result hypoxia for both area (left) and charge (right) for L2/3 and L4. Comparisons: P5-10 L4 area ($p \leq 0.0001$), L4 charge ($p \leq 0.0001$); P18-23 L2/3 area ($p \leq 0.001$), L2/3 charge ($p \leq 0.05$).

Hypoxia results in increased response gains in the acoustic startle reflex

Acoustic startle responses are often used as way to behaviorally detect changes in excitability of the brain. The acoustic startle response (ASR) is a way to examine auditory function (Rybalko et al., 2015). However it is important to note that the ASR is a reflexive auditory behavior that does not need animal training and therefore can be used for studies investigating of early ontogeny (Rybalko et al., 2015). One measure we used was the response gain ratio in order to see if this reflected hemispheric excitability due to hypoxia. The response gain ratio is a ratio of the response amplitude at the highest startle level of 105 dB normalized by the lowest level at 55 dB. The higher the ratio, the more strongly the animal responds to the loudest level compared to the lowest level. Thus, we used a startle behavior paradigm investigating the sensitivity levels of rats from P13-16 after hypoxia (see methods – Ch.2) (N = 9 rats; 5 rats for control, and 4 rats for hypoxia). We used rats from P13-16 because that is after the onset of hearing, which is around P11-12. We did not find changes in the sensitivity startle thresholds of the hypoxia rats; however, we did find that after hypoxia there is an increase in the ratio of the response gain from P13-16 from (Fig. 7.13).

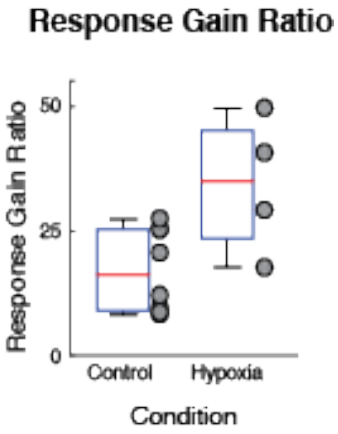

Figure 7.13: Response gain ratio increases in startle reflex of hypoxic rats. p = 0.0491, one-way ANOVA.

Discussion:

Here we show that an animal model of hypoxia alone causes distinct changes to functional cortical microcircuits over development in the neonatal rodent. While we did see functional circuit changes for input to L4 neurons from P5-10 and P18-23, the effects of hypoxia were most pronounced SPNs from P5-10. This suggests that SPNs are also selectively vulnerable as early as P5 to hypoxia exposure (5% oxygen) at P1-2. Therefore functional microcircuit mapping is a sensitive enough measure in order to detect and identify functional connectivity changes on a laminar-specific microcircuit level as a result of neonatal hypoxia. Additionally, we are able to delineate distinct changes throughout development of L4 circuits after hypoxia. Our results suggest that subplate is selectively vulnerable to hypoxia (5% oxygen). Is it

important to note that many other studies of hypoxia are at higher percentages of oxygen therefore one must note the percentage of oxygen across studies.

SPNs are the earliest born cortical neurons and are first to receive thalamic input as well as from intercortical sources and project to L4(Zhao et al., 2009); (Kanold and Luhmann, 2010) (Meng et al., 2014) (Viswanathan et al., 2016). Importantly, SPNs are required for the maturation of excitatory and inhibitory circuitry to thalamorecipient layer 4 (Kanold et al., 2003); (Kanold and Shatz, 2006); (Tolner et al., 2012). With excitatory input projected from subplate to L4, the altered SPN connectivity we reveal here would similarly predict altered connections to L4 neurons. Surprisingly, while we do see hyperconnectivity of excitatory input within SP after hypoxia, by P5-10 input to L4 neurons end up becoming hypoconnected excitatory input to L4 from L2/3. However by P18-23, that hypoconnectivity we saw for L4 input becomes diminished by P18-23. This suggests a cortical rewiring of not only SP circuits by of L4 circuits throughout development as a result of hypoxia. We also see that the excitatory rostral-caudal extent for L4 input becomes narrowed only from P5-10, but by P18-23 excitatory input width does not change after hypoxia. Additionally, this reveals that there is an extended window of therapeutic treatment for L4 circuitry, however for SP circuitry that window is from P5-10 in the neonatal rat. However with regards to tonotopy, the time window for adjusting the microcircuitry of excitatory L4 input is up until P10. Thus if one were to treat hypoxia auditory function, treatment before P10 (rat) is optimal in order to catch the L4 circuitry when it is most dynamic and in process of rewiring on a more subtle manner.

However with regards to GABAergic inhibitory connectivity, we see that hypoxia results in hyperconnectivity of input from above SP, such as from L5/6 and 4. But for input to L4 circuits, we see that that there is no hyperconnectivity in the total area from either L2/3 or L4 from P5-10. Likewise, by P18-23 the inhibitory connectivity stays unchanged after hypoxia. Thus inhibitory connectivity has a time window of P5-10 where the circuitry is dynamically altered after hypoxia. Additionally, GABAergic circuits are stable and consistent for input to L4 over development despite the hypoxia exposure. Thus layer 4 circuitry is selectively vulnerable up until about P10 in the auditory cortex of the neonatal rat.

With respect to the dynamic changes in the excitatory postsynaptic charge differences over development, here we show that the subplate from P5-10 and L4 from P18-23 have mirrored increased in the strengths of the mean charges. However again we see that during, P5-10 L4 changes do not mirror SP changes for mean EPSC charge. Instead we see that L4 excitatory circuitry is weakened from P5-10 after hypoxia, but then by P18-23 there is an increase in the strength of the EPSC connections to L4 after hypoxia. Thus this suggests that after hypoxia, L4 circuitry attempts to readjust the strength of connections in order to preserve L4 connections that are becoming weakened from P5-10 after hypoxia.

Next, we show that inhibitory postsynaptic charge of input to SPNs is altered after neonatal hypoxia. Specifically, hypoxia results in a strengthening of inhibitory mean charge to SPNs. However the strengths of the IPSC input to L4 neurons throughout development are unaltered after hypoxia. This suggests that the strength of

the inhibition of SP from P5-10 is selectively vulnerable to hypoxia from P1-2 in the neonatal rat.

Next, we show that hypoxia results in an imbalance of excitation to inhibition of L4 circuits over development despite the balance, but altered circuitry of SPNs earlier in development. When we investigate the EI ratio of the subplate from P5-10, hypoxia does not result in an imbalance of any of the input from L4, L5/6, or within SP. However, the EI ratios are differential imbalanced for input to L4 over development. Specifically, the source of the imbalance for during P5-10 is for input from within L4, where the EI ratio is reduced and thus the inhibition component is greater. However by P18 to 23, hypoxia results in an increase in the EI ratio arising from L2/3 and thus represents an increase in the excitatory component for both area and charge from superficial inputs. Therefore the investigative role SPNs in the recurrent loop of SP to L4 and L4 to SP connectivity is altered after hypoxia. Thus while the inhibition is greater during P5-10 for input within L4, over development superficial sources of excitation sprout from L2/3 to L4 as a result of hypoxia.

Behaviorally, the acoustic startle reflexes we see from P13-16 increase the response gain ratio and this suggests that the loudest sound level elicits a greater startle reflex in the hypoxia rats. This helps to reflect the state of the L4 input connectivity in the EI balances we see at P18-23 rather than P5-10 since during P18-23 the excitation component is greater relative to inhibition after hypoxia. Thus the startle behavior suggests that P13 is when the shift in the EI balance of L4 input initiates, and this shift persists by P18-23. However the startle behavior does not reflect the changes seen in the EI balances from P5-10. This suggests that the

increased inhibition component of the EI balance persists up until about P12. At P18-23 we see that for the EI balance, input from within L4 excitation and inhibition are balanced after hypoxia. Thus this suggests that L2/3 may be contributing to altered cortical perception to acoustic stimuli since the EI balance, while increased in the ratio and therefore increased in the excitatory component. This suggests that if an infant were to perceive sound, the source of excitation due to sound stimuli may result in hyperactivity responses from the child. Additionally, from the rostral-caudal width information we see increasing laterally in SP, but the narrowed width we see in L4, this may suggest that hypoxia is resulting in the integration of fewer neighboring frequency regions, and this this has potential to impair the frequency tuning selectivity within L4 and L2/3 compared to a normoxic infant.

Chapter 8: General Discussion

For the brain to properly develop and mature, we know that the normal anatomical organization and function of the cortex is dependent on sensory experience. We also know that subplate neurons (SPNs) play a crucial role in the development of thalamocortical circuitry. From previous work done in the visual cortex of cats, we know that ablation of these SPNs disrupts the proper formation of ocular dominance columns (Ghosh and Shatz, 1993; Kanold and Shatz, 2006). In early development of the normal brain, GABAergic activity is depolarizing and excitatory due to low KCC2 levels (and thus the equilibrium potential for chloride is high), however as the brain develops there is a developmental switch resulting in the upregulation of KCC2 expression levels (and therefore decreasing the equilibrium potential of chloride) and in turn this causes GABAergic activity to become hyperpolarizing and inhibitory (Rivera et al., 1999; Kanold and Shatz, 2006; Kanold, 2009). Additionally, we know that removal of subplate neurons from P6-9 from developing brain circuitry prevents the maturation of GABAergic inhibition in the cat (Kanold and Shatz, 2006). Thus in order for the brain to strengthen both excitatory and inhibitory circuits, the GABAergic circuits might need to be established first so that the depolarizing GABA can then assist in the maturation of excitatory glutamatergic connections (Kanold, 2009). Also from previous work, we know that removal of SPNs from the visual cortex of cats resulted in the weakening of excitatory postsynaptic currents (EPSCs) in L4, and SPN ablation disrupts orientation maps and prevents the sharpening of orientation tuning of the visual cortex (Kanold et

al., 2003). Thus SPNs ultimately aid in the targeting and refinement of thalamocortical axons to thalamorecipient layer 4.

However, are SPNs universal across all cortical areas and are they species specific? Thus we continued to investigate the role of SPNs when they are removed from the rat somatosensory cortex. In normal development of somatosensory cortex, barrels reside in thalamorecipient layer 4. We found that removal of SPNs right after birth, from the primary somatosensory cortex barrel field, also disrupted the proper formation of anatomical barrel patterning. Like in the cat visual cortex, we also found that removal of SPNs in the rat somatosensory cortex resulted in weakened EPSCs in L4 of the barrel field (Tolner et al., 2012). Additionally, removal of SPNs abolished spindle burst activity in the limb region of the primary somatosensory cortex (Tolner et al., 2012). From these experiments, we now know that SPNs are not particular to a specific cortical region. In fact, SPNs are located in the developing subcortical white matter of all cortical regions (Luskin and Shatz, 1985; Valverde and Facal-Valverde, 1987; Kostovic and Rakic, 1990; Allendoerfer and Shatz, 1994; Kostovic et al., 2002; Kanold, 2009). Additionally, from the SPN ablation in both cat and rat sensory regions, SPNs played similar roles in both the refinement of columns and barrels in L4, as well as being required for the strengthening of thalamocortical synapses. Now while these studies were able to identify common roles of SPNs across visual and somatosensory cortices in animal models, these studies involved the surgical and focal removal of these SPNs through injections of p75 immunotoxin. Thus while systematically removing SPNs in a controlled way aided us in understanding the role

of SPNs in sensory cortices, we do not know how other human disorders impact the role of SPNs in the development of injured neonatal brains.

Therefore we continued to investigate the role of SPNs in a disease paradigm of subplate death such as from hypoxia-ischemia. Hypoxia-ischemia encephalopathy (HIE) affects thousands of infants a year and the current treatment for this neonatal disorder is hypothermia to reduce the incidence of seizures in the brain (Lai and Yang, 2011). However hypoxia-ischemia (HI) is a difficult disorder to develop treatment for because it results in a wide variety of severities of injury to the neonate. However we know from other studies that SPNs are selectively vulnerable to HI (McQuillen et al., 2003). In the preterm human, HI results in damage to subcortical developing white matter, referred to as periventricular leukomalacia (PVL) (Ferriero, 2004). Thus this led us to investigate the role of SPNs in a clinically relevant disorder where the brain injury is not controlled, and the disorder is present in humans who develop a wide variety of defects such as severe motor loss, fine and gross motor dysfunction, sensorineural hearing loss, speech and language development, cerebral palsy, epilepsy, and abnormalities in cognitive function (Robertson and Perlman, 2006).

Therefore in order to investigate the changes of the microcircuitry of the injured brain after HI, we had to first establish the functional synaptic maps of microcircuitry in the Sprague-Dawley rat over development by recording from L4 neurons of primary auditory cortex. We focused on developmental differences in the spatial distribution connectivity maps and strengths of connections on L4 neurons because later in development, the majority of SPNs die off as thalamocortical

connections become strengthened and secured. Thus, we sought out to investigate these developmental differences by using laser-scanning photostimulation (LSPS) of caged glutamate combined with whole-cell patch clamp recordings to map the photostimulation-evoked postsynaptic current (PSC) responses through the laminae. LSPS is a powerful technique in that it is able to provide us with maps revealing differences in spatial distributions of synaptic connectivity and changes in the strengths of connections with respect to the function of these circuits.

However, LSPS is not a commonly used technique and therefore we needed to establish the changes in the spatial distribution of synaptic connectivity in primary auditory cortex of the developing brain, particularly with respect to input to SPNs and L4 neurons. We know that there is auditory tonotopy on a global scale (Zhang et al., 2001) across the auditory cortex, however on a finer scale, we also know that within L2/3, there is increased heterogeneity of auditory responses in the rodent (Bandyopadhyay et al., 2010; Rothschild et al., 2010). Thus with LSPS, we are also able to visually discern the changes to the width of the synaptic connectivity within layers along the rostral-caudal axis as done in other studies (Meng et al., 2015). For example, input from a wider marginal area indicates a larger range of integration across the tonotopic axis. Thus with LSPS, we are able to investigate the spatial differences in connectivity in multiple laminae across the cortex in vitro. Therefore, we set out to investigate the spatial distribution and connection strength changes for input to L4 neurons from P5-10 and from P18-23, which is later in the auditory critical period which follows the onset of hearing from P11-12 up until about the first postnatal month in the rat (de Villers-Sidani et al., 2007).

We found that in from P5-23, there were distinct laminar changes in the excitatory and inhibitory inputs to L4 neurons. Generally, the functional microcircuit changes we found were more pronounced within L4 for excitatory input and from L2/3 for inhibitory input over development. Specifically, development revealed a hyperconnectivity of excitatory and inhibitory input from L2/3 and L4. Additionally, we see an expansion of AMPA-mediated activity and GABAergic activity along the rostral-caudal extent over development, which suggests broader tuning across the primary auditory cortex on a microcircuit level. However the excitatory and inhibitory input to L4 are differentially focused to particular cortical layers. Specifically, excitation expands along the rostral-caudal axis within L4, but inhibition expands within most within L2/3. While there are expansions in both layers for excitatory and inhibitory activity, if one compares the degree of significance in which the circuitries change along that axis, the majority of the expansion differences are focused to different laminae depending on if the activity is excitatory or inhibitory. Nevertheless, development results in an expansion along this axis for both layers and for excitation and inhibition for input to L4 in primary auditory cortex. With lateral expansion along the rostral-caudal axis, our results suggest that input to L4 is coming from more lateral connections and thus input may reside from more frequency regions ultimately accumulating in a greater mixture of frequencies. In order to investigate if that were true, one would have to do in vivo whole-cell patch clamp recordings of rats in auditory cortex and would have to play different frequencies to see which neurons would be responding to which frequencies and then repeat this later in development. However, with LSPS we are able to see the total spatial distribution of connections,

while in vivo patch clamp would not reveal that unless under two-photon imaging for example. Nevertheless, we see expansion in the excitatory and inhibitory input total area from L2/3 and within L4 as a result of normal development in the rat.

These results of developmental differences in primary auditory cortex (A1) suggest that as the rat grows and is exposed to more sounds over development, that there is general expansion of the cortical areas in which neurons in layer 4 receive input in A1 along the tonotopic extent. However because these experiments were conducted in vitro, we do not know which neurons respond to which frequency specifically. Therefore we can at least compare the compare the width of inputs along the tonotopic gradient with respect to overall expansion and narrowing and this suggests the relative degree of frequency mixing for tuning for inputs to the recorded neuron. However if we compare the expansion of L2/3 to L4, L4 has a wider extent for which is receives input thus suggesting that there is greater integration of input from within L4 over development than from L2/3. Thus expansion along the rostral-caudal extent suggests broader tuning across A1 over development and the majority of this expansion lies within L4 throughout the auditory critical period.

Because we did not see seizures in the normally developing rat, but we did see changes for excitatory and inhibitory connection densities and the strengths of these connections, we investigated if these rats had imbalanced EI ratios. For normal development, it is imperative that there be a balance of excitation and inhibition. However when we investigate AMPA-mediated and GABAergic inputs to L4, we found that development results in an overall imbalance of excitation and inhibition. However the sources of the EI imbalances were also differential based upon laminae.

Specifically, excitation increased in the EI ratio within L4. In addition, the shift of the EI ratio with respect to charge revealed more inhibition. We also found that there was a greater shift in the EI ratio from L2/3 therefore, since more of the ratio changed within L2/3 than in L4 for charge, we consider that to be a shift in the source of the imbalance and this arises from the supragranular layer over development. Thus we see stronger inhibition from L2/3 and a larger area of excitatory connections in L4. However regardless of these EI imbalances, we did not observe epileptic seizures resulting in convulsions in these rats over development right before recordings. One must remember that convulsions are seizures with a motor manifestation and epilepsy is disorder of the brain due to cerebral injuries. It is possible that the EI imbalances were not large enough to cause seizures and convulsions, however one can test to see if there is epileptiform activity in future studies using a 3D-microelectrode array. A 3D-microelectrode array allows of us to look at a larger network of neurons in an in vitro slice preparation and allows us to look at the activity of multiple neurons and their spatial and temporal patterns across a slice. Thus MEA recordings would indicate if there is enough hyperexcitability to show epileptiform activity but not enough to result in epilepsy.

Thus we then looked at inhibitory connections to see if changes in inhibition were enough to counter the changes in excitation to prevent seizures in normally developing rats. We found that for IPSC charge that there was a strengthening in inhibition arising from L2/3 and within L4. Thus this may have prevented the brain from developing seizures as the circuitry expands from P5 and if the timing of inputs is synchronized together. Since we know that SPNs receive thalamic input and project

to L4 (Zhao et al., 2009) and that there are also corticothalamic projections from L4 back to SP (Viswanathan et al., 2016), our results suggest that A1 undergoes considerable changes in microcircuitry while preserving the basic thalamocortical circuitry over development in the rat. Additionally, the emphasis on L2/3 suggests increased lateral inhibition and lateral excitatory input form L4 for the dynamic restabilization of functional microcircuitry throughout the auditory critical period.

Next, we investigated the effects of neonatal hypoxia-ischemia on the rat from P5-10 in SP and in L4. We know from other studies that SPNs are selectively vulnerable to injury and result in death after hypoxia-ischemia (McQuillen et al., 2003). In our hands, we induced two severities of hypoxia-ischemia: mild and moderate in the auditory cortex from P1-2. We found that a few days later, from P5-10, the functional circuit changes we saw were most pronounced in the SP and therefore this suggested that early HI insults to the developing cortex exert most of their influence on SPNs.

We also investigated the gross histology of these HI brains in order to see if the changes we see in cortical shrinkage were similar to what is seen in other studies (Failor et al., 2010). With the ligation suture technique we used to induce a more moderate form of ischemia (Mod HI), we did see more cortical shrinkage in the auditory cortex. This shrinkage was already detectable by P5-10 however, Mild HI did not result in gross histological changes. Nevertheless, we found that in both conditions SPNs showed changes in functional microcircuitry, particularly excitatory hyperconnectivity of SPNs. This is especially important to highlight because in the clinic, MRI is often used to examine anatomical differences after brain injury.

However if one were to do MRI on these Mild HI brains, one would not be able to detect differences in the brain circuitry, yet with LSPS one is able to reveal those functional specific differences in vitro. Thus, MRI on milder forms of HI may be misleading one into thinking that the brain may be functioning normally, when it in fact has deficits on a microcircuit level that are harder to detect with current machines in the clinic.

With regards to functional circuitry changes, other studies showed that HI resulted in decreased cortical activity through EEG however EEG measures larger network activity and thus incorporates multiple layers of circuitries (Ranasinghe et al., 2015). However LSPS allows us to examine the laminar differences in the microcircuitries after brain injury. Unfortunately, LSPS is for in vitro brain slices and thus does not allow us to examine laminar differences in vivo because the laser light would cause scatter in the tissue and the caged glutamate would not be able to penetrate through all the layers of the cortex. Therefore we would not be able to uncage the glutamate in deeper layers. Nevertheless the spatial distribution information available to us from LSPS provides us with important spatial distribution changes in a visual manner.

Regardless, using LSPS and whole-cell patch clamp recordings of individual neurons, we found that our results suggest that while reduced SPN activity is due to the relative increase in inhibition, this leads to changes in the spatial patterning of excitatory inputs to L4. While we know that Mod HI results in SP cell loss (McQuillen et al., 2003), the cell loss within the SP leads to the loss of connections to L4. Additionally, we investigated the EI ratios of these different groups of neurons in

order to see if HI leads to an imbalance of excitation to inhibition and thus resulting in observable seizures in the more moderate form of HI.

We found that HI does indeed cause an imbalance in the excitatory and inhibitory intracortical inputs to SPNs. Therefore SPNs have a more integrative role, which is altered after HI. Since we know that SPNs are required for the maturation of excitatory and inhibitory circuits to L4 (Kanold et al., 2003; Kanold and Shatz, 2006; Tolner et al., 2012), and given the excitatory input from SP to L4, the altered SPN connections we see would predict similarly altered connections to L4 neurons. In fact, we do observe hypoconnectivity of excitatory connections in L4 after Mod HI, which is consistent with the cell loss and connection changes we see in the SP. Additionally, moderate HI results in decreased excitatory GluR1 expression in L4 and L6 (Ranasinghe et al., 2015), and this is also consistent with our results. Therefore we speculate that because Mod HI is associated with SPN loss, the total SPN-mediated activity to L4 neurons is reduced thus leading to hypoconnectivity.

In addition, we know that SPNs are involved in the generation of spontaneous cortical oscillations (Dupont et al., 2006) and SPN lesions abolish spindle burst activity in S1 (Tolner et al., 2012). Moderate HI in rodents results in transiently diminished background EEG activity (Ranasinghe et al., 2015), our results suggest that altered SPN and L4 circuitries are what underlie the changed EEG signals after neonatal HI.

Regardless of the severity of HI, the basic interlaminar circuitry remains intact in the primary auditory cortex. This is important to point out because this suggests that HI does not alter reelin expression. Reelin is an extracellular matrix glycoprotein

that is secreted by Cajal-Retzius cells in the marginal zone during corticogenesis in order to allow for proper organization of laminae (Hoerder-Suabedissen and Molnar, 2015). This suggests that HI did not lesion Cajal-Retzius cells. The normal laminar organization suggests that it is possible for the observed circuit changes we see after Mild HI, which did not result in cell death, to be reversed. Therefore targeted interventions, which can selectively strengthen SP circuits, might be able to reverse the early effects of HI. Currently, the clinical treatment after HI is hypothermia (Lai and Yang, 2011), which presumably decreases the activity in all neurons. Thus this will also prevent strengthening of proper connections to SPNs. Therefore treatments might be made more effective if they involve the targeting of different, SPN-specific receptors, instead of trying to use a more global treatment that affects the activity of the entire brain. For example, SPNs express many neuromodulatory receptors such as serotonin and ACh (Hanganu and Luhmann, 2004; Kilb et al., 2008; Liao and Lee, 2011) and thus the transient activation of these systems might mediate the effects of HI. Since SPNs are a diverse cell population selectively expressing multiple genes (Hoerder-Suabedissen et al., 2009; Kanold and Luhmann, 2010; Hoerder-Suabedissen and Molnar, 2015; Viswanathan et al., 2016), the development of SPN-specific pharmacological treatments might be a promising avenue for more efficient treatments. Finally, our results showed that subplate neuron circuits are vulnerable to hypoxic-ischemic brain injury and it is likely that other insults to the developing brain at the earliest stages also alter SPN circuitry. This information nicely compliments the work done by McQuillen et al. in trying to understand the effects of HI and how HI impacts SPNs over development.

Thus our results provide added information on a microcircuit cortical level of the dynamic and laminar-specific effects of differing severities of HI and a possible explanation for how seizures result due to an imbalance of excitation and inhibition as early as P5-10 days in the rodent which translates to about gestational weeks (GW) 25-30 in the human (Howdeshell, 2002).

We then investigated to see if the functional microcircuit changes we see from P5-10 in the auditory cortex persist later in the auditory critical period from P18-23. Here, we focused on changes in input to L4 since earlier in development SPNs aid in establishing feedforward connections to L4. Additionally, from P18-23 the observable seizures we saw earlier in development as a result of HI were no longer observable. Thus this led us to investigate if there were any subtle functional changes on a microcircuit level. By P18-23, we show that the majority of the defects we saw earlier in development were less numerous and less severe in auditory cortex. This compliments the lack of observable seizures from P18-23. Also, this suggests that there was a rebalancing of excitation and inhibition. However, in order to rebalance this suggests that there may be pruning of weaker synapses as a result of injury since other studies reveal that HI results in decreased dendritic complexity (Ranasinghe et al., 2015). This additional pruning compared to the refinement seen in P18-23 of L4 may not necessarily be beneficial as fewer connections may compromise the overall computational processing of the auditory cortex. Therefore the strongest connections would be the ones to be preserved by P18-23. However in our hands, by P18-23 we do not see changes in the input area of excitation or inhibition, but Mod HI only strengthened the mean EPSC charge within L4 and we see that for IPSCs the width of

input increased within L2/3 and L4. Therefore, this suggests that it may not be pruning of weakened synapses after all that rebalance the excitation and inhibition, but it is the widening of the inhibitory connections that engulf the strengthened excitatory connections within L4 after Mod HI. Also, this suggests that as the excitation becomes stronger within L4 after Mod HI, that the inhibitory connections spread to balance out the strengthened excitatory inputs so that by P18-23 we do not see observable seizures.

Regardless, we found that Mod HI was severe enough to have deficits persist through P18-23 in L4. However Mild HI did not alter L4 circuitry from P18-23. Therefore this suggests that the brain is able to recover after Mild HI by P18-23. Specifically, the effects of Mild HI appeared to be transient and restricted up until before P18. Therefore our results suggest differential time windows for treatment intervention of HI. Since Mild HI has deficits detectable from P5-10 but Mod HI has deficits that persist up until P23, this suggests that Mild HI has a smaller time window for treatment. Additionally, since majority of the differences we saw occur earlier in development from P5-10, and even less from P18-23, our results suggest that treatment intervention for the neonate is optimal earlier in development rather than later. Nevertheless, despite the reduced differences by P18-23, we are also able to show that LSPS is powerful enough to detect differential changes in circuitry throughout development.

While the basic interlaminar circuitry of primary auditory cortex remains intact from P18-23 after hypoxic-ischemic injury, the observed circuit changes we see

from P18-23 are possibly still reversible for moderate HI injury without compromising basic circuitry components of the cortex for thalamocortical circuits.

Again, the current treatment for HI is hypothermia, and while the effects of hypothermia on subplate circuits are not known, L4 is still impacted by Mod HI injury from P18-23. However we do not know how hypothermia impacts L4 circuits later in the critical period of auditory cortex of rats. Typically, hypothermia is applied by reducing the body temperature by about 5 degrees below the normal body temperature in order to reduce cerebral injury (Lai and Yang, 2011). Hypothermia has been shown to penetrate into deep cortical layers such as layer 5/6 in mice (Kida et al., 2013). Therefore, it is worth investigating of hypothermia is able to alter L4 circuitry of A1. This would provide additional insight into the effectiveness of the hypothermia treatment around birth of the human (GW 40). However it is important to note that hypothermia treatment for infants with mild HI may not be as effective as by P18-23 in the rat, since by then the L4 circuitry is unchanged compared to control. Regardless, mild HI by P18-23 did not result in severe seizures. Thus mild HI may not be an injury to be as worried about later in development of L4 circuitries since our investigation shows no differences due to Mild HI from P18-23. In fact, by P18-23 neither mild nor moderate HI resulted in observable seizures and this may reflect the rebalanced excitation to inhibition of layer 4 circuits of A1.

Nevertheless, while mild and moderate HI show no changes to the EI balance by P18-23, infants still develop to have language and communication difficulties. A clinical study examined the effects of HI on seventy children from 1 month to 24 months old and they found that as the children aged, language tasks became more

dependent and specific on the direct action of the subject rather than the subjective interpretation of their guardian (Martinez et al., 2014). This suggested that HI delayed language development. Thus while excitation and inhibition in A1 appear balanced by P18-23 in the rat, this suggests that the greatest impact of HI alters the circuitry from P5-10. Therefore by P18-23 the changes that have altered circuitry have passed through that dynamic window of subtle circuit remodeling are able to compensate for the injury in order to rebalance excitation and inhibition to preserve brain function and attempt to reduce seizure occurrence that would otherwise further damage circuitry through mechanisms such as glutamatergic excitotoxicity.

The transient nature of the microcircuit changes after mild HI are similar to previous work where we investigated the effects of hypoxia and inflammation through IL-1B in the mouse primary somatosensory barrel cortex to examine changes in epileptiform activity. There we found that by P28-30 in the hypoxic mouse, evoked epileptiform activity was reduced and this indicated that cortical dysfunction was transient (Mordel et al., 2016).

Therefore this dissertation continued to examine the effects of only hypoxia over development from P5-10 in SP and L4, and P18-23 in L4 of auditory cortex in the neonatal rat. Here, we showed that an animal model of hypoxia alone caused distinct changes to functional cortical microcircuits over development in the neonatal rodent. While we did see functional circuit changes for input to L4 neurons from P5-10 and P18-23, the effects of hypoxia were most pronounced SPNs from P5-10. This suggests that SPNs are also selectively vulnerable as early as P5 to hypoxia exposure

(5% oxygen) at P1-2. Therefore, this echoes the similar vulnerability of SPNs to HI we saw in earlier in the dissertation.

While we do see hyperconnectivity of excitatory input within SP after hypoxia by P5-10, input to L4 neurons end up becoming hypoconnected excitatory input to L4 from L2/3. When comparing the control to the hypoxic tissue, this hyperconnectivity we see in L4 neurons in primary auditory cortex is similar to what is seen in primary somatosensory cortex in other studies. Work done by Ranasinghe *et al*. show that when they compare the hypoxic hemisphere to a control brain, that there is decreased number of dendrites in S1 for at least the first branch order around P14(Ranasinghe et al., 2015). Therefore this suggests that with hypoconnectivity seen up until P10 in A1 and reduced dendritic complexity seen in S1 that hypoxia potentially has similar effects across cortical regions. This is not surprising as hypoxia affects the entire brain and not solely one cortical region. However by P18-23, that degree of relative hypoconnectivity compared to P5-10 for L4 input is not present by P18-23. This suggests a cortical rewiring of not only SP circuits by of L4 circuits throughout development as a result of hypoxia and that this rewiring is a transient phenomenon as by P18-23 there are no differences in connectivity of L4 neurons as a result of hypoxia. This is similar to the effects we see from Mild HI. Thus in order to distinguish the effects of the mild hypoxia-ischemia we investigated earlier in this dissertation and hypoxia alone, one would have to do further analysis to compare the quantitative single-cell analysis of mild HI and hypoxia alone in the same layers at the same ages because the effects of Mild HI could be considered misleading. However since we used the same time points and recorded from the same layers of

auditory cortex across this dissertation, we will be able to do those cross comparisons in future to get a more in-depth insight into the effects if mild ischemic events result in very subtle, but detectable differences to auditory developmental circuitry.

On a cursory examination of the differences between hypoxia and mild HI, one particular example showed that the excitatory rostral-caudal extent for L4 input becomes narrowed only from P5-10, but by P18-23 excitatory input width does not change after hypoxia, whereas Mild HI did not alter either the excitatory or inhibitory width for L4 input. However more analysis is needed in future for differentiating all possible differences between hypoxia and mild HI. Thus our results suggest that, at a quick look, mild ischemia when combined with hypoxia does result in distinct changes to the L4 circuitry from P5-10, but further analysis is needed to differentiate the effects of the mild ischemia on SP and L4 circuitries over development of the primary auditory cortex.

Additionally, we revealed that there is an extended window of therapeutic treatment for L4 circuitry, however for SP circuitry that window is from P5-10 in the neonatal rat after hypoxia. However with regards to tonotopy, the time window for adjusting the microcircuitry of excitatory L4 input is up until P10 since the majority of the observed changes seen in the rostral-caudal width are from P5-10. Since P10 is around the time of ear opening, this suggests that these changes in microcircuitry occur before the onset of hearing and before the rat auditory critical period. Thus if one were to treat hypoxia auditory function, treatment before P10 (rat) is optimal in order to alter L4 circuitry when it is most dynamic and in process of rewiring on a more subtle manner. In another study done in the CA1 region of the hippocampus of

the neonatal rat, others found that after 20 min exposure to hypoxia at P1 (100% N2) that by after one week post-insult, there was apoptosis and decreased neuronal loss, however this apoptosis event was followed by increased neurogenesis and anatomical recovery (Daval et al., 2004). Therefore this suggested to them that the brain may have a higher capacity for self-repair (Daval et al., 2004). This is similar to what we saw with HI in the developing rat, in that there was also a limited time window where the majority of functional circuitry changes occur during P5-10. Thus this also suggests to us that there is possible self-repair as a result of hypoxia in primary auditory cortex. Thus this suggests that the self-repair due to hypoxia is not specific to one brain region.

However with regards to GABAergic inhibitory connectivity, we saw that hypoxia results in hyperconnectivity of input from above SP, such as from L5/6 and 4. This differs from HI in the fact that only Mild HI resulted in an increase in the width of L5/6 but not in L4. This suggests that for subplate, with increased connectivity from L5/6 to subplate that the strength of the thalamic drive to subplate may be decreased to compensate for the hyperconnectivity. In order to test this one would have to stimulate the auditory thalamus (MG) and record in the subplate to compare the amplitudes and charge of the IPSCs. But for input to L4 circuits, we see that that there is no hyperconnectivity in the total area from either L2/3 or L4 from P5-10 after hypoxia, similar to both Mild and Mod HI. Likewise, by P18-23 the inhibitory connectivity stays unchanged after hypoxia and this is similar to Mild HI from P18-23. Thus inhibitory connectivity also has a time window of P5-10 where the circuitry is dynamically altered after hypoxia. Thus GABAergic circuits are stable

and consistent for input to L4 over development despite the hypoxic exposure. This suggests that layer 4 circuitry is selectively vulnerable up until about P10 in the auditory cortex of the neonatal rat. This highlights that hypoxia results in different results compared to Mod HI in that from P18-23, it is because the ischemia is more moderate that we see pronounced differences in functional circuitry later in development. Thus the severity of the ischemia has the power to influence differential circuit changes over development of auditory cortex.

With respect to the dynamic changes in the excitatory postsynaptic charge differences over development, here we show that the subplate from P5-10 and L4 from P18-23 have mirrored increased in the strengths of the mean charges. However again we see that during P5-10, L4 changes do not mirror SP changes for mean EPSC charge. Instead we see that L4 excitatory circuitry is weakened from P5-10 after hypoxia, but then by P18-23 there is an increase in the strength of the EPSC connections to L4 after hypoxia. This is similar to the effects of Mod HI from P18-23 where the mean EPSC charge becomes strengthened within L4. Thus this suggests that after hypoxia, L4 circuitry attempts to readjust the strength of connections in order to preserve L4 connections that are becoming weakened from P5-10 after hypoxia.

Next, we show that inhibitory postsynaptic charge of input to SPNs is altered after neonatal hypoxia. This highlights a key difference with SPNs in that SPNs are affected after Mild HI by way of an increase in inhibitory connections laterally within the subplate. Specifically hypoxia results in a strengthening of inhibitory mean charge to SPNs, whereas the mean IPSC charge to SPNs is unaltered after mild or moderate

HI. However the strengths of the IPSC input to L4 neurons throughout development are unaltered after hypoxia. This suggests that the strength of the inhibition of SP from P5-10 is selectively vulnerable to hypoxia from P1-2 in the neonatal rat. Additionally, this begins to also help separate differences between hypoxia and the two severities of HI over development of A1.

Next, we show that hypoxia results in an imbalance of excitation to inhibition of L4 circuits over development despite the balance, but altered circuitry of SPNs earlier in development. While the imbalance of excitation to inhibition from hypoxia for inputs to L4 is similar to the effects of mild and moderate HI on L4 inputs, the subplate is where the key difference resides. While after hypoxia, the subplate has balanced excitation and inhibition, mild HI does not, thus again we see another difference from the mild ischemic event over the hypoxia, which helps us in distinguishing hypoxia and mild HI.

When we investigate the EI ratio of the subplate from P5-10, hypoxia does not result in an imbalance of any of the input from L4, L5/6, or within SP. However, the EI ratios are differentially imbalanced for input to L4 over development. Specifically, the source of the imbalance for during P5-10 is for input from within L4, where the EI ratio is reduced and thus the inhibition component is greater. This differential sourcing of imbalance is similar to HI. However the more moderate form of HI causes differences in the balance in L2/3 (such as an increased EI ratio and thus increased excitation), whereas mild HI causes differences in L4 (such as decreased EI ratio and thus increased inhibition). However by P18 to P23, hypoxia results in an increase in the EI ratio arising from L2/3 and thus represents an increase in the

excitatory component for both area and charge from superficial inputs. Therefore, hypoxia differs from HI by P18-23 for L4 in that both severities of HI do not alter the EI ratio, and thus are balanced. Therefore, the investigative role SPNs in the recurrent loop of SP to L4 and L4 to SP connectivity is altered after hypoxia. Thus while the inhibition is greater during P5-10 for input within L4, over development superficial sources of excitation arise from L2/3 to L4 as a result of hypoxia. Therefore another distinguishing factor between mild HI and hypoxia for subplate input is that while hypoxia alters excitation and inhibitory for input to SP, the EI ratio for subplate input is balanced while the EI ratio for subplate input after mild HI is imbalanced. Therefore this suggests to us that the mild ischemic event does differentiate mild HI from hypoxia alone. However, further analysis is needed to thoroughly confirm that suggestion.

Behaviorally, the acoustic startle reflexes we see from P13-16 increase the response gain ratio and this suggests that the loudest sound level elicits a greater startle reflex in the hypoxia rats. This helps to reflect the state of the L4 input connectivity in the EI balances we see at P18-23 rather than P5-10 since during P18-23 the excitation component is greater relative to inhibition after hypoxia. Thus the startle behavior suggests that P13 is when there is a shift in the EI balance of L4 input initiates, and this shift persists by P18-23. However since hypoxia affects the entire animal, not just the auditory cortex but also other cortical areas and possibly the brainstem could be altered since the startle response is a reflex. However the startle behavior does not reflect the changes seen in the EI balances from P5-10. This suggests that the increased inhibition component of the EI balance persists up until

about P12. At P18-23 we see that for the EI balance, input from within L4, excitation and inhibition are balanced after hypoxia. Additionally, from the rostral-caudal width information we see increasing laterally in SP, but the narrowed width we see in L4, this suggests that hypoxia is resulting in the integration of fewer neighboring frequency regions, and this this has potential to impair the frequency tuning selectivity within L4 and L2/3 compared to a normoxic infant. In addition, we did conduct startle experiments on HI rats for both severities of injuries (not pictured) but the results were not significant, however this may reflect that there is high variability of injury in HI rats as reflected in the cortical shrinkage data presented earlier in this dissertation. Thus in order to see if there are any differences in either severity of HI, more rats would have to be startled and analyzed.

Importantly, this dissertation highlights the role of SPNs over development. Specifically, how damage to subplate alters cortical anatomical and functional development. From this work and works of others on SPNs, we now know that SPNs are functionally necessary over visual, somatosensory, and auditory cortices and the removal of SPNs have similar effects to thalamocortical circuit function and anatomical structuring regardless of the species or sensory region. SPNs are necessary for the strengthening of thalamocortical circuits and are required for the proper targeting and refinement in multiple sensory regions. Thus removal of SPNs via focal ablation or brain injury result in altered L4 circuitry function. Additionally, we now know that SPNs are selectively vulnerable in multiple sensory cortices. This dissertation also provides information about the possible expansion and thus broader tuning of the auditory cortex on a microcircuit level as a result of HI. Overall, this

dissertation provides an extensive investigation of the effects of hypoxia and hypoxia-ischemia, and its differing severities, on the functional microcircuitry of the developing rat auditory cortex. After recording over hundreds of neurons throughout these projects over SP and L4, and over development, we are able to gain insight on the changes that occur on a laminar-specific level and how they differ with respect to the severity of injury. This is potentially why HIE is an incredibly difficult disorder to treat in humans. Fortunately, with the use of LSPS we are able to gain a microcircuit view of laminar and columnar differences between hypoxia, mild HI, and moderate HI on developing A1 circuitries in order to help explain possible sources of seizure activity in early developing brains. Additionally, we now know that cell death in moderate HI leads to altered L4 cortical function in the neonatal rat and that cell death could be triggering reorganization programs that are not triggered by non-lethal injuries.

In conclusion, SPNs have a shared role across mammalian species, across sensory regions, and even in the aftermath of HI brain injury in that SPNs are necessary for the refined, organized, and targeted strengthening of connections to L4. Without SPNs anatomical sensory organization of circuits become disrupted, and thalamocortical connections become weakened. Thus when SPNs are injured or die off earlier than before thalamocortical circuitry is secure, we find that after HI the brain attempts to rebalance excitation and inhibition. This may be an attempt for the brain to prevent further seizures than are initiated in the incidence of SPN damage after HI.

References

Aboitiz F (2009) Neocortex: Origins. Elsevier Ltd.

Adelsberger H, Garaschuk O, Konnerth A (2005) Cortical calcium waves in resting newborn mice. Nat Neurosci 8:988-990.

Agmon A, Connors BW (1991) Thalamocortical responses of mouse somatosensory (barrel) cortex in vitro. Neuroscience 41:365-379.

Agmon A, Yang LT, Jones EG, O'Dowd DK (1995) Topological precision in the thalamic projection to neonatal mouse barrel cortex. The Journal of neuroscience : the official journal of the Society for Neuroscience 15:549-561.

Allendoerfer KL, Shatz CJ (1994) The subplate, a transient neocortical structure: its role in the development of connections between thalamus and cortex. Annual review of neuroscience 17:185-218.

Anderson CA, Arciniegas DB (2010) Cognitive sequelae of hypoxic-ischemic brain injury: a review. NeuroRehabilitation 26:47-63.

Bandyopadhyay S, Shamma SA, Kanold PO (2010) Dichotomy of functional organization in the mouse auditory cortex. Nature neuroscience 13:361-368.

Ben Ari Y (2001) Developing networks play a similar melody. Trends Neurosci 24:353-360.

Bernard C, Milh M, Morozov YM, Ben-Ari Y, Freund TF, Gozlan H (2005) Altering cannabinoid signaling during development disrupts neuronal activity.

Proceedings of the National Academy of Sciences of the United States of America 102:9388-9393.

Blaesse P, Airaksinen MS, Rivera C, Kaila K (2009) Cation-chloride cotransporters and neuronal function. Neuron 61:820-838.

Bokor H, Acsady L, Deschenes M (2008) Vibrissal responses of thalamic cells that project to the septal columns of the barrel cortex and to the second somatosensory area. The Journal of neuroscience : the official journal of the Society for Neuroscience 28:5169-5177.

Book AA, Wiley RG, Schweitzer JB (1995) 192 IgG-saporin. 2. Neuropathology in the rat brain. Acta neuropathologica 89:519-526.

Bos AF, Martijn A, Okken A, Prechtl HF (1998) Quality of general movements in preterm infants with transient periventricular echodensities. Acta Paediatr 87:328-335.

Bromfield EB, Cavazos JE, Sirven JI (2006) An Introduction to Epilepsy In: (Bromfield EB, Cavazos JE, Sirven JI, eds). West Hartford (CT): American Epilepsy Society.

Bureau I, von Saint Paul F, Svoboda K (2006) Interdigitated paralemniscal and lemniscal pathways in the mouse barrel cortex. PLoS biology 4:e382.

Calderon DP, Leverkova N, Peinado A (2005) Gq/11-induced and spontaneous waves of coordinated network activation in developing frontal cortex. J Neurosci 25:1737-1749.

Chapman B, Jacobson MD, Reiter HO, Stryker MP (1986) Ocular dominance shift in kitten visual cortex caused by imbalance in retinal electrical activity. Nature 324:154-156.

Chmielowska J, Carvell GE, Simons DJ (1989) Spatial organization of thalamocortical and corticothalamic projection systems in the rat SmI barrel cortex. The Journal of comparative neurology 285:325-338.

Colonnese MT, Khazipov R (2010) "Slow activity transients" in infant rat visual cortex: a spreading synchronous oscillation patterned by retinal waves. J Neurosci 30:4325-4337.

Colonnese MT, Kaminska A, Minlebaev M, Milh M, Bloem B, Lescure S, Moriette G, Chiron C, Ben-Ari Y, Khazipov R (2010) A conserved switch in sensory processing prepares developing neocortex for vision. Neuron 67:480-498.

Daval JL, Pourie G, Grojean S, Lievre V, Strazielle C, Blaise S, Vert P (2004) Neonatal hypoxia triggers transient apoptosis followed by neurogenesis in the rat CA1 hippocampus. Pediatr Res 55:561-567.

de Villers-Sidani E, Chang EF, Bao S, Merzenich MM (2007) Critical period window for spectral tuning defined in the primary auditory cortex (A1) in the rat. The Journal of neuroscience : the official journal of the Society for Neuroscience 27:180-189.

Diamond ME, von Heimendahl M, Knutsen PM, Kleinfeld D, Ahissar E (2008) 'Where' and 'what' in the whisker sensorimotor system. Nat Rev Neurosci 9:601-612.

Douglas RJ, Martin KA (2004) Neuronal circuits of the neocortex. Annual review of neuroscience 27:419-451.

Dupont E, Hanganu IL, Kilb W, Hirsch S, Luhmann HJ (2006) Rapid developmental switch in the mechanisms driving early cortical columnar networks. Nature 439:79-83.

Erzurumlu RS, Kind PC (2001) Neural activity: sculptor of 'barrels' in the neocortex. Trends Neurosci 24:589-595.

Evrard A, Ropert N (2009) Early development of the thalamic inhibitory feedback loop in the primary somatosensory system of the newborn mice. J Neurosci 29:9930-9940.

Failor S, Evans M, Cang J, Stryker M, McQuillen P (2006) Impaired cortical plasticity after early hypoxia--ischemia. In: Program number 717.14, 2006 Neuroscience Meeting Planner. San Diego, CA: Society for Neuroscience. Online.

Failor S, Nguyen V, Darcy DP, Cang J, Wendland MF, Stryker MP, McQuillen PS (2010) Neonatal cerebral hypoxia-ischemia impairs plasticity in rat visual cortex. The Journal of neuroscience : the official journal of the Society for Neuroscience 30:81-92.

Feldman DE, Brecht M (2005) Map plasticity in somatosensory cortex. Science 310:810-815.

Ferriero DM (2004) Neonatal brain injury. The New England journal of medicine 351:1985-1995.

Fox K, Schlaggar BL, Glazewski S, O'Leary DD (1996) Glutamate receptor blockade at cortical synapses disrupts development of thalamocortical and columnar organization in somatosensory cortex. Proceedings of the National Academy of Sciences of the United States of America 93:5584-5589.

Friauf E, Shatz CJ (1991) Changing patterns of synaptic input to subplate and cortical plate during development of visual cortex. Journal of neurophysiology 66:2059-2071.

Ganguly K, Schinder AF, Wong ST, Poo M (2001) GABA itself promotes the developmental switch of neuronal GABAergic responses from excitation to inhibition. Cell 105:521-532.

Garaschuk O, Linn J, Eilers J, Konnerth A (2000) Large-scale oscillatory calcium waves in the immature cortex. Nat Neurosci 3:452-459.

Ghosh A, Shatz CJ (1992) Involvement of subplate neurons in the formation of ocular dominance columns. Science (New York, NY 255:1441-1443.

Ghosh A, Shatz CJ (1993) A role for subplate neurons in the patterning of connections from thalamus to neocortex. Development 117:1031-1047.

Gonzalez-Islas C, Wenner P (2006) Spontaneous network activity in the embryonic spinal cord regulates AMPAergic and GABAergic synaptic strength. Neuron 49:563-575.

Hackett TA, Barkat TR, O'Brien BM, Hensch TK, Polley DB (2011) Linking topography to tonotopy in the mouse auditory thalamocortical circuit. The Journal of neuroscience : the official journal of the Society for Neuroscience 31:2983-2995.

Hadders-Algra M (2007) Putative neural substrate of normal and abnormal general movements. Neuroscience and biobehavioral reviews 31:1181-1190.

Haidarliu S, Ahissar E (2001) Size gradients of barreloids in the rat thalamus. The Journal of comparative neurology 429:372-387.

Hanganu IL, Luhmann HJ (2004) Functional nicotinic acetylcholine receptors on subplate neurons in neonatal rat somatosensory cortex. Journal of neurophysiology 92:189-198.

Hanganu IL, Kilb W, Luhmann HJ (2002) Functional synaptic projections onto subplate neurons in neonatal rat somatosensory cortex. The Journal of neuroscience : the official journal of the Society for Neuroscience 22:7165-7176.

Hanganu IL, Ben-Ari Y, Khazipov R (2006) Retinal waves trigger spindle bursts in the neonatal rat visual cortex. J Neurosci 26:6728-6736.

Harris KD, Shepherd GM (2015) The neocortical circuit: themes and variations. Nature neuroscience 18:170-181.

Hensch TK, Fagiolini M (2004) Excitatory-inhibitory balance : synapses, circuits, systems. New York: Kluwer Academic/Plenum.

Herkenham M (1980) Laminar organization of thalamic projections to the rat neocortex. Science 207:532-535.

Hirsch S, Luhmann HJ (2008) Pathway-specificity in N-methyl-D-aspartate receptor-mediated synaptic inputs onto subplate neurons. Neuroscience 153:1092-1102.

Hoerder-Suabedissen A, Molnar Z (2012) Morphology of mouse subplate cells with identified projection targets changes with age. The Journal of comparative neurology 520:174-185.

Hoerder-Suabedissen A, Molnar Z (2015) Development, evolution and pathology of neocortical subplate neurons. Nat Rev Neurosci 16:133-146.

Hoerder-Suabedissen A, Wang WZ, Lee S, Davies KE, Goffinet AM, Rakic S, Parnavelas J, Reim K, Nicolic M, Paulsen O, Molnar Z (2009) Novel markers reveal subpopulations of subplate neurons in the murine cerebral cortex. Cereb Cortex 19:1738-1750.

Hoogland PV, Welker E, Van der Loos H (1987) Organization of the projections from barrel cortex to thalamus in mice studied with Phaseolus vulgaris-leucoagglutinin and HRP. Experimental brain research Experimentelle Hirnforschung Experimentation cerebrale 68:73-87.

Howdeshell KL (2002) A model of the development of the brain as a construct of the thyroid system. Environ Health Perspect 110 Suppl 3:337-348.

Hu K, Carroll J, Rickman C, Davletov B (2002) Action of complexin on SNARE complex. The Journal of biological chemistry 277:41652-41656.

Inan M, Crair MC (2007) Development of cortical maps: perspectives from the barrel cortex. Neuroscientist 13:49-61.

Iwasato T, Datwani A, Wolf AM, Nishiyama H, Taguchi Y, Tonegawa S, Knopfel T, Erzurumlu RS, Itohara S (2000) Cortex-restricted disruption of NMDAR1 impairs neuronal patterns in the barrel cortex. Nature 406:726-731.

Jantzie LL, Corbett CJ, Firl DJ, Robinson S (2014) Postnatal Erythropoietin Mitigates Impaired Cerebral Cortical Development Following Subplate Loss from Prenatal Hypoxia-Ischemia. Cereb Cortex.

Kanold PO (2009) Subplate neurons: crucial regulators of cortical development and plasticity. Frontiers in neuroanatomy 3:16.

Kanold PO, Shatz CJ (2006) Subplate neurons regulate maturation of cortical inhibition and outcome of ocular dominance plasticity. Neuron 51:627-638.

Kanold PO, Luhmann HJ (2010) The subplate and early cortical circuits. Annual review of neuroscience 33:23-48.

Kanold PO, Kara P, Reid RC, Shatz CJ (2003) Role of subplate neurons in functional maturation of visual cortical columns. Science (New York, NY 301:521-525.

Kao JPY (2006) Caged molecules: principles and practical considerations. In: Current protocols in neuroscience (Gerfen C, Holmes A, Rogawski M, Sibley D, Skolnick P, Wray S, eds). Hoboken, NJ: Wiley.

Katz LC, Shatz CJ (1996) Synaptic activity and the construction of cortical circuits. Science (New York, NY 274:1133-1138.

Khazipov R, Sirota A, Leinekugel X, Holmes GL, Ben-Ari Y, Buzsaki G (2004) Early motor activity drives spindle bursts in the developing somatosensory cortex. Nature 432:758-761.

Kida H, Nomura S, Shinoyama M, Ideguchi M, Owada Y, Suzuki M (2013) The effect of hypothermia therapy on cortical laminar disruption following ischemic injury in neonatal mice. PloS one 8:e68877.

Kilb W, Hanganu IL, Okabe A, Sava BA, Shimizu-Okabe C, Fukuda A, Luhmann HJ (2008) Glycine receptors mediate excitation of subplate neurons in neonatal rat cerebral cortex. Journal of neurophysiology 100:698-707.

Koh S, Loy R (1989) Localization and development of nerve growth factor-sensitive rat basal forebrain neurons and their afferent projections to hippocampus and neocortex. J Neurosci 9:2999-0318.

Koralek KA, Jensen KF, Killackey HP (1988) Evidence for two complementary patterns of thalamic input to the rat somatosensory cortex. Brain research 463:346-351.

Kostovic I, Rakic P (1980) Cytology and time of origin of interstitial neurons in the white matter in infant and adult human and monkey telencephalon. J Neurocytol 9:219-242.

Kostovic I, Rakic P (1990) Developmental history of the transient subplate zone in the visual and somatosensory cortex of the macaque monkey and human brain. The Journal of comparative neurology 297:441-470.

Kostovic I, Judas M, Rados M, Hrabac P (2002) Laminar organization of the human fetal cerebrum revealed by histochemical markers and magnetic resonance imaging. Cereb Cortex 12:536-544.

Lai MC, Yang SN (2011) Perinatal hypoxic-ischemic encephalopathy. Journal of biomedicine & biotechnology 2011:609813.

Land PW, Erickson SL (2005) Subbarrel domains in rat somatosensory (S1) cortex. The Journal of comparative neurology 490:414-426.

Liao CC, Lee LJ (2011) Neonatal fluoxetine exposure affects the action potential properties and dendritic development in cortical subplate neurons of rats. Toxicol Lett 207:314-321.

Liao CC, Lee LJ (2014) Presynaptic 5-HT1B receptor-mediated synaptic suppression to the subplate neurons in the somatosensory cortex of neonatal rats. Neuropharmacology 77:81-89.

Lu SM, Lin RC (1993) Thalamic afferents of the rat barrel cortex: a light- and electron-microscopic study using Phaseolus vulgaris leucoagglutinin as an anterograde tracer. Somatosens Mot Res 10:1-16.

Luskin MB, Shatz CJ (1985) Studies of the earliest generated cells of the cat's visual cortex: cogeneration of subplate and marginal zones. The Journal of neuroscience : the official journal of the Society for Neuroscience 5:1062-1075.

Marcano-Reik AJ, Blumberg MS (2008) The corpus callosum modulates spindle-burst activity within homotopic regions of somatosensory cortex in newborn rats. The European journal of neuroscience 28:1457-1466.

Marcano-Reik AJ, Prasad T, Weiner JA, Blumberg MS (2010) An abrupt developmental shift in callosal modulation of sleep-related spindle bursts coincides with the emergence of excitatory-inhibitory balance and a reduction of somatosensory cortical plasticity. Behavioral neuroscience 124:600-611.

Martinez C, Carneiro L, Vernier L, Cesa C, Guardiola A, Vidor D (2014) Language in children with neonatal hypoxic-ischemic encephalopathy. Int Arch Otorhinolaryngol 18:255-259.

McQuillen PS, Sheldon RA, Shatz CJ, Ferriero DM (2003) Selective vulnerability of subplate neurons after early neonatal hypoxia-ischemia. The Journal of neuroscience : the official journal of the Society for Neuroscience 23:3308-3315.

Meng X, Kao JP, Kanold PO (2014) Differential signaling to subplate neurons by spatially specific silent synapses in developing auditory cortex. The Journal of neuroscience : the official journal of the Society for Neuroscience 34:8855-8864.

Meng X, Kao JP, Lee HK, Kanold PO (2015) Visual Deprivation Causes Refinement of Intracortical Circuits in the Auditory Cortex. Cell Rep 12:955-964.

Meyer HS, Wimmer VC, Hemberger M, Bruno RM, de Kock CP, Frick A, Sakmann B, Helmstaedter M (2010) Cell type-specific thalamic innervation in a column of rat vibrissal cortex. Cereb Cortex 20:2287-2303.

Milh M, Kaminska A, Huon C, Lapillonne A, Ben-Ari Y, Khazipov R (2007) Rapid cortical oscillations and early motor activity in premature human neonate. Cereb Cortex 17:1582-1594.

Minlebaev M, Ben-Ari Y, Khazipov R (2007) Network mechanisms of spindle-burst oscillations in the neonatal rat barrel cortex in vivo. Journal of neurophysiology 97:692-700.

Minlebaev M, Ben-Ari Y, Khazipov R (2009) NMDA receptors pattern early activity in the developing barrel cortex in vivo. Cereb Cortex 19:688-696.

Mohns EJ, Blumberg MS (2010) Neocortical activation of the hippocampus during sleep in infant rats. J Neurosci 30:3438-3449.

Molyneaux BJ, Arlotta P, Menezes JR, Macklis JD (2007) Neuronal subtype specification in the cerebral cortex. Nat Rev Neurosci 8:427-437.

Moore AR, Zhou WL, Jakovcevski I, Zecevic N, Antic SD (2011) Spontaneous electrical activity in the human fetal cortex in vitro. J Neurosci 31:2391-2398.

Mordel J, Sheikh A, Tsohataridis S, Kanold PO, Zehendner CM, Luhmann HJ (2016) Mild systemic inflammation and moderate hypoxia transiently alter neuronal excitability in mouse somatosensory cortex. Neurobiology of disease 88:29-43.

Muralidharan S, Dirda ND, Katz EJ, Tang CM, Bandyopadhyay S, Kanold PO, Kao JP (2016) Ncm, a Photolabile Group for Preparation of Caged Molecules: Synthesis and Biological Application. PLoS One 11:e0163937.

O'Leary DD, Schlaggar BL, Tuttle R (1994) Specification of neocortical areas and thalamocortical connections. Annu Rev Neurosci 17:419-439.

Pierret T, Lavallee P, Deschenes M (2000) Parallel streams for the relay of vibrissal information through thalamic barreloids. The Journal of neuroscience : the official journal of the Society for Neuroscience 20:7455-7462.

Pinon MC, Jethwa A, Jacobs E, Campagnoni A, Molnar Z (2009) Dynamic integration of subplate neurons into the cortical barrel field circuitry during postnatal development in the Golli-tau-eGFP (GTE) mouse. J Physiol 587:1903-1915.

Polley DB, Seidl AH, Wang Y, J.T. S (2013) Functional circuit development in the auditory system. In: Neural circuit development and function in the healthy

and diseased brain (Rubenstein JLR, Rakic P, eds), pp 21-39. Amsterdam: Elsevier.

Purves D (2008) Neuroscience. Sunderland, Massachusetts: Sinauer Associates, Inc. .

Quairiaux C, Sizonenko SV, Megevand P, Michel CM, Kiss JZ (2010) Functional deficit and recovery of developing sensorimotor networks following neonatal hypoxic-ischemic injury in the rat. Cereb Cortex 20:2080-2091.

Raghuveer TS, Cox AJ (2011) Neonatal resuscitation: an update. American family physician 83:911-918.

Ranasinghe S, Or G, Wang EY, Ievins A, McLean MA, Niell CM, Chau V, Wong PK, Glass HC, Sullivan J, McQuillen PS (2015) Reduced Cortical Activity Impairs Development and Plasticity after Neonatal Hypoxia Ischemia. The Journal of neuroscience : the official journal of the Society for Neuroscience 35:11946-11959.

Reim K, Wegmeyer H, Brandstatter JH, Xue M, Rosenmund C, Dresbach T, Hofmann K, Brose N (2005) Structurally and functionally unique complexins at retinal ribbon synapses. The Journal of cell biology 169:669-680.

Reim K, Regus-Leidig H, Ammermuller J, El-Kordi A, Radyushkin K, Ehrenreich H, Brandstatter JH, Brose N (2009) Aberrant function and structure of retinal ribbon synapses in the absence of complexin 3 and complexin 4. J Cell Sci 122:1352-1361.

Rheims S, Minlebaev M, Ivanov A, Represa A, Khazipov R, Holmes GL, Ben Ari Y, Zilberter Y (2008) Excitatory GABA in rodent developing neocortex in vitro. Journal of neurophysiology:90402.

Rivera C, Voipio J, Payne JA, Ruusuvuori E, Lahtinen H, Lamsa K, Pirvola U, Saarma M, Kaila K (1999) The K+/Cl- co-transporter KCC2 renders GABA hyperpolarizing during neuronal maturation. Nature 397:251-255.

Robertson CM, Perlman M (2006) Follow-up of the term infant after hypoxic-ischemic encephalopathy. Paediatrics & child health 11:278-282.

Rothschild G, Nelken I, Mizrahi A (2010) Functional organization and population dynamics in the mouse primary auditory cortex. Nature neuroscience 13:353-360.

Rumajogee P, Bregman T, Miller SP, Yager JY, Fehlings MG (2016) Rodent Hypoxia-Ischemia Models for Cerebral Palsy Research: A Systematic Review. Front Neurol 7:57.

Rybalko N, Chumak T, Bures Z, Popelar J, Suta D, Syka J (2015) Development of the acoustic startle response in rats and its change after early acoustic trauma. Behavioural brain research 286:212-221.

Schlaggar BL, Fox K, O'Leary DD (1993) Postsynaptic control of plasticity in developing somatosensory cortex [see comments]. Nature 364:623-626.

Seelke AM, Blumberg MS (2010) Developmental appearance and disappearance of cortical events and oscillations in infant rats. Brain Res 1324:34-42.

Sengpiel F, Kind PC (2002) The role of activity in development of the visual system. Curr Biol 12:R818-826.

Shatz CJ (1996) Emergence of order in visual system development. J Physiol Paris 90:141-150.

Shepherd GM, Pologruto TA, Svoboda K (2003) Circuit analysis of experience-dependent plasticity in the developing rat barrel cortex. Neuron 38:277-289.

Shimizu-Okabe C, Yokokura M, Okabe A, Ikeda M, Sato K, Kilb W, Luhmann HJ, Fukuda A (2002) Layer-specific expression of Cl- transporters and differential [Cl-]i in newborn rat cortex. Neuroreport 13:2433-2437.

Sipila ST, Schuchmann S, Voipio J, Yamada J, Kaila K (2006) The cation-chloride cotransporter NKCC1 promotes sharp waves in the neonatal rat hippocampus. J Physiol 573:765-773.

Stiebler I, Neulist R, Fichtel I, Ehret G (1997) The auditory cortex of the house mouse: left-right differences, tonotopic organization and quantitative analysis of frequency representation. J Comp Physiol A 181:559-571.

Sun JJ, Luhmann HJ (2007) Spatio-temporal dynamics of oscillatory network activity in the neonatal mouse cerebral cortex. The European journal of neuroscience 26:1995-2004.

Suter BA, O'Connor T, Iyer V, Petreanu LT, Hooks BM, Kiritani T, Svoboda K, Shepherd GM (2010) Ephus: multipurpose data acquisition software for neuroscience experiments. Front Neural Circuits 4:100.

Tolner EA, Sheikh A, Yukin AY, Kaila K, Kanold PO (2012) Subplate neurons promote spindle bursts and thalamocortical patterning in the neonatal rat somatosensory cortex. The Journal of neuroscience : the official journal of the Society for Neuroscience 32:692-702.

Turrigiano G (2011) Too many cooks? Intrinsic and synaptic homeostatic mechanisms in cortical circuit refinement. Annual review of neuroscience 34:89-103.

Turrigiano G (2012) Homeostatic synaptic plasticity: local and global mechanisms for stabilizing neuronal function. Cold Spring Harbor perspectives in biology 4:a005736.

Turrigiano GG (1999) Homeostatic plasticity in neuronal networks: the more things change, the more they stay the same. Trends in neurosciences 22:221-227.

Turrigiano GG, Nelson SB (2004) Homeostatic plasticity in the developing nervous system. Nat Rev Neurosci 5:97-107.

Urbain N, Deschenes M (2007) A new thalamic pathway of vibrissal information modulated by the motor cortex. The Journal of neuroscience : the official journal of the Society for Neuroscience 27:12407-12412.

Vaithianathan T, Henry D, Akmentin W, Matthews G (2015) Functional roles of complexin in neurotransmitter release at ribbon synapses of mouse retinal bipolar neurons. The Journal of neuroscience : the official journal of the Society for Neuroscience 35:4065-4070.

Valverde F, Facal-Valverde MV (1987) Transitory population of cells in the temporal cortex of kittens. Brain research 429:283-288.

Vanhatalo S, Kaila K (2010) Emergence of spontaneous and evoked electroencephalographic activity in the human brain. In: The Newborn Brain: Neuroscience and Clinical Applications 2nd Edition (Lagercrantz H, Hanson

M, Evrard P, Rod C, eds), pp 229-244. Cambridge: Cambridge University Press.

Vanhatalo S, Jousmaki V, Andersson S, Metsaranta M (2009) An easy and practical method for routine, bedside testing of somatosensory systems in extremely low birth weight infants. Pediatr Res 66:710-713.

Vanhatalo S, Tallgren P, Andersson S, Sainio K, Voipio J, Kaila K (2002) DC-EEG discloses prominent, very slow activity patterns during sleep in preterm infants. Clinical Neurophysiology 113:1822-1825.

Vanhatalo S, Palva JM, Andersson S, Rivera C, Voipio J, Kaila K (2005) Slow endogenous activity transients and developmental expression of K+-Cl- cotransporter 2 in the immature human cortex. The European journal of neuroscience 22:2799-2804.

Varga C, Sik A, Lavallee P, Deschenes M (2002) Dendroarchitecture of relay cells in thalamic barreloids: a substrate for cross-whisker modulation. The Journal of neuroscience : the official journal of the Society for Neuroscience 22:6186-6194.

Vasung L, Huang H, Jovanov-Milosevic N, Pletikos M, Mori S, Kostovic I (2010) Development of axonal pathways in the human fetal fronto-limbic brain: histochemical characterization and diffusion tensor imaging. Journal of anatomy 217:400-417.

Viswanathan S, Bandyopadhyay S, Kao JP, Kanold PO (2012) Changing microcircuits in the subplate of the developing cortex. The Journal of

neuroscience : the official journal of the Society for Neuroscience 32:1589-1601.

Viswanathan S, Sheikh A, Looger LL, Kanold PO (2016) Molecularly defined subplate neurons project both to thalamocortical recipient layers and thalamus. Cereb Cortex (In press).

Volpe JJ (1996) Subplate neurons--missing link in brain injury of the premature infant? Pediatrics 97:112-113.

Wimmer VC, Bruno RM, de Kock CP, Kuner T, Sakmann B (2010) Dimensions of a projection column and architecture of VPM and POm axons in rat vibrissal cortex. Cereb Cortex 20:2265-2276.

Winkowski DE, Kanold PO (2013) Laminar transformation of frequency organization in auditory cortex. The Journal of neuroscience : the official journal of the Society for Neuroscience 33:1498-1508.

Xu HP, Furman M, Mineur YS, Chen H, King SL, Zenisek D, Zhou ZJ, Butts DA, Tian N, Picciotto MR, Crair MC (2011) An instructive role for patterned spontaneous retinal activity in mouse visual map development. Neuron 70:1115-1127.

Xue M, Stradomska A, Chen H, Brose N, Zhang W, Rosenmund C, Reim K (2008) Complexins facilitate neurotransmitter release at excitatory and inhibitory synapses in mammalian central nervous system. Proceedings of the National Academy of Sciences of the United States of America 105:7875-7880.

Yang JW, Hanganu-Opatz IL, Sun JJ, Luhmann HJ (2009) Three patterns of oscillatory activity differentially synchronize developing neocortical networks in vivo. J Neurosci 29:9011-9025.

Yuste R, Denk W (1995) Dendritic spines as basic functional units of neuronal integration. Nature 375:682-684.

Zhang LI, Poo MM (2001) Electrical activity and development of neural circuits. Nat Neurosci 4 Suppl:1207-1214.

Zhang LI, Bao S, Merzenich MM (2001) Persistent and specific influences of early acoustic environments on primary auditory cortex. Nature neuroscience 4:1123-1130.

Zhao C, Kao JP, Kanold PO (2009) Functional excitatory microcircuits in neonatal cortex connect thalamus and layer 4. The Journal of neuroscience : the official journal of the Society for Neuroscience 29:15479-15488.